DTIC FILE COPY

(2)

AD-A200 581

SACLANTCEN REPORT
serial no.: SR-113

SACLANT UNDERSEA
RESEARCH CENTRE

REPORT

SAFARI

Seismo-Acoustic Fast field Algorithm for Range-Independent environments

User's Guide

H. Schmidt

DTIC
ELECTE
NOV 23 1988
S D
E

September 1988

DISTRIBUTION STATEMENT A
Approved for public release;
Distribution Unlimited

The SACLANT Undersea Research Centre provides the Supreme Allied Commander Atlantic (SACLANT) with scientific and technical assistance under the terms of its NATO charter, which entered into force on 1 February 1963. Without prejudice to this main task—and under the policy direction of SACLANT—the Centre also renders scientific and technical assistance to the individual NATO nations.

88 1122 055

This document is released to a NATO Government at the direction of SACLANT Undersea Research Centre subject to the following conditions:

- The recipient NATO Government agrees to use its best endeavours to ensure that the information herein disclosed, whether or not it bears a security classification, is not dealt with in any manner (a) contrary to the intent of the provisions of the Charter of the Centre, or (b) prejudicial to the rights of the owner thereof to obtain patent, copyright, or other like statutory protection therefor.

- If the technical information was originally released to the Centre by a NATO Government subject to restrictions clearly marked on this document the recipient NATO Government agrees to use its best endeavours to abide by the terms of the restrictions so imposed by the releasing Government.

Page count for SR-113
(excluding covers)

Pages	Total
i–v	5
1–152	152
	157

SACLANT Undersea Research Centre
Viale San Bartolomeo 400
19026 San Bartolomeo (SP), Italy

tel: 0187 540 111
telex: 271148 SACENT I

NORTH ATLANTIC TREATY ORGANIZATION

SACLANTCEN SR-113

SAFARI

Seismo-Acoustic Fast field Algorithm for Range-Independent environments

User's Guide

H. Schmidt

The content of this document pertains to work performed under Project 19 of the SACLANTCEN Programme of Work. The document has been approved for release by The Director, SACLANTCEN.

Peter C. Wille
Director

DTIC
ELECTE
NOV 23 1988
S D
E

intentionally blank page

SAFARI

Seismo-Acoustic Fast field Algorithm for Range-Independent environments

User's Guide

H. Schmidt

continuous wave

Abstract: An efficient algorithm has been developed for solving the depth-separated wave equation in general fluid/solid horizontally stratified media. The algorithm has been built into a general-purpose package of computer codes called SAFARI. The package consists of three modules providing plane wave reflection coefficients, ~~and~~ transmission losses, and broadband pulse response. This document ~~first~~ describes the mathematical model for seismo-acoustic propagation in stratified media. Then the numerical solution technique is outlined followed by a description of the three different SAFARI modules and their implementation. ~~Finally,~~ the actual use of the different modules is described, including a detailed discussion on the numerical considerations that are crucial for successful use of this type of numerical model. SAFARI is applicable to a wide range of problems in many disciplines, from seismology to ultrasonics. Here its use is illustrated by a series of examples from underwater acoustics.

Keywords: attenuation; beam propagation; fast field program; Green's function; normal mode propagation; numerical modelling; pulse propagation; reflection coefficient; ~~SAFARI~~; seismic interface wave; seismo-acoustic propagation; stratified media; transmission loss; underwater acoustics; wave equations; wave propagation.
(NATO-furnished, edc)

QUALITY INSPECTED 2

Accession For	
NTIS GRA&I	☑
DTIC TAB	☐
Unannounced	☐
Justification	
By	
Distribution/	
Availability Codes	
Dist	Avail and/or Special
A-1	

Contents

1. Introduction 1
2. The environmental model 5
3. The mathematical model 7
3.1. The depth-separated wave equation 7
3.2. Homogeneous fluid medium 9
3.3. Inhomogeneous fluid medium 11
3.4. Homogeneous solid medium 15
3.5. Boundary conditions 17
3.6. Attenuation 18
4. Numerical solution technique 21
4.1. Depth-dependent Green's function 22
4.2. Reflection coefficients 30
4.3. Wavenumber integration 31
4.4. Frequency integration 37
5. Installation of SAFARI 39
5.1. Precision requirements 39
5.2. Memory requirements 40
5.3. Source files 40
5.4. Compiling the SAFARI *codes* 42
5.5. Linking the SAFARI *codes* 43
5.6. Running the SAFARI *codes* 43
6. Running SAFARI-FIPR 46
6.1. Input files for SAFARI-FIPR 47
6.2. Numerical considerations 58
6.3. SAFARI-FIPR *examples* 58
7. Running SAFARI-FIP 67
7.1. Input files for SAFARI-FIP 68
7.2. Numerical considerations 83
7.3. SAFARI-FIP *examples* 86
8. Running SAFARI-FIPP 102
8.1. Input files for SAFARI-FIPP 104
8.2. Numerical considerations 127

8.3 SAFARI-FIPP *examples* *129*

References *139*

Appendix A – Installing and running SAFARI on the FPS164 . . *143*
Appendix B – Running FIPPLOT *146*
Appendix C – Running CONTUR *150*

Acknowledgement: The author would like to thank the significant number of persons who had impact on the development of SAFARI. Prime in this respect has been Finn Jensen, SACLANTCEN, who proposed several features of importance in underwater acoustics. Gerard Tango, NORDA, was the first to use SAFARI outside SACLANTCEN and has proposed output features convenient for examining phenomena in crustal and exploration geophysics. The opportunity to work jointly with Tango on presenting SAFARI to the seismic community was highly appreciated. The collaboration with Bill Kuperman, NRL, on generalising his scattering theory to solid media and implementing it in SAFARI is likewise appreciated. I would also like to thank John Glattetre, NDRE, for the very fruitful collaboration in connection with the development of a three-dimensional version of SAFARI; Neil Fraser of the Hawaii Geophysical Institute, for many discussions on numerical integration which have had significant impact on the efficiency of the code; Steve Wales, NRL, for the supply of subroutines for generating Airy functions.

Many SAFARI users have been feeding back information on inconveniences and problems. In this context a special thanks to Robert Koch, ARL; Dave Thomson, DREP; Ralph Stephen, WHOI; and Greg Duckworth, MIT.

Finally I would like to thank Tom Muir and Finn Jensen, SACLANTCEN, for carefully 'testing out' the original version of this user's guide and for pointing out necessary changes and clarifications.

1. Introduction

The seismo-acoustic environments encountered in nature are in general very complex. Sound velocity in the ocean varies with both range and depth due to changes in temperature, salinity and density, induced by solar heating, gravity, currents and eddies. The water depth can vary significantly, in particular near the shore and at the continental rise. In addition, the bottom will often be characterised by irregular stratification and anisotropy. Since the seismo-acoustic propagation is highly dependent on the material properties, an exact computer modelling would require exact knowledge of the environmental properties to the smallest detail, which is of course prohibitive. Some kind of approximation therefore has to be applied in order to obtain a physical model of the environment for which the wave equation can be solved numerically. Solution techniques such as the finite-difference technique [1] and the finite-element method [2] require only a few approximations of the environment. These techniques are therefore the most general, but the computational requirements are extensive, in reality prohibiting their application to large scale propagation modelling. None of the more efficient techniques are applicable to the general problem since they are based on specific assumptions concerning the environment. The parabolic equation technique [3] can treat propagation in a range-dependent environment, but the shear properties of the ocean bottom are ignored and the results are only accurate for moderate grazing angles. One class of solution techniques requires the environment to be described by a physical model for which the wave equation is separable. This class includes the normal mode [4] technique, which, however, in most implementations ignores shear and is limited to propagation at grazing angles less than critical (by means of mode coupling, the normal mode technique may be applied to non-seperable problems as well [5]). Another solution technique requiring the wave equation to be separable is the Fast Field (FFP) or full wavefield technique applied in SAFARI. This technique yields – at least in principle – an exact solution to the wave equation in a horizontally stratified fluid/solid environment.

The principle of wave equation separation for horizontally stratified media was introduced in underwater acoustics by Pekeris [6], who treated the problem of acoustic propagation in plane layered waveguides using simple two- and three-layered environmental models. Later, Jardetsky [7] and Ewing, Jardetsky and Press [8] used the same technique to investigate seismic propagation in few-layered waveguides. The technique was to apply a series of integral transforms to the Helmholtz wave equation to reduce the original four-dimensional partial differential equation (3 space dimensions and 1 of time) to a series of ordinary differential equations in the depth coordinate. These differential equations were then solved analytically within each layer in terms of unknown amplitudes which were determined by matching of the

boundary conditions at the interfaces. The displacement and stress quantities were finally determined by evaluation of the inverse integral transforms.

For the few-layered cases originally presented, the linear system of equations in the unknown wavefield amplitudes, expressing the boundary conditions, can easily be solved analytically. For more complicated environmental models, however, this procedure is inconvenient and has to be replaced by a numerical technique.

Traditionally, computation of the depth dependence of the field has been performed by means of propagator matrix methods as introduced by Thomson [9] and Haskell [10]. The propagator matrix approach has the computational advantage that it only requires a small amount of computer memory due to its recursive nature. However, it was realised quite early that special numerical treatment is required in order to ensure numerical stability, and several modified propagator matrix schemes have been proposed. In general, however, these have resulted in much more time consuming codes. Further, the propagator technique is not well suited to problems where the field has to be determined at more than a single receiver depth. A review of the propagator approaches is given by Kenneth [11] who himself introduced the elegant invariant embedding formulation [12] which has the interpretational advantage that arrivals resulting from reflections from a single interface can be isolated.

The propagator matrix approach has formed the basis of several application codes in both underwater acoustics [13] and seismology [14]. The so-called Fast Field program developed by DiNapoli [15] applies a very elegant recursive technique to determine the depth-dependent solution for many horizontal wavenumbers simultaneously, and is therefore extremely efficient. In contrast to the other techniques, however, the depth-dependent solution is approximate, and the technique is only applicable to a limited class of fluid problems.

In SAFARI a direct, global matrix approach is taken to determine the depth dependence of the field solution, known as the depth-dependent Green's function. The SAFARI technique is in fact a general numerical implementation of the original solution technique of Ewing et al. [8], but implemented using efficient numerical techniques adopted from modern finite-element programs.

In what might be termed a direct global matrix or 'finite wave element' approach, the wavefield in each layer is considered as a superposition of the field produced by an arbitrary number of sources and an unknown field satisfying homogeneous wave equations. These unknown fields are then determined from the boundary conditions to be satisfied simultaneously at all interfaces. The local boundary conditions at each interface lead to a linear system of equations in the Hankel transforms of the potentials in the adjacent layers. These *local* systems of equations are then straightforwardly assembled in a *global* system of equations expressing the boundary conditions at all interfaces simultaneously. The resulting global coefficient matrix is organised to be block-bidiagonal and diagonally dominant in close analogy

to the global stiffness matrix arising in the finite-element method. Unconditionally numerically-stable solutions are determined efficiently by gaussian elimination, yielding the field in all layers simultaneously.

Despite the analytical equivalence of the propagator and global matrix solutions for the depth-dependent Green's function, there are a number of important advantages of the latter technique for application to general wave propagation problems in underwater acoustics and seismology as well as in ultrasonics:

- The field produced by multiple sources, e.g. in phased arrays, is easily determined since the fields produced by the individual sources within a layer are simply superimposed, and no dummy interfaces are required at the source depths.
- The field can be determined at any number of receiver depths in a single solution pass, since the wavefield potentials are found in all layers simultaneously.
- In contrast to the situation for techniques based on propagator matrices, mixed problems with fluid, solid and vacuum layers are readily treated in an efficient manner, as the global system of equations is set up to involve only non-vanishing potential functions.
- Time consuming stability assurance problems do not arise, because they are removed automatically by choosing an appropriate coordinate system within each layer together with a specific organization of the global system of equations.
- The solution is unconditionally numerically-stable for any number of layers.
- Due to the global nature, many operations can be vectorized, making the code efficient on modern array and vector processors, in particular in cases with many layers.

These properties make the global matrix approach well suited for implementation in a general applications program like SAFARI, rendering it applicable to a large range of seismo-acoustic propagation problems in underwater acoustics, seismology and ultrasonics.

Although the solution for the depth-dependence of the field is exact to within machine accuracy, it is a common characteristic of all numerical models of the full wavefield type that they are not easy to use. They are what might be termed 'scientific' numerical models which require the user to possess a significant knowledge of the physics involved in wave propagation phenomena in stratified waveguides and at the same time be confident with numerical analysis. This is due to the fact that the evaluation of the inverse integral transforms has to be made numerically, which requires both truncation and discretisation of the integration interval, both of which introduce errors and numerical artifacts which have to be reduced to insignificance. There are no general rules to follow, because the necessary sampling depends on the

characteristics of the actual problem. This is particularly true in cases where only selected parts of the solution are of interest. The numerical integration therefore cannot be fully automated, but has to be controlled by the user.

The present document is not intended for teaching waveguide propagation and numerical analysis to the new SAFARI user. Those topics are treated in many different textbooks. Thus the intention is solely to present a self-contained user's guide which should introduce the new user to the SAFARI model and at the same time act as a reference manual for the experienced user.

In order to describe the basic assumptions underlying the SAFARI codes, the mathematical model for wave propagation in stratified media is first outlined. Secondly, the numerical implementation of the mathematical model is discussed in detail, presenting first the global matrix solution technique particular to SAFARI and then the different numerical integration schemes available for evaluating the total field. In the third part, the implementation of the three basic SAFARI modules is discussed in general terms; the precise procedure of course depends on the actual installation. Finally, the last and most important part treats the process of running the codes, including preparation of input files and the necessary numerical considerations concerning the numerical integrations in particular. The actual use is illustrated by a series of characteristic numerical examples from underwater acoustics. Applications of SAFARI to other problems, both from seismology and ultrasonics, are given in [16–27].

2. The environmental model

The mathematical description of the seismo-acoustic propagation used in SAFARI requires the environment to be represented as a horizontally stratified medium as illustrated in Fig. 1. All interfaces are plane and parallel, and the layer properties are range-independent. The layers, including the upper and lower halfspaces, may be either viscoelastic solids or fluids, or they may be empty space, i.e. vacuum.

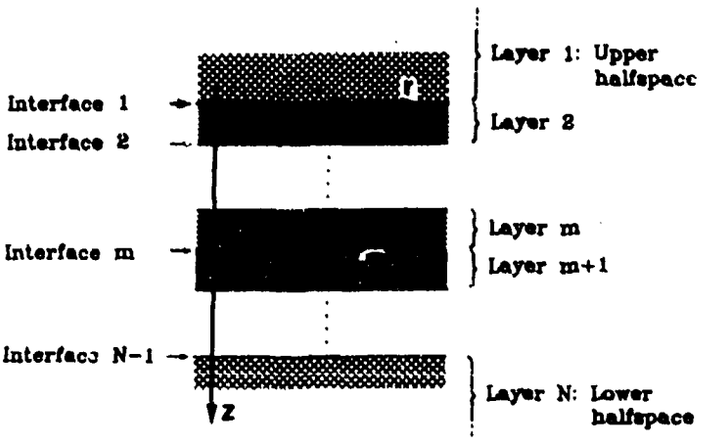

Fig. 1. Horizontally stratified environment.

The solid layers are required to be homogeneous and isotropic with Lamé constants λ and μ and density ρ. The corresponding compressional wave speed is

$$c_c = \sqrt{(\lambda + 2\mu)/\rho}, \tag{1}$$

and the shear speed is

$$c_s = \sqrt{\mu/\rho}. \tag{2}$$

In order for the solid medium to have positive compressibility, it is required that the bulk modulus, $K = \lambda + \frac{2}{3}\mu$, be positive. A physically realistic material therefore requires

$$c_s < \sqrt{0.75}\, c_c. \tag{3}$$

In the fluid layers the density ρ must be constant, whereas the nonvanishing Lamé constant λ is allowed to vary with depth according to the linear law:

$$\frac{1}{\lambda(z)} = az + b \tag{4}$$

which corresponds to the following depth dependence for the sound speed, Eq. (1),

$$c_c(z) = \sqrt{1/(\rho(az + b))}. \tag{5}$$

The special case of a homogeneous fluid medium corresponds to $a = 0$.

3. The mathematical model

Only two-dimensional propagation problems can be treated by the standard SAFARI package, although a special three-dimensional version has been developed [28]. Thus the seismo-acoustic field has to be either plane or axisymmetric, restricting the sources to be either line sources perpendicular to the plane of propagation or omni-directional point sources placed on a common vertical axis. In underwater acoustics the last type is the most common, and therefore we here describe the mathematical model for the axisymmetric case. The corresponding model for the plane case is described in [21].

The full wavefield solution technique is based on the fact that for a horizontally stratified environment, it is possible to obtain exact integral representations for the field within each layer in terms of a set of unknown coefficients. These coefficients are found by matching the boundary conditions simultaneously at all interfaces, and the total field is determined by evaluation of the integral representations. In this section the basic principle of the solution of the wave equation by depth-separation is first described. Then the resulting field representations will be given for both fluid and solid media, and finally the pertinent boundary conditions are discussed. The actual numerical implementation is discussed in Sect. 4.

3.1. THE DEPTH-SEPARATED WAVE EQUATION

A cylindrical coordinate system $\{r, \theta, z\}$ is introduced, Fig. 1, with the z-axis passing through the sources, making the field independent of asimuthal angle θ. For the isotropic media considered here, the seismo-acoustic wavefield can then be expressed in terms of scalar wavefield potentials $\Psi(r, z, t)$, which satisfy the linear wave equation

$$\left(\nabla^2 - \frac{1}{c(r,z)^2}\frac{\partial^2}{\partial t^2}\right)\Psi(r,z,t) = F_s(r,z,t). \tag{6}$$

Here $c(r, z)$ is a wave speed and $F_s(r, z, t)$ a forcing term which in the present case is due to the seismo-acoustic sources. We now utilise the Fourier transform pair

$$f(\omega) = \frac{1}{2\pi}\int_{-\infty}^{\infty} F(t)e^{-i\omega t}\,\mathrm{d}t, \tag{7}$$

$$F(t) = \int_{-\infty}^{\infty} f(\omega)e^{i\omega t}\,\mathrm{d}\omega. \tag{8}$$

By applying the forward transform, Eq. (7), to the wave equation, Eq. (6), the frequency domain wave equation is obtained:

$$\left(\nabla^2 + k_m^2(r,z)\right)\Psi(r,z,\omega) = f_s(r,z,\omega), \tag{9}$$

where ω is the angular frequency and $k_m(r,z)$ is the medium wavenumber,

$$k_m(r,z) = \omega/c(r,z). \tag{10}$$

Since the environment is range independent and the sources are confined to the vertical axis, Eq. (9) can be rewritten as

$$\left(\nabla^2 + k_m^2(z)\right)\Psi(r,z,\omega) = \frac{f_s(z,\omega)\delta(r)}{2\pi r}. \tag{11}$$

In the following the ω dependence will be generally suppressed.

Next, we employ the Hankel transform pair

$$g(k) = \int_0^\infty G(r)J_0(kr)r\,\mathrm{d}r, \tag{12}$$

$$G(r) = \int_0^\infty g(k)J_0(kr)k\,\mathrm{d}k, \tag{13}$$

where k is the horizontal wavenumber, and apply the forward transform, Eq. (12), to Eq. (11), obtaining the depth-separated wave equation

$$\left(\frac{\mathrm{d}^2}{\mathrm{d}z^2} - \left(k^2 - k_m^2(z)\right)\right)\Psi(k,z) = \frac{f_s(z)}{2\pi}, \tag{14}$$

i.e. an ordinary differential equation in depth. The solution is the sum of a particular solution $\widehat{\Psi}(k,z)$ to Eq. (14) and any linear combination of the two independent solutions $\Psi^-(k,z)$ and $\Psi^+(k,z)$ to the homogeneous equation

$$\left(\frac{\mathrm{d}^2}{\mathrm{d}z^2} - \left(k^2 - k_m^2(z)\right)\right)\Psi(k,z) = 0. \tag{15}$$

The total solution for the depth dependence of the field, the so-called depth-dependent Green's function, is therefore

$$\Psi(k,z) = \widehat{\Psi}(k,z) + A^-(k)\Psi^-(k,z) + A^+(k)\Psi^+(k,z), \tag{16}$$

where $A^-(k)$ and $A^+(k)$ are arbitrary coefficients to be determined from the boundary conditions. The particular solution to Eq. (14) is most conveniently chosen to be the field produced by the sources in the absence of boundaries.

When the unknown coefficients are found, the total field at the angular frequency ω is found at any range r by carrying out the inverse Hankel transform, Eq. (13). Similarly, the time response is determined by evaluating the inverse Fourier transform, Eq. (8).

The basic property of the full wavefield solution technique is to restrict the depth dependence of $k_m^2(z)$ to cases where Eqs. (14) and (15) can be solved analytically, limiting the numerical effort to determining the unknown coefficients $A^-(k)$ and $A^+(k)$ from the boundary conditions and to evaluating the inverse integral transforms.

In the following, the analytical field representations will be given for the media included in the SAFARI model, followed by a discussion of the boundary conditions to be satisfied at the interfaces.

3.2. HOMOGENEOUS FLUID MEDIUM

For an ideal fluid, the equation of motion for angular frequency ω is easily shown to be satisfied if the displacements are expressed in terms of a scalar displacement potential as

$$u = \frac{\partial \Phi}{\partial r}, \tag{17}$$

$$w = \frac{\partial \Phi}{\partial z}, \tag{18}$$

where u and w are the radial and vertical components, respectively, and the potential $\Phi(r, z)$ satisfies the wave equation, Eq. (9). The depth dependence of the field is therefore of the form given by Eq. (16).

In the case of a homogeneous fluid layer, the medium wavenumber is

$$k_m(z) = h_m, \tag{19}$$

i.e. the compressional velocity c_c is constant not only in range but also in depth, and the homogeneous solutions obtained from Eq. (15) are simply exponential functions,

$$\Phi^+(k, z) = e^{\alpha z}, \tag{20}$$

$$\Phi^-(k, z) = e^{-\alpha z}, \tag{21}$$

where

$$\alpha(k) = \sqrt{k^2 - h_m^2}. \tag{22}$$

If no sources are present in the layer, the total field then follows directly from Eq. (13) as

$$\Phi(r,z) = \int_0^\infty \left[A^- e^{-\alpha z} + A^+ e^{\alpha z}\right] J_0(kr) k \, dk. \tag{23}$$

In physical terms, Eq. (23) is a decomposition of the total wavefield in upgoing ($e^{\alpha z}$) and downgoing ($e^{-\alpha z}$) conical waves with horizontal wavenumber k.

The boundary conditions for fluid layers , discussed in Sect. 3.5, involve the vertical displacement w and the normal stress σ_{zz} (equivalent to negative pressure in a fluid medium). The vertical displacement follows from Eq. (18),

$$w(r,z) = \int_0^\infty \left[-\alpha A^- e^{-\alpha z} + \alpha A^+ e^{\alpha z}\right] J_0(kr) k \, dk, \tag{24}$$

whereas the normal stress follow from Hooke's law,

$$\sigma_{zz}(r,z) = \lambda \nabla^2 \Phi(r,z) = -\rho\omega^2 \Phi(r,z) = -\rho\omega^2 \int_0^\infty \left[A^- e^{-\alpha z} + A^+ e^{\alpha z}\right] J_0(kr) k \, dk. \tag{25}$$

If a source is present in the layer, the particular solution to Eq. (14) has to added. In the case of an omnidirectional point source, the term $f_s(z,\omega)$ in Eq. (11) takes the form

$$f_s(z,\omega) = -S_\omega \delta(z - z_s), \tag{26}$$

where S_ω is the source strength and z_s is the source depth. It can be shown [30], that in this case the particular solution to Eq. (14) is

$$\widehat{\Phi}(k,z) = \frac{S_\omega}{4\pi} \frac{e^{-\alpha|z-z_s|}}{\alpha}, \tag{27}$$

and the corresponding source contribution to the total field again follows from Eq. (13),

$$\widehat{\Phi}(r,z) = \frac{S_\omega}{4\pi} \int_0^\infty \frac{e^{-\alpha|z-z_s|}}{\alpha} J_0(kr) k \, dk. \tag{28}$$

If more sources are present in the layer their contributions are simply superimposed. The displacements and stresses are derived analogously to Eqs. (24) and (25) and become

$$\widehat{w}(r,z) = -\frac{S_\omega}{4\pi} \int_0^\infty \operatorname{sign}(z - z_s) e^{-\alpha|z-z_s|} J_0(kr) k \, dk, \tag{29}$$

$$\widehat{\sigma}_{zz}(r,z) = -\frac{S_\omega \rho\omega^2}{4\pi} \int_0^\infty \frac{e^{-\alpha|z-z_s|}}{\alpha} J_0(kr) k \, dk. \tag{30}$$

3.3. INHOMOGENEOUS FLUID MEDIUM

In a real ocean environment the sound velocity varies with depth, and it is well known that this variation has significant impact on the acoustic propagation. The ocean waveguide can therefore not in general be represented by a single homogeneous fluid layer. It can be shown, however, that if the range-independent ocean waveguide is represented by an increasing number of homogeneous layers, a numerical solution based on the field representation for homogeneous layers will converge towards the correct solution. However, a satisfactory convergence requires the layers to be less than one quarter of a wavelength thick. Such a technique is therefore only convenient for low frequency propagation in shallow water, and modelling of deep water or high frequency propagation does require some sort of velocity profile to be incorporated.

Since it is still necessary that Eq. (14) can be solved analytically it is obvious that the ocean cannot in general be represented by a single layer, but has to be approximated by a series of layers, within which the depth dependence of the field has an analytic representation. A few examples of sound speed interpolation functions for which this is possible are given in [15]. However, the actual choice of interpolation function is not very critical since the profile is usually measured at discrete depths with a finite uncertainty. In the SAFARI code the solution corresponding to the sound-speed variation given in Eq. (5) has been implemented. In this case the homogeneous depth-separated wave equation, Eq. (15), becomes

$$\left(\frac{\mathrm{d}^2}{\mathrm{d}z^2} - \left(k^2 - \rho\omega^2(az+b)\right)\right)\Phi(k,z) = 0. \tag{31}$$

By introducing the variable transformation,

$$\begin{aligned}\zeta &= c^{-2/3}(cz+d)\\ &= (\rho\omega^2 a)^{-2/3}(k^2 - \rho\omega^2(az+b)),\end{aligned} \tag{32}$$

the following equation is obtained:

$$\left(\frac{\mathrm{d}^2}{\mathrm{d}\zeta^2} - \zeta\right)\Phi(\zeta) = 0. \tag{33}$$

This is a special form of the Bessel differential equation, for which two independent solutions are the Airy functions $Ai(\zeta)$ and $Bi(\zeta)$, [29]. Independent homogeneous solutions to Eq. (31) are therefore

$$\Phi^+(k,z) = Ai(c^{-2/3}(k^2 - (cz+d)), \tag{34}$$

$$\Phi^-(k,z) = Bi(c^{-2/3}(k^2 - (cz+d)). \tag{35}$$

The total field at angular frequency ω is again obtained by evaluation of the inverse Hankel transform, Eq. (13),

$$\Phi(r,z) = \int_0^\infty [A^+ Ai(\zeta) + A^- Bi(\zeta)] J_0(kr) k \, dk, \tag{36}$$

with the corresponding displacement and stress given by

$$w(r,z) = -c^{1/3} \int_0^\infty [A^+ Ai'(\zeta) + A^- Bi'(\zeta)] J_0(kr) k \, dk, \tag{37}$$

$$\sigma_{zz}(r,z) = -\rho\omega^2 \int_0^\infty [A^+ Ai(\zeta) + A^- Bi(\zeta)] J_0(kr) k \, dk, \tag{38}$$

where a prime denotes the derivative with respect to the argument.

When a source is present in the layer the corresponding particular solution to Eq. (14) again has to be added. However, even in the case of a point source it is not straightforward to find such a particular solution. We will apply a small 'trick' to obtain analytical representations for the depth dependence of the field produced by a point source at depth z_s in an infinite medium with the sound velocity given by Eq. (5). A thin homogeneous layer of thickness ϵ with sound speed $c_c = c_c(z_s)$ is introduced containing the source, Fig. 2. In the limit $\epsilon \to 0$, the solution of this layered problem converges to the solution of the original problem.

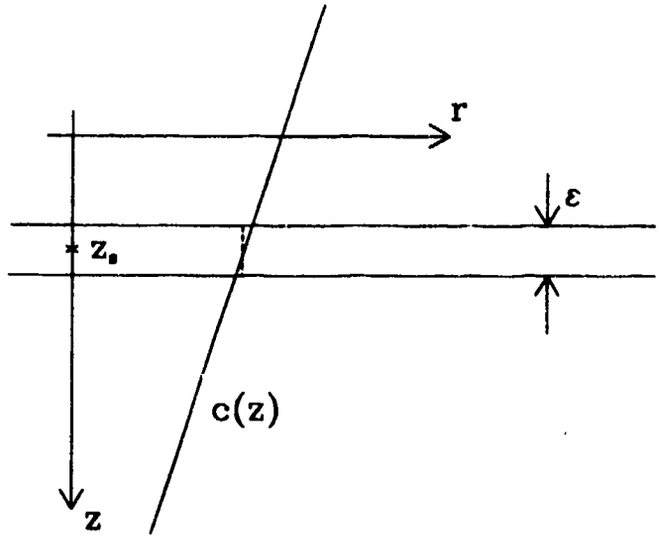

Fig. 2. Point source in inhomogeneous fluid medium.

This 3-layer problem is solved in exactly the same way in which the general multi-layered problem is solved in SAFARI. As an illustration of this solution technique, we shall here go through the details. In Fig. 2 the sound speed variation is shown for the case in which $a > 0$, i.e. $\lim_{z\to\infty} c_c(z) = 0$ and $\lim_{z\to -b/a} c_c(z) = \infty$. The argument ζ to the Airy functions, Eq. (32), therefore has the limits

$$\lim_{z\to\infty} \zeta = -\infty, \tag{39}$$

$$\lim_{z\to-\infty} \zeta = \infty. \tag{40}$$

Since no sources are present in the two halfspaces, the field in both is given by Eq. (36). The field, however, must satisfy the radiation condition for $z \to \pm\infty$, which immediately reduces the number of unknown coefficients. Since the field must be limited and $\lim_{\zeta\to\infty} Bi(\zeta) = \infty$, the depth dependence of the field in the upper halfspace must be of the form

$$\Phi_1(k,z) = A_1^+ Ai(\zeta). \tag{41}$$

Similarly, the radiation condition requires that only downgoing waves exist for $z \to \infty$. Because of the asymptotic behaviour of the Airy functions for $\zeta \to -\infty$ [29], it is required that the field in the lower halfspace be

$$\Phi_3(k,z) = A_3^-(Ai(\zeta) + iBi(\zeta)). \tag{42}$$

For the intermediate isovelocity layer, the depth dependence of the field is directly obtained from Eqs. (20), (21) and (27) as

$$\Phi_2(k,z) = A_2^- e^{-\alpha z} + A_2^+ e^{\alpha z} + \frac{S_\omega}{4\pi}\frac{e^{-\alpha|z-z_s|}}{\alpha}. \tag{43}$$

The next step is to satisfy the boundary conditions of continuous vertical displacement and stress at the two interfaces, which are so close together that they can both be considered to be at depth z_s, leading to the following system of equations:

$$A_1^+(-c^{1/3}Ai'(\zeta_s)) - \alpha(-A_2^- + A_2^+) = \frac{S_\omega}{4\pi}, \tag{44}$$

$$-A_1^+ Ai(\zeta_s) + (A_2^- + A_2^+) = -\frac{S_\omega}{4\pi\alpha}, \tag{45}$$

$$\alpha(-A_2^- + A_2^+) - A_3^-(-c^{1/3}(Ai'(\zeta_s) + iBi'(\zeta_s))) = \frac{S_\omega}{4\pi}, \tag{46}$$

$$-(A_2^- + A_2^+) + A_3^-(Ai(\zeta_s) + iBi(\zeta_s)) = \frac{S_\omega}{4\pi\alpha}. \tag{47}$$

All terms involving the coefficients A_2^- and A_2^+ are easily eliminated by pairwise addition, and the resulting two equations give the following solutions:

$$A_1^+ = -\frac{S_\omega}{4\pi}\frac{2c^{-1/3}(Ai(\zeta_s)+iBi(\zeta_s))}{Ai'(\zeta_s)(Ai(\zeta_s)+iBi(\zeta_s))-Ai(\zeta_s)(Ai'(\zeta_s)+iBi'(\zeta_s))}, \tag{48}$$

$$A_3^- = -\frac{S_\omega}{4\pi}\frac{2c^{-1/3}Ai(\zeta_s)}{Ai'(\zeta_s)(Ai(\zeta_s)+iBi(\zeta_s))-Ai(\zeta_s)(Ai'(\zeta_s)+iBi'(\zeta_s))}. \tag{49}$$

The source field representations for the case where the sound speed increases with depth, i.e. $a < 0$, can of course be determined in the same way, but it can also be determined right away by symmetry considerations. The choice of depth axis z is arbitrary, and we can therefore perform the variable transformation $z \to -z$. This will also change the sign of a in Eq. (5), and, as can be observed from Eq. (32), ζ is then invariant to this transformation, and the results above are therefore still valid; they just have to be interchanged between the two halfspaces. The field produced by a source in an inhomogeneous fluid layer therefore has the integral representation

$$\widehat{\Phi}(r,z) = -\frac{S_\omega}{4\pi}\int_0^\infty J_0(kr)k\,\mathrm{d}k$$
$$\times\begin{cases} \dfrac{2c^{-1/3}(Ai(\zeta_s)+iBi(\zeta_s))Ai(\zeta)}{Ai'(\zeta_s)(Ai(\zeta_s)+iBi(\zeta_s))-Ai(\zeta_s)(Ai'(\zeta_s)+iBi'(\zeta_s))}, & a(z-z_s)\le 0, \\[2ex] \dfrac{2c^{-1/3}Ai(\zeta_s)(Ai(\zeta)+iBi(\zeta))}{Ai'(\zeta_s)(Ai(\zeta_s)+iBi(\zeta_s))-Ai(\zeta_s)(Ai'(\zeta_s)+iBi'(\zeta_s))}, & a(z-z_s)\ge 0. \end{cases} \tag{50}$$

The resulting stresses and displacements are derived as they are for the homogeneous case. Note that, as was the case for a source in a homogeneous layer, the kernel in the integral representation for $\widehat{\Phi}(r,z)$ is continuous at the source depth, but the depth derivative is discontinuous. If more sources are present, their contributions are simply superimposed.

3.4. HOMOGENEOUS SOLID MEDIUM

For a homogeneous and isotropic elastic solid, it can be shown [8], that the equation of motion is satisfied if the displacements are expressed in terms of scalar potentials $\{\Phi, \Psi\}$ as

$$u(r,z) = \frac{\partial}{\partial r}\Phi(r,z) + \frac{\partial^2}{\partial r \partial z}\Psi(r,z), \tag{51}$$

$$w(r,z) = \frac{\partial}{\partial z}\Phi(r,z) - \frac{1}{r}\frac{\partial}{\partial r} r \frac{\partial}{\partial r}\Psi(r,z), \tag{52}$$

where the potentials in the absence of sources satisfy the uncoupled homogeneous wave equations

$$\left(\nabla^2 - \frac{1}{c_c^2}\frac{\partial^2}{\partial t^2}\right)\Phi(r,z,t) = 0, \tag{53}$$

$$\left(\nabla^2 - \frac{1}{c_s^2}\frac{\partial^2}{\partial t^2}\right)\Psi(r,z,t) = 0, \tag{54}$$

c_c and c_s being the compressional and shear velocities, respectively, given in terms of the Lamé constants in Eqs. (1) and (2). Both these equations are of the same form as Eq. (6) and can therefore be depth-separated. As in the case of a homogeneous fluid, the constant wave speeds lead to simple exponential functions in depth, and the potentials therefore have the following integral representations for angular frequency ω:

$$\Phi(r,z) = \int_0^\infty [A^- e^{-\alpha z} + A^+ e^{\alpha z}] J_0(kr) k \, dk, \tag{55}$$

$$\Psi(r,z) = \int_0^\infty [B^- e^{-\beta z} + B^+ e^{\beta z}] J_0(kr) \, dk, \tag{56}$$

where

$$\alpha(k) = \sqrt{k^2 - h_m^2}, \tag{57}$$

$$\beta(k) = \sqrt{k^2 - k_m^2}. \tag{58}$$

The medium wavenumbers h_m and k_m are for compressional and shear waves, respectively. By means of Eqs. (51) and (52), the following integral representations are obtained for the displacements,

$$u(r,z) = \int_0^\infty \left[-\alpha A^- e^{-\alpha z} - \alpha A^+ e^{\alpha z} + \beta B^- e^{-\beta z} - \beta B^+ e^{\beta z}\right] J_1(kr) k \, dk, \tag{59}$$

$$w(r,z) = \int_0^\infty \left[-\alpha A^- e^{-\alpha z} + \alpha A^+ e^{\alpha z} + k B^- e^{-\beta z} + k B^+ e^{\beta z}\right] J_0(kr) k \, dk, \tag{60}$$

and the normal stress σ_{zz} and tangential stress σ_{rz} follow from Hooke's law,

$$\begin{aligned}\sigma_{zz}(r,z) &= (\lambda+2\mu)\frac{\partial w}{\partial z}+\lambda\frac{\partial u}{\partial r}\\ &= \mu\int_0^\infty \Big[(2k^2-k_m^2)[A^-e^{-\alpha z}+A^+e^{\alpha z}]\\ &\qquad -2k\beta[B^-e^{-\beta z}-B^+e^{\beta z}]\Big]J_0(kr)k\,\mathrm{d}k, \end{aligned} \tag{61}$$

$$\begin{aligned}\sigma_{rz}(r,z) &= \mu\left(\frac{\partial u}{\partial z}+\frac{\partial w}{\partial r}\right)\\ &= \mu\int_0^\infty \Big[2k\alpha[A^-e^{-\alpha z}-A^+e^{\alpha z}]\\ &\qquad -(2k^2-k_m^2)[B^-e^{-\beta z}+B^+e^{\beta z}]\Big]J_1(kr)k\,\mathrm{d}k. \end{aligned} \tag{62}$$

In a solid medium, integral representations for several types of sources can be derived, including point forces and force couples. A number of examples are given by Harkrider [31]. In the SAFARI code, two source types are available for solid media. One is a compressional point source equivalent to the one used in fluid media. The compressional point source involves the compressional potential Φ only, with the integral representation

$$\widehat{\Phi}(r,z)=\frac{S_\omega}{4\pi}\int_0^\infty \frac{e^{-\alpha|z-z_s|}}{\alpha}J_0(kr)k\,\mathrm{d}k. \tag{63}$$

The corresponding displacement and stresses again follow from Eqs. (51),(52) and Hooke's law:

$$\widehat{u}(r,z)=-\frac{S_\omega}{4\pi}\int_0^\infty \frac{ke^{-\alpha|z-z_s|}}{\alpha}J_1(kr)k\,\mathrm{d}k, \tag{64}$$

$$\widehat{w}(r,z)=-\frac{S_\omega}{4\pi}\int_0^\infty \mathrm{sign}(z-z_s)e^{-\alpha|z-z_s|}J_0(kr)k\,\mathrm{d}k, \tag{65}$$

$$\widehat{\sigma}_{zz}(r,z)=\frac{S_\omega\mu}{4\pi}\int_0^\infty (2k^2-k_m^2)\frac{e^{-\alpha|z-z_s|}}{\alpha}J_0(kr)k\,\mathrm{d}k, \tag{66}$$

$$\widehat{\sigma}_{rz}(r,z)=\frac{S_\omega\mu}{4\pi}\int_0^\infty 2k\,\mathrm{sign}(z-z_s)e^{-\alpha|z-z_s|}J_1(kr)k\,\mathrm{d}k. \tag{67}$$

The second implemented source type is a vertical point force, with the following integral representations for the potentials [8]:

$$\widehat{\Phi}(r,z)=\frac{S_\omega}{4\pi}\int_0^\infty \mathrm{sign}(z-z_s)e^{-\alpha|z-z_s|}J_0(kr)k\,\mathrm{d}k, \tag{68}$$

$$\widehat{\Phi}(r,z) = \frac{S_\omega}{4\pi}\int_0^\infty \frac{e^{-\beta|z-z_s|}}{\beta} J_0(kr)k\,\mathrm{d}k. \tag{69}$$

Integral representations for the displacements and stresses are again obtained from Eqs. (51),(52) and Hooke's law:

$$\widehat{u}(r,z) = -\frac{S_\omega}{4\pi}\int_0^\infty \mathrm{sign}(z-z_s)k\left[e^{-\alpha|z-z_s|} - e^{-\beta|z-z_s|}\right] J_1(kr)k\,\mathrm{d}k, \tag{70}$$

$$\widehat{w}(r,z) = -\frac{S_\omega}{4\pi}\int_0^\infty \left[\alpha e^{-\alpha|z-z_s|} - k^2\beta^{-1}e^{-\beta|z-z_s|}\right] J_0(kr)k\,\mathrm{d}k, \tag{71}$$

$$\widehat{\sigma}_{zz}(r,z) = \frac{S_\omega\mu}{4\pi}\int_0^\infty \mathrm{sign}(z-z_s) \times \left[(2k^2-k_m^2)e^{-\alpha|z-z_s|} - 2k^2e^{-\beta|z-z_s|}\right] J_0(kr)k\,\mathrm{d}k, \tag{72}$$

$$\widehat{\sigma}_{rz}(r,z) = \frac{S_\omega\mu}{4\pi}\int_0^\infty \left[2k\alpha e^{-\alpha|z-z_s|} - (k^3\beta^{-1}+k\beta)e^{-\beta|z-z_s|}\right] J_1(kr)k\,\mathrm{d}k. \tag{73}$$

3.5. BOUNDARY CONDITIONS

The field at each interface now has two distinct integral representations, one from the layer above and one from the layer below. Depending on the type of interface, a certain set of boundary conditions has to be satisfied.

- If the interface is separating two fluid layers, the vertical displacement w and the normal stress σ_{zz} have to be continuous. If one of the media is a vacuum, the normal stress σ_{zz} must vanish.
- If one of the layers is solid and the other is a vacuum, both σ_{zz} and σ_{rz} must vanish, whereas the fluid/solid interface requires that w and σ_{zz} must be continuous and σ_{rz} must vanish.
- At a welded interface between two solid media, w, u, σ_{zz} and σ_{rz} all have to be continuous.

The boundary conditions for the different types of interfaces are summarised in Table 1.

Since the boundary conditions have to be satisfied at all ranges r, it is obvious that they must be satisfied by the kernels in the integral representations as well. The radiation conditions for $z \to \pm\infty$ together with the conditions to be satisfied at all interfaces simultaneously, lead to a linear system of equations in the unknown kernel coefficients A^-, A^+, B^- and B^+. In principle, this system has to be solved for all

Table 1
Boundary conditions*

Type	Field parameter			
	w	u	σ_{zz}	σ_{rz}
fluid/vacuum	-	-	0	-
fluid/fluid	=	-	=	-
fluid/solid	=	-	=	0
solid/vacuum	-	-	0	0
solid/solid	=	=	=	=

* Symbols used: =, continuous; 0, vanishing; -, not involved.

values of the horizontal wavenumber k, and the total field can then be determined by evaluating the inverse transforms. Except for a few trivial cases, however, both the solution of the linear system of equations and the evaluation of the inverse transforms have to be done numerically, requiring truncation and discretisation of the horizontal wavenumber axis.

3.6. ATTENUATION

It is well known that sound propagating in the ocean bottom undergoes a significant attenuation due to the dissipation of seismo-acoustic energy into heat. It is therefore crucial to a realistic prediction of the propagation characteristics that volume attenuation be taken into account. In the present full wavefield solution technique this is straightforwardly done as shown below.

Assume a plane harmonic wave of angular frequency ω propagating in a homogeneous medium along the positive x-axis of a cartesian coordinate system. With the present choice of time-frequency transform pair, Eqs. (7),(8), such a wave has the form

$$F(x,t) = Ae^{i(\omega t - k_m x)}, \tag{74}$$

where k_m is the medium wavenumber for either compressional or shear waves and A is the amplitude. If k_m is real, this wave has constant amplitude for all ranges x. It can be shown [32], however, that viscoelastic attenuation can be accounted for by letting the medium wavenumber k_m be complex, i.e.

$$\tilde{k}_m = k_m(1 - i\delta), \qquad \delta > 0. \tag{75}$$

. the wavefield becomes

$$F(x,t) = Ae^{-\delta k_m x} e^{i(\omega t - k_m x)}. \tag{76}$$

Now the amplitude is decaying exponentially in range as is required for linear viscoelastic fluid and solid media. Since the full wavefield solution technique is based on plane-wave decomposition as described above, it is obvious that a viscoelastic attenuation is taken into account by letting the medium wavenumbers and therefore also the Lamé constants be complex:

$$\tilde{\lambda} = \lambda + i\lambda', \tag{77}$$

$$\tilde{\mu} = \mu + i\mu'. \tag{78}$$

It has been experimentally observed [8,32], that most solid media exhibit an attenuation that increases linearly with frequency, i.e. δ = const. For these solids,

$$\frac{\lambda' + 2\mu'}{\lambda + 2\mu} = \frac{1}{Q_c}, \tag{79}$$

$$\frac{\mu'}{\mu} = \frac{1}{Q_s}, \tag{80}$$

where Q_c and Q_s are constants. By inserting the complex Lamé constants in Eqs. (1) and (2), we get from Eqs. (10) and (75) the following value of δ for compressional and shear waves respectively, assuming $Q_c, Q_s \gg 1$:

$$\delta_c = \frac{1}{2Q_c}, \tag{81}$$

$$\delta_s = \frac{1}{2Q_s}. \tag{82}$$

In underwater acoustics it is more common to express the linear frequency-dependent attenuation in dB/Λ (where Λ is the wavelength):

$$\gamma = -20\log\left|\frac{F(x+\Lambda,t)}{F(x,t)}\right| = -20\log\left[e^{-\delta k_m \Lambda}\right] = 40\pi\delta\log e \simeq \frac{27.29}{Q}. \tag{83}$$

Although the solution technique is valid for any value of the attenuations, these must be physically meaningful. Thus it is required that a pure dilatation of a solid medium does not produce energy. Therefore the bulk modulus, $K = \lambda + \frac{2}{3}\mu$, must have a positive imaginary part, which is easily shown to require

$$\frac{\gamma_s}{\gamma_c} = \frac{\delta_s}{\delta_c} < \frac{3}{4}\left(\frac{c_c}{c_s}\right)^2. \tag{84}$$

The linear-elastic fluid media are merely limiting cases of solids with $\mu \to 0$, and the attenuation is therefore introduced accordingly.

In addition to the volume attenuation described above, scattering at rough interfaces also attenuates the stress waves in stratified environments. Since the depth-separation solution technique requires all interfaces to be plane and parallel, a deterministic treatment of rough surface scattering is not possible by means of the present method. Such a deterministic treatment is, however, only of academic interest, since the roughness appearing in nature is either rapidly changing (as in the case of ocean surface waves) or is not sufficiently well described to permit direct modelling. The statistical roughness characteristics, on the contrary, are relatively slowly varying and can be more easily determined even for the ocean bottom.

If the roughness is small compared to the acoustic wavelength involved and the roughness characteristics are stationary in both space and time, it is possible by means of a perturbational approach to modify the boundary conditions in such a way that the effect of the roughness on the coherent (mean) part of the field can be taken into account by the present solution technique. Such a technique, originally developed for fluid media only, has been generalised to interfaces between solid media and implemented in the SAFARI code [25]. The actual perturbation theory is not of importance to the general use of the code, and therefore only the underlying assumptions concerning the roughness characteristics will be given here. For details reference is made to [25].

The interface elevation at a point with the horizontal coordinates given by the vector $\mathbf{r}$ is $\gamma(\mathbf{r})$. This function is only determined in terms of its correlation function $N(\mathbf{R})$, defined by

$$N(\mathbf{R}) = \langle \gamma(\mathbf{r}_1)\gamma(\mathbf{r}_2)\rangle, \qquad \mathbf{R} = \mathbf{r}_1 - \mathbf{r}_2 \tag{85}$$

or in terms of the two-dimensional Fourier transform of the interface-roughness power spectrum $P(\mathbf{s})$,

$$N(\mathbf{R}) = \langle \gamma^2 \rangle \frac{1}{2\pi} \int \mathrm{d}^2\mathbf{s}\, P(\mathbf{s})\, e^{-i\mathbf{s}\cdot\mathbf{R}}, \tag{86}$$

where $\langle \gamma^2 \rangle$ is the rms value of the roughness. In SAFARI only isotropic roughness can be treated, i.e. the interface correlation depends only on the horizontal distance $|R|$ between two points, not the direction. Further, the spectrum – of course also isotropic – is assumed to be gaussian:

$$P(\mathbf{s}) = L^2 e^{-\frac{1}{2}L^2|\mathbf{s}|^2}, \tag{87}$$

where L is a characteristic correlation length for the interface roughness. The interface roughness statistics are therefore described entirely by the rms roughness $\langle \gamma^2 \rangle$ and the correlation length L. These parameters may, of course, vary from interface to interface. For the perturbation expansion to be valid, it is required that $\gamma/L < 1$.

4. Numerical solution technique

The numerical solution of the full wavefield problem divides naturally into three parts. First the depth-dependent Green's function is found at a discrete number of horizontal wavenumbers for the selected receiver depths. Secondly, the wavenumber integral, Eq. (13), is evaluated, yielding the transfer function at the selected depths and ranges. Finally, upon repetition of the first two steps at selected frequencies, the frequency integration, Eq. (8), is performed to yield the total response in time.

It is clear that the three steps are not independent. In particular, the frequency and wavenumber sampling cannot be chosen arbitrarily, but have to satisfy the requirements of the sampling theorem. The frequency interval depends on the bandwidth of the source and the time window must be sufficiently large to contain the whole signal in order to avoid wrap-around, which again imposes requirements on the frequency sampling. Similarly, the wavenumber sampling must be sufficiently large to allow accurate integration of the often rapidly varying and oscillating integrand in Eq. (13).

Depending on the time/frequency and range/depth requirements, the determination of the depth-dependent Green's function may have to be performed a substantial number of times. The efficiency of the code is therefore highly dependent on this part, and it is precisely here – in the global matrix approach – that the SAFARI code differs in computational approach from recursive propagator matrix techniques used in earlier codes of the same type.

The global matrix solution technique forms the basis for all three SAFARI modules. SAFARI-FIPR calculates plane-wave reflection coefficients for an arbitrarily stratified halfspace. SAFARI-FIP first calculates the depth-dependent Green's function and then evaluates the wavenumber integrals to obtain the single-frequency seismo-acoustic field at selected receiver depths and ranges. The last module, SAFARI-FIPP, performs the same operation for a number of frequencies, and after weighting with a source spectrum it determines the pulse response at any receiver by evaluating the frequency integrals. In this section we will describe in detail the numerical techniques applied in all three program modules.

4.1. DEPTH-DEPENDENT GREEN'S FUNCTION

The use of digital computers for numerically solving field problems in continuous media in general requires some kind of discretization. One possibility is to set up the exact field equations for the continuum and subsequently find an approximate solution by discretization of the equations. This is the approach taken in finite difference techniques. The other possibility is to discretize the medium itself and then in effect let the computer numerically determine an exact solution to this now approximate problem. The best-known example of this latter approach is the finite element method [2]. This technique is based on the division of the continuum into finite blocks or elements connected to each other at a finite number of discrete nodes. Exact local solutions for the single elements, together with the continuity between the elements, concentrated in the nodes, lead directly to an exact solution for the approximated global problem. This, however, requires the solution of very large linear systems of equations in the unknown degrees of freedom (typically node displacements). The unavailability of sufficient computing power until the last decade delayed the widespread use of this powerful technique, which today is the most widely employed methodology in structural and fluid mechanics, for example.

In this regard, it is easily observed [19,23] that the integral transform solution of the wave equation for horizontally stratified environments is of the 'finite element' category. The local expressions for the depth-dependent Green's function are exact within each layer (*element*), and thus an exact global solution can be obtained directly from the boundary conditions to be satisfied at all interfaces (*nodes*). It is therefore not surprising that the numerical implementation can be performed in close analogy with the finite element method using efficient numerical tools created within the last decades.

In order to develop this analogy formally, the basic properties of the finite element method will be briefly outlined at this point. For details reference is made to the pertinent literature [2].

The simple static element in Fig. 3a is chosen as a representative example. It has four degrees of freedom, here the four independent node displacements $\{u\}_m = \{u_1, u_2, u_3, u_4\}$. The corresponding node forces $\{p\}_m = \{p_1, p_2, p_3, p_4\}$ are then given by

$$\{p\}_m = [k]_m \{u\}_m, \qquad m = 1, 2 \ldots N, \tag{88}$$

where $[k]_m$ is the local element stiffness matrix and the subscript refers to the actual element number. N is the total number of elements. As the nodes are in general common to more elements, it is here convenient to introduce a global degree-of-freedom vector $\{U\}$ defined by

$$\{u\}_m = [L]_m \{U\}, \qquad m = 1, 2 \ldots N, \tag{89}$$

where $[L]_m$, a topology or connectivity matrix for element m, is an extremely sparse matrix with only four non-vanishing elements equal to unity. The mapping de-

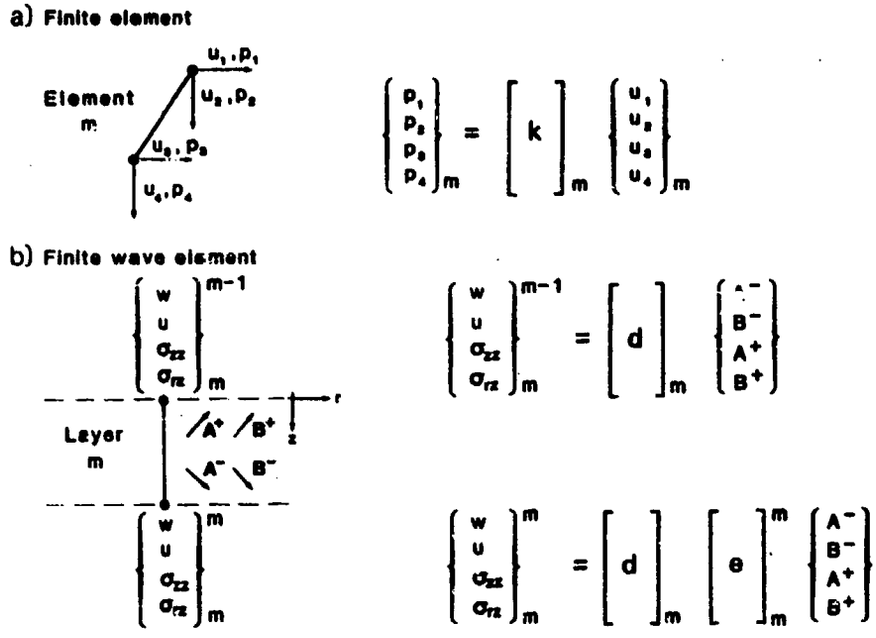

Fig. 3. Analogy to finite element method: (a) finite element with four degrees of freedom; (b) finite wave element with four degrees of freedom.

fined by Eq. (89) directly reflects the connectivity conditions governing the globally assembled element system in question.

At this point a variational principle, often Hamilton's principle of stationary energy, together with Eqs. (88),(89) leads to the following linear system of equations having to be satisfied:

$$[K]\{U\} = \{R\}, \tag{90}$$

where $[K]$ is the global stiffness matrix

$$[K] = \sum_{m=1}^{N} [L]_m^T [k]_m [L]_m, \tag{91}$$

and $\{R\}$ is the global external force vector

$$\{R\} = \sum_{m=1}^{N} [L]_m^T \{r\}_m. \tag{92}$$

The local vector $\{r\}_m$ represents the external forces acting on element number m, again concentrated in the nodes.

It is not necessary here to go into details concerning the actual implementation of the finite element equations, but it is important to note the structure of the global system of equations, Eq. (90). Since the topology matrices contain only zeros and ones, the matrix multiplications in Eqs. (90) and (91) never need to be performed, but can be replaced by a set of indices (pointers) indicating the row and column of the global stiffness matrix where each element of the local ones have to be added. The actual generation of the global stiffness matrix can therefore be performed very efficiently once the local ones have been determined.

Returning to the determination of the depth-dependent Green's function in stratified media, the fact that the horizontal range dependence has been removed by the depth-separation yields the possibility of effectively representing each layer as a one dimensional 'finite wave element', as shown in Fig. 3b, in formal analogy to the standard finite element discussed above. The degrees of freedom for this element are simply the amplitudes A_m^-, A_m^+, B_m^- and B_m^+ of the cortical waves in layer number m. These are conveniently collected in a local degree-of-freedom vector $\{a(k)\}_m$, where k is the horizontal wavenumber:

$$\{a(k)\}_m = \begin{Bmatrix} A_m^-(k) \\ B_m^-(k) \\ A_m^+(k) \\ B_m^+(k) \end{Bmatrix}, \qquad m = 1, 2 \ldots N. \tag{93}$$

If the kernels for the field parameters involved in the boundary conditions are expressed in vector form as

$$\{v(k,z)\}_m = \begin{Bmatrix} w(k,z) \\ u(k,z) \\ \sigma_{zz}(k,z) \\ \sigma_{rz}(k,z) \end{Bmatrix}_m, \qquad m = 1, 2 \ldots N, \tag{94}$$

the following matrix relation is obtained for the homogeneous part of the solution in layer number m

$$\{v(k,z)\}_m = [c(k,z)]_m \{a(k)\}_m, \qquad m = 1, 2 \ldots N. \tag{95}$$

The local coefficient matrix $[c(k,z)]_m$ is a function of the horizontal wavenumber k and the depth z. For the homogeneous layers the depth is involved in the exponential functions only, and in these cases the coefficient matrix can be factorized as

$$[c(k,z)]_m = [d(k)]_m [e(k,z)]_m, \tag{96}$$

where $[d(k)]_m$ is a depth-independent matrix containing only simple functions of k, and $[e(k,z]_m$ is a diagonal matrix containing the exponentials.

The kernels for the source field $\{\hat{v}(k,z)\}_m$ are now superimposed with the kernels for the homogeneous solution, and the continuity of the field parameters at interface number m separating the layers m and $m+1$ can then be expressed as

$$\{v(k)\}_m^m + \{\hat{v}(k)\}_m^m = \{v(k)\}_{m+1}^m + \{\hat{v}(k)\}_{m+1}^m, \qquad m = 1,2\ldots N-1, \tag{97}$$

where the depth z of the interface has been removed and replaced by a superscript indicating the interface number. If Eq. (97) is rewritten as

$$\{v(k)\}_m^m - \{v(k)\}_{m+1}^m = \{\hat{v}(k)\}_{m+1}^m - \{\hat{v}(k)\}_m^m, \qquad m = 1,2\ldots N-1, \tag{98}$$

it expresses the cancellation of the discontinuity in the source field by the discontinuity in the homogeneous solution. The interface discontinuity vector $\{v(k)\}^m$ is therefore introduced as

$$\{v(k)\}^m = \{v(k)\}_m^m - \{v(k)\}_{m+1}^m, \qquad m = 1,2\ldots N-1, \tag{99}$$

and similarly for the source field discontinuity vector $\{\hat{v}(k)\}^m$.

In order to assemble the local equations, Eq. (98), into a global system, the global degree-of-freedom vector $\{A(k)\}$ in the upgoing and downgoing wavefield amplitudes is first introduced, defined by the unique local-to-global mapping

$$\{a(k)\}_m = [S]_m\{A(k)\}, \qquad m = 1,2\ldots N. \tag{100}$$

After insertion of Eqs. (95) and (100), the discontinuity vector, Eq. (99), takes the form

$$\{v(k)\}^m = \left([c(k)]_m^m[S]_m - [c(k)]_{m+}^m[S]_{m+1}\right)\{A(k)\}, \qquad m = 1,2\ldots N-1. \tag{101}$$

We now introduce a second unique mapping, collecting the local field discontinuity vectors $\{v(k)\}^m$ into one global discontinuity vector $\{V(k)\}$,

$$\{V(k)\} = \sum_{m=1}^{N-1}[T]^m\{v(k)\}^m, \tag{102}$$

which after insertion of Eq. (101) becomes

$$\{V(k)\} = \sum_{m=1}^{N-1}[T]^m\left([c(k)]_m^m[S]_m - [c(k)]_{m+}^m[S]_{m+1}\right)\{A(k)\}. \tag{103}$$

Similarly the global source-field discontinuity vector $\{\hat{V}(k)\}$ is

$$\{\hat{V}(k)\} = \sum_{m=1}^{N-1}[T]^m\left(\{\hat{v}(k)\}_m^m - \{\hat{v}(k)\}_{m+1}^m\right). \tag{104}$$

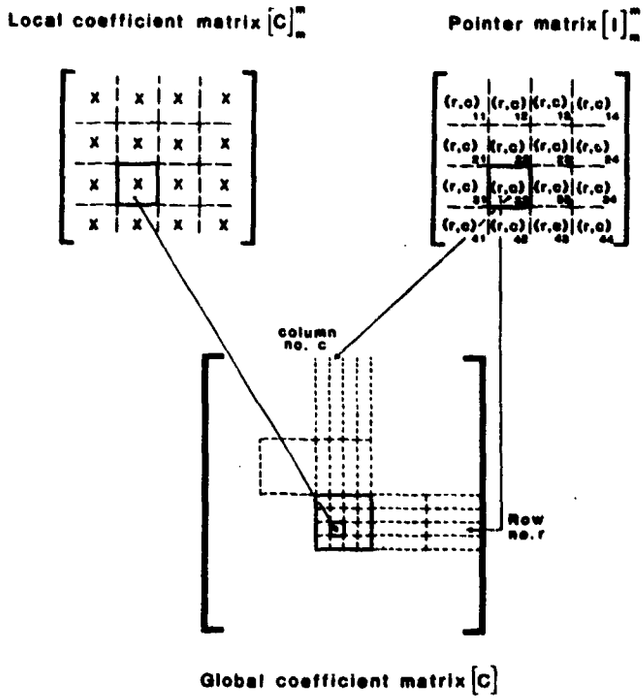

Fig. 4. Mapping between local and global coefficient matrices by means of row and column pointers.

The global cancellation of Eq. (103) by Eq. (104) therefore requires the following linear system of equations to be satisfied:

$$[C(k)]\{A(k)\} = -\{\hat{V}(k)\}, \tag{105}$$

where $[C(k)]$ is the global coefficient matrix

$$[C(k)] = \sum_{m=1}^{N-1} [T]^m \left([c(k)]^m_m [S]_m - [c(k)]^m_{m+} [S]_{m+1} \right) . \tag{106}$$

As can be observed, the global system, Eq. (105), is very similar to the finite element system, Eq. (90). The mapping matrices $[T]^m$ and $[S]_m$ are equivalent to the topology matrices $[L]_m$ defined for the finite element method in Eq. (89). However, due to the fact that the governing boundary conditions for the wave equation are not set up in the unknowns directly, but in derived quantities, two sets of topology matrices are needed here: one for the local-to-global mapping of the degrees of freedom, i.e. the wavefield amplitudes, and one for the physical parameters, i.e. displacement and stresses involved in the boundary conditions.

The matrices $[S]_m$ and $[T]^m$ are extremely sparse, containing only zeros and ones. Since the mappings of Eqs. (100) and (102) are unique, the corresponding summations and matrix multiplications in Eqs. (104) and (106) need never actually be performed but can be replaced by a unique set of pointers, connecting the elements of the local systems with those of the global system, as illustrated in Fig. 4. As is the case in finite element programs, the topology matrices are therefore never set up in the actual computer code. Their formal use in Eqs. (104) and (106) is, however, very convenient in the general fluid/solid/vacuum case. The topology matrix $[S]_m$ is set up to include only the non-vanishing wavefield amplitudes, e.g. in the upper and lower halfspaces only those corresponding to upgoing (A^+, B^+) and downgoing (A^-, B^-) waves respectively, and in fluid media only A^- and A^+. Similarly, $[T]^m$ is set up to include only the actual number of boundary conditions at interface m, as described in Sect. 3.5. This ensures that the global coefficient matrix is a square matrix and also reduces the total number of equations and unknowns compared to the purely solid case.

The pointer indices defined by the mappings of Eqs. (100) and (102) depend solely on the number of unknowns within each layer and the boundary conditions at each interface. They are therefore both frequency and wavenumber independent and can be determined *a priori*.

In this notation, the set-up of the global coefficient matrix requires only the calculation of the elements of the local coefficient matrices $[c(k)]_m$, followed by the indexed move defined by the mappings given in Fig. 4. The subsequent solution of Eq. (105) then yields the unknown wavefield amplitudes in all layers simultaneously.

Although the global system of equations, Eq. (105), is analytically well conditioned, apart from poles corresponding to normal modes and interface waves, its numerical solution is not necessarily stable. However, by choosing the mappings such that the coefficient matrix becomes block-diagonally dominant it is possible to ensure unconditionally stable solutions using gaussian elimination with partial pivoting. This important feature will be discussed in the following.

The difference in absolute dimension between the displacements and stresses can yield a difference of several orders of magnitude between the coefficients in the corresponding rows for both the local and global systems. As is well known in such cases, simple gaussian elimination, with or without partial pivoting, will not guarantee unconditional numerical stability. In the SAFARI implementation, the coefficient matrices are therefore scaled to make all elements physically dimensionless.

Although from a theoretical point of view the origin of the depth axis can be chosen arbitrarily, its choice is quite critical for the numerical stability. The Airy function solutions for the inhomogeneous fluid layers are invariant to the choice of origin, but this is obviously not the case for the isovelocity layers. First of all, a common origin for all layers is inconvenient due to the limited allowed arguments to the

exponential functions. A local origin is therefore used for each layer, but this still does not ensure numerical stability for large layer thicknesses and large horizontal wavenumbers where the real parts of arguments to the exponential functions become significant (the evanescent regime). In these cases argument overflow may of course appear, but even before this happens numerical instability may appear due to the fact that the difference between the growing and decaying exponentials exceeds the machine precision. This problem can be avoided by factorising out the exponential functions growing in depth [33], but unconditional stability can also be obtained by very simple means *not requiring any additional computational effort*, just by observing the physical significance of the problem and adopting a numerical 'trick' from the finite element technique. This is the key to the efficiency of the SAFARI code and will therefore be discussed at this point.

The physical significance of the evanescent regime for a certain layer is that the wavefield in the absence of a source is a superposition of two exponentially decaying fields, one arising from a non-vanishing field at the interface above, the other from the interface below. Now assume that sources are only present above the actual layer. Then the field decaying away from the lower interface ($e^{\alpha z}$) can only be due to 'reflection' from this interface of the field decaying away from the upper interface ($e^{-\alpha z}$). If, however, the layer is very thick or the horizontal wavenumber is large, the amplitude at the lower interface of the downwards decaying field is insignificant, and the upwards decaying field will be practically non-existent. In other words, the layer containing the evanescent field will behave exactly like an infinite halfspace.

It is obvious that numerical stability can be obtained in these cases if the environmental model is truncated by replacing the thick layer by an infinite halfspace. This would, however, introduce significant book-keeping problems and rearrangements of the global system of equations, seriously affecting the computation time.

Instead it is possible to take advantage of the knowledge about the vanishing upwards decaying wavefield in another way, simply adopting a numerical trick from implementations of the finite element technique. If a certain node displacement is known to vanish it is not removed from the degrees of freedom; instead the corresponding diagonal element in the global stiffness matrix is set to a very large number. This automatically ensures that the node displacement obtained by the solution will vanish numerically.

In the present case we know that the amplitude of the upward-decaying field must vanish. This could be accomplished by placing a large number in the corresponding diagonal element in the global coefficient matrix. Again, however, complicated book-keeping is involved. The same result can be obtained almost free of charge in the following way. First the interface above the layer is selected as the local origin for the depth axis. This removes the exponential functions from the local coefficient matrix at this interface. Then the argument to the exponential function is truncated at a value close to the maximum allowed for the actual computer.

This avoids overflow problems and at the same time yields very large numbers in the columns of the global coefficient matrix corresponding to the upward-decaying fields. It can now be shown [20,21], that gaussian elimination with pivoting by columns will automatically force the corresponding amplitudes to vanish numerically if the mappings of Eq. (100) and (102) are chosen such that the global coefficient matrix becomes block-diagonally dominant. In essence this is obtained by assembling the local systems in consecutive order and placing the coefficients involving the large exponential functions close to the diagonal of the global matrix. When the amplitude of the upward-decaying field is thus forced to vanish, the solution obtained for all wavefield amplitudes in the other layers is indistinguishable from the one obtained if the thick layer had been replaced by a halfspace.

Similar arguments can be used to show that also in the case of sources below or within the thick layer the SAFARI technique is unconditionally numerically stable. Concerning the inhomogeneous fluid layers, the two independent solutions $Ai(\zeta)$ and $Bi(\zeta)$ exponentially decay and grow respectively for $\zeta \rightarrow \infty$. The stability in cases where these are involved is therefore ensured in exactly the same way as described above.

In summary, unconditionally stable solutions are obtained simply by choosing a proper local coordinate system and a proper local-to-global mapping in connection with gaussian elimination with partial pivoting. The solution technique is stable for any machine precision. Double precision is therefore not required for stability purpose, but the dynamic range is of course limited to the number of mantissa digits available, due to the global nature of the solution. For most purposes, however, the 6–7 orders of magnitude offered by single precision is more than enough.

When the global system of equations, Eq. (105), has been solved, the kernels in the integral representations can readily be evaluated at any depth. The present technique is therefore highly efficient in cases where the total wavefield is to be determined at many depths, e.g. for depth-range contouring of single frequency transmission loss and for synthetic vertical seismic profiling (VSP).

4.2. REFLECTION COEFFICIENTS

The determination of plane-wave reflection coefficients of a stratified halfspace is of great interest in both underwater acoustics and seismology for several reasons. It is required as input to the widespread ray-tracing codes and it forms the basis of the synthetic reflectivity seismograms commonly used in crustal seismology [23]. Further, the plane-wave reflection coefficients are often used for ocean bottom-property inversion schemes.

The full wavefield solution technique is based on a decomposition of the total wavefield in conical waves for cylindrical geometry and plane waves for plane cartesian geometry. We have here given the field representations in cylindrical geometry, but the similar plane-geometry representations are obtained simply by replacing the Hankel transform with the Fourier transform; the kernels are identical in the two cases [21]. The relation between the horizontal wavenumber k and the grazing angle θ of propagation for an isovelocity layer is

$$k = k_m \cos\theta, \tag{107}$$

where the medium wavenumber k_m may correspond to either compressional or shear waves. As can be observed, only wavenumbers $k \leq k_m$ correspond to real angles.

We shall now demonstrate that the plane-wave reflection coefficient $R(\theta)$ for a wave incident from above at angle θ on a certain interface is straightforwardly found by the present solution technique. The layer above the interface is replaced by an infinite halfspace. By letting the source field be a plane wave incident at angle θ and with amplitude $A^-(k) = A^-(k_m \cos\theta)$ at the interface, the solution of the global system of equations for this new layered problem will directly yield the complex amplitude of the reflected plane wave $A^+(k) = A^+(k_m \cos\theta)$, and the reflection coefficient can be determined by

$$R(\theta) = \frac{A^+(k_m \cos\theta)}{A^-(k_m \cos\theta)}. \tag{108}$$

Both the incident and reflected waves may of course in general be either compressional or shear waves. As the global solution is exact to within machine accuracy, the same is the case for the reflection coefficients, i.e. no approximation except for the environmental model is involved.

The SAFARI-FIPR module computes the plane-wave reflection coefficients for incident compressional waves only, since a standard SAFARI compressional line source – placed just above the interface – is used to produce the incident plane wave; however the calculated reflection coefficient may be either for reflected compressional waves or for reflected shear waves.

It should be pointed out that the reflection coefficients calculated in this way are for *true plane waves*. Plane-wave reflection coefficients are difficult to determine

experimentally [22], which should be kept in mind when comparing synthetic and experimental reflection data.

4.3. WAVENUMBER INTEGRATION

The horizontal wavenumbers at which the depth-dependent Green's functions have to be determined are controlled by the numerical integration scheme used for evaluating the integral representations for the displacements and stresses. Those Hankel transform integrals are of the form

$$G(r,z) = \int_0^\infty g(k,z) J_m(kr) k \, dk, \tag{109}$$

where $m = 0$ except for the horizontal displacement and shear stress where $m = 1$.

To evaluate these integrals numerically, a truncation of the infinite integration interval is required. Due to the exponentially decaying kernels for $k \to \infty$ this can be done to any degree of accuracy. In most cases a truncation point 10 to 20% higher than the maximum medium wavenumber in the problem will include everything. There are, however, exceptions when solid layers are present. In these cases poles may exist due to evanescent surface, interface or plate modes. Especially in the case of thin plates, very large wavenumbers are involved. It is therefore important to be aware of the behaviour and significance of these waves in order to choose a proper integration interval.

Even with a proper truncation there are two factors complicating the numerical evaluation of the Hankel transforms. One is the kernel, which in the case of guided propagation in lossless media is known to have poles on the real axis corresponding to normal modes and interface waves [6]. In the more realistic cases where volume attenuation is included, these poles will move out into the complex plane, in principle making real axis integration possible, but the kernel will in most cases remain rapidly varying. The second complicating factor is the Bessel function $J_m(kr)$, which especially for long ranges r oscillates very rapidly in k. Therefore an accurate evaluation of the Hankel transform will usually require a very fine sampling in the wavenumber k.

There are algorithms available for directly evaluating the Hankel transform. The one developed by Tsang [34], however, requires the evaluation of an FFT for every range selected, but even more importantly it requires a numerical separation parameter which is not easily selected. The so-called Fast Hankel Transform [35] is very efficient for relatively smooth kernels, but not well suited for the rapidly varying kernels of the waveguide problems.

Nevertheless it has been shown [15] that except for ranges shorter than a few wavelengths and very steep propagation angles, accurate evaluation can be obtained by

an asymptotic approximation. First the Bessel function is expressed in terms of two Hankel functions

$$J_m(kr) = \tfrac{1}{2}\left(H_m^{(1)}(kr) + H_m^{(2)}(kr)\right). \tag{110}$$

With the present choice of time/frequency transform the term $H_m^{(1)}(kr)$ corresponds to incoming waves which are only important for representing the standing wavefield at very short ranges. This term is therefore neglected, and $H_m^{(2)}(kr)$ is replaced by its asymptotic approximation

$$\lim_{kr\to\infty} H_m^{(2)}(kr) = \sqrt{\frac{2}{\pi kr}}\, e^{-i\left(kr-(m+\frac{1}{2})\frac{1}{2}\pi\right)}. \tag{111}$$

The inverse Hankel transform then takes the form

$$G(r,z) = \sqrt{\frac{1}{2\pi r}}\, e^{i(m+\frac{1}{2})\frac{1}{2}\pi} \int_0^\infty g(k,z)\sqrt{k}\, e^{-irk}\, \mathrm{d}k. \tag{112}$$

Due to the desire for generality, which excludes the use of dedicated quadrature schemes, the truncated wavenumber space is discretised equidistantly in SAFARI as follows:

$$k_l = k_{\min} + l\Delta k, \qquad l = 0, 1 \ldots (M-1), \tag{113}$$

where M is the total number of sampling points.

The value of the field is often required at a large number of ranges r, in particular in connection with the common underwater acoustics problem of determining transmission loss as function of range. In these cases the Fourier integral in Eq. (112) is very efficiently evaluated by means of the so-called 'Fast Field' approach [15]. This technique is therefore applied in the single-frequency transmission-loss program SAFARI-FIP. The range axis r is discretised as

$$r_j = r_{\min} + j\Delta r, \qquad j = 0, 1 \ldots (M-1), \tag{114}$$

where the range step Δr is determined by the relation

$$\Delta r \Delta k = 2\pi/M, \tag{115}$$

and M is an integral power of 2. The following discrete approximation of Eq. (112) is then obtained:

$$G(r_j,z) \approx \frac{\Delta k}{\sqrt{2\pi r_j}}\, e^{-i\left(k_{\min} r_j - (m+\frac{1}{2})\frac{1}{2}\pi\right)} \sum_{l=0}^{M-1} \left[g(k_l,z)\, e^{-ir_{\min} l\Delta k}\sqrt{k_l}\right] e^{-i(2\pi lj/M)}, \tag{116}$$

where the summation can be performed by means of an FFT yielding the field at all M ranges, Eq. (114), simultaneously.

It is well known from the use of the FFT for time/frequency transformations that undersampling in one domain causes aliasing (wrap-around) in the other domain. This is also the case here, where the kernel is often rapidly varying due to poles and branch points close to the integration axis. The reason is [36] that the evaluation of Eq. (116) does not yield $G(r,z)$ but instead $\sum_{n=-\infty}^{\infty} G(r+nR,z)$, where $R = 2\pi/\Delta k$, i.e. a sum of the signals in all range windows of width $R = M\Delta r$. As can be observed, wrap-around will happen from both sides of the actual interval and therefore also from ranges smaller than r_{min}. The negative range axis does not give any significant wrap-around due to the fact that only waves travelling in the positive range direction are included. However if $r_{min} > 0$ the signals in the interval $[0, r_{min}]$ are wrapped into the interval $[R, r_{min} + R]$. *Consequently the maximum useable range is always $R = M\Delta r$, independent of the choice of r_{min}.*

In the case of lossy media, the aliasing from ranges larger than $r_{min} + R$ can be reduced by choosing R so large that the signal is known to die out within the range window. However, we see from Eq. (115) that a long range may require a substantial number of wavenumber samples, especially when the wavenumber interval is fixed.

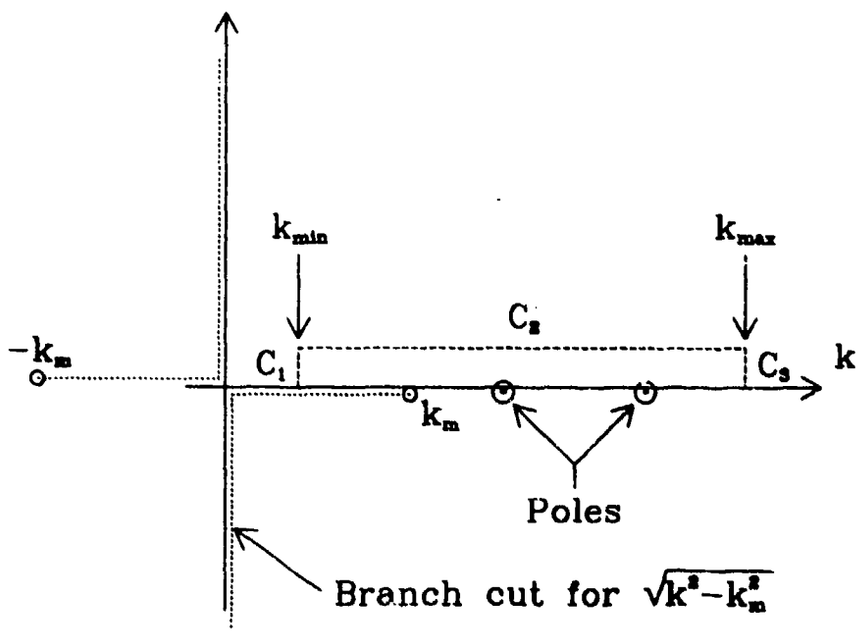

Fig. 5. Complex integration contour.

The aliasing problem can, however, be solved by moving the integration contour away from the poles, i.e. by smoothing the kernels. According to Cauchy's theorem

the integrals in the complex plane between two points is invariant to a change in the integration contour. Therefore Eq. (112) can be replaced by

$$G(r,z) = \sqrt{\frac{1}{2\pi r}} e^{i(m+\frac{1}{2})\frac{1}{2}\pi} \int_C g(k,z)\sqrt{k} e^{-irk}\, dk, \tag{117}$$

where C is the contour shown in Fig. 5. The contour consists of three linear sections C_1, C_2 and C_3, where the vertical sections of length ϵ are chosen at the points where the wavenumber axis would in any case be truncated. If these points are chosen where the kernels are small, i.e $g(k_{\min},z)\sqrt{k_{\min}}$, $g(k_{\max},z)\sqrt{k_{\max}} \approx 0$, and $\epsilon \ll k_{\max} - k_{\min}$ then the contributions from the vertical sections become insignificant compared to the integral along the horizontal section defined by $\tilde{k} = k + i\epsilon$. By inserting $\tilde{k}$ in Eq. (117), we obtain

$$G(r,z)e^{-\epsilon r} \simeq \sqrt{\frac{1}{2\pi r}} e^{i(m+\frac{1}{2})\frac{1}{2}\pi} \int_{k_{\min}}^{k_{\max}} g(k+i\epsilon,z)\sqrt{k+i\epsilon} e^{-irk}\, dk. \tag{118}$$

This integral can again be determined by means of an FFT, with the result

$$\begin{aligned}\sum_{n=-\infty}^{\infty} G(r_j,z)e^{-\epsilon(r_j+nR)} \simeq & \\ & \frac{\Delta k}{\sqrt{2\pi r_j}} e^{-i(k_{\min} r_j - (m+\frac{1}{2})\frac{1}{2}\pi)} \\ & \times \sum_{l=0}^{M-1} \left[g(k_l+i\epsilon,z) e^{-ir_{\min} l\Delta k} \sqrt{k_l+i\epsilon} \right] e^{-i(2\pi lj)/M},\end{aligned} \tag{119}$$

or, after multiplication with $e^{\epsilon r_j}$,

$$\begin{aligned}G(r_j,z) \simeq & \frac{\Delta k}{\sqrt{2\pi r_j}} e^{\epsilon r_j - i(k_{\min} r_j - (m+\frac{1}{2})\frac{1}{2}\pi)} \\ & \times \sum_{l=0}^{M-1} \left[g(k_l+i\epsilon,z) e^{-ir_{\min} l\Delta k} \sqrt{k_l+i\epsilon} \right] e^{-i(2\pi lj/M)} \\ & - \sum_{n\neq 0} G(r_j+nR,z)e^{-\epsilon nR}.\end{aligned} \tag{120}$$

It is now clear that all signals wrapped around from ranges larger than $r_{\min} + R$ will be attenuated by at least $e^{-\epsilon R}$. On the other hand signals wrapped around from ranges smaller than $r_{\min}$ will be amplified by at least $e^{\epsilon R}$. As was the case for the real axis integration the maximum range is therefore $r_{\max} = R$ also for the offset contour integration.

The actual value of ϵ is not extremely critical. However, if it is chosen too large the contributions from the two vertical parts of the contour may become significant. On the other hand a too small value will require a very large number of sampling points. For most practical purposes an attenuation of the wrap-around by 60 dB is more than enough. The corresponding value of the contour offset is

$$\epsilon = \frac{3}{R \log e} = \frac{3}{2\pi(M-1)\log e}(k_{\max} - k_{\min}) \tag{121}$$

which even for a relatively small number of sampling points M will ensure that $\epsilon \ll k_{\max} - k_{\min}$, and thus yield insignificant contributions from the vertical contours.

Whereas the Fast Field integration technique is highly efficient for single-frequency transmission-loss calculations, its use is inconvenient in the case of wideband pulse calculations. If the pulse response is required at more than a single range, the wavenumber sampling distance Δk would have to be frequency independent in order to satisfy Eq. (115). Furthermore, the pulse response will usually only be required for a relatively small number of ranges, so that direct numerical integration for each individual range is feasible. This is therefore the approach taken in the pulse program SAFARI-FIPP.

There is an optional choice of two different quadrature schemes. The first, which is the default scheme, performs a standard trapezoidal rule evaluation of the integral in Eq. (112), still with equidistant wavenumber sampling. The trapezoidal rule integration approximates the integrand by a function varying linearly between the sampling points. It is therefore obvious that this technique is only applicable out to ranges where the product of the kernel and the exponential function is well represented by a linear function. The kernel can be smoothed by moving the contour out into the complex plane as described above, but the exponential function varies rapidly at long ranges. To ensure that the exponential function alone is well represented by a linear function, the wavenumber sampling must satisfy the following inequality [36]

$$\Delta k R < \tfrac{1}{4}\pi, \tag{122}$$

which by comparison with Eq. (115) translates into a maximum range which is much shorter than the one obtained by the Fast Field technique. Here it should be pointed out, however, that the FFT technique has a degraded accuracy at longer ranges, which is insignificant on the logarithmic scale used for representation of transmission loss but which definitely is important in connection with wideband pulse calculations. For accurate pulse calculations the maximum ranges for the two techniques are almost identical and determined by Eq. (122).

It is possible, however, to obtain accurate solutions at much larger ranges by applying

the generalised Filon integration scheme [37]:

$$\int_a^b f(k)e^{Sg(k)}\,\mathrm{d}k = \begin{cases} \dfrac{\Delta k}{S\Delta g}\left[\Delta\left[fe^{Sg}\right] - \dfrac{\Delta f \Delta[e^{Sg}]}{S\Delta g}\right], & \Delta g \neq 0, \\ \dfrac{\Delta k}{2}\left[f(a)e^{Sg(a)} + f(b)e^{Sg(b)}\right], & \Delta g = 0, \end{cases} \tag{123}$$

where $\Delta f = f(b) - f(a)$ and similarly for the other functions. This quadrature scheme is exact for linear variations of $f(k)$ and $g(k)$. In the present case $S = -ir$ and $g(k) = k$, i.e. a linear function of k. The Filon scheme is therefore applicable to any range provided that the kernels are well represented by linear interpolation between the sample points. On the other hand the error due to the 'nonlinearity' of the kernel will increase with range, and the Filon scheme therefore also has a finite range of applicability. Since this range of applicability depends on the smoothness of the kernel, it is not possible to give any specific value. Mallick and Fraser [36] have found that whereas the wavenumber sampling required for the trapezoidal rule of integration is inversely proportional to ωr, the Filon scheme requires a sampling which is approximately inversely proportional to $\sqrt{\omega r}$. The additional computations involved in the Filon scheme are insignificant compared to the total calculation time involving the determination of the depth-dependence of the field. It is clear that this scheme has significant computational advantages due to the reduction in the required sampling, in particular if combined with the kernel-smoothing contour offset.

For all the numerical integration schemes described above the kernels must vary smoothly between the sampling points. One of the effects of a too rapidly varying kernel is the wrap-around, but as demonstrated, this problem can be overcome by choosing a complex integration contour, which in effect smooths the kernels by moving the contour away from the poles and branch points. If, however, the integration interval is truncated at points where the kernel amplitude is significant, the discontinuities so introduced will also give rise to wrap-around. In broadband calculations, in particular, this will cause artificial arrivals which will often be indistinguishable from true arrivals. These discontinuities therefore must be smoothed. In SAFARI-FIP and SAFARI-FIPP this is done by extrapolating the kernels by a first-order Hermite polynomial, where the coefficients are chosen such that the kernel and its first derivative become continuous at the truncation points.

In summary, it should be stressed that the evaluation of the wavenumber integrals is by far the most critical part of the full-wavefield solution technique. Whereas the depth-dependent Green's function is exact to within the computer accuracy once the environmental model has been chosen, the integration requires both truncation and discretisation of the wavenumber interval, a procedure which is not easily automated since the significance of the errors introduced is highly dependent on the characteristics of the actual problem. As described above there are remedies available for reducing the errors to insignificance, but these tools have to be selected carefully, involving a significant portion of physical knowledge and experience. The best rule of thumb that can be given for the use of this type of model is therefore:

Never be satisfied with the first result – check the convergence!

4.4. FREQUENCY INTEGRATION

The last step involved in determining the full pulse response is the evaluation of the inverse Fourier transform, Eq. (8). This integral has to be evaluated for all field parameters, ranges, and depths of interest, i.e.

$$F(r,z,t) = \int_{-\infty}^{\infty} G(r,z,\omega)e^{i\omega t}\,\mathrm{d}\omega. \tag{124}$$

Due to the fact that the frequency interval is predetermined by the source spectrum, i.e. the frequency dependence of S_ω, the frequency axis is easily truncated and the Fourier integral is therefore most conveniently evaluated by means of an FFT, i.e.

$$F(r,z,t) \simeq \Delta\omega e^{i\omega_{\min} t_j} \sum_{l=0}^{N-1} \left[G(r,z,\omega_l)e^{it_{\min} l\Delta\omega}\right] e^{i(2\pi lj/N)}, \tag{125}$$

where the frequency and time axes have been discretized as follows,

$$t_j = t_{\min} + j\Delta t, \qquad lj = 0,1\ldots(N-1), \tag{126}$$

$$\omega_l = \omega_{\min} + l\Delta\omega, \qquad l = 0,1\ldots(N-1), \tag{127}$$

and the samplings satisfy the relation

$$\Delta t\Delta\omega = 2\pi/N. \tag{128}$$

Due to the symmetry relation $G(r,z,-\omega) = \overline{G(r,z,\omega)}$ it is clear that the time function $F(r,z,t)$ determined by Eq. (124) is real. In order for the discrete form, Eq. (125), to yield a real time series it is required that the frequency discretization, Eq. (127), be symmetric around $\omega = 0$. There are algorithms available, the so-called real FFT's (RFFT), which take advantage of the symmetry relation of the kernel and therefore only require input of $G(r,z,\omega)$ at the $N/2$ discrete frequencies

$$\omega_l = l\Delta\omega, \qquad l = 0,1\ldots N/2-1, \tag{129}$$

and still yield the time series at all N times, Eq. (126). Due to the computational savings, the RFFT is always used to evaluate the time series in SAFARI-FIPP.

The discretisation of the frequency axis again introduces wrap-around due to the limited time window T, which is related to the angular frequency sampling $\Delta\omega$ by

$$T = N\Delta t = 2\pi/\Delta\omega. \tag{130}$$

As was the case for the wavenumber integration, the wrap-around can be eliminated – or at least reduced – in two ways. One way is to smooth the kernel $G(r, z, \omega)$ by moving the integration contour, which is the technique called complex frequency integration [36]. The other way is to choose T so large that the whole signal is included in the time window. Although the first approach definitely has computational advantages, the latter is the one chosen in SAFARI-FIPP. This is due to the transient nature of wideband signals which makes it much easier to perform a truncation of the time window than of the range window. No signal can arrive to a receiver at a higher speed than the fastest wave speed in the problem. This therefore determines the beginning of the time window for which no wrap-around will happen from earlier times. The length T of the time window is more difficult to determine, but with some experience in conjunction with convergence tests it becomes relatively straightforward. One approach is to make an initial calculation with a very long time window but with a narrow source spectrum. This will of course yield relatively wide pulses, but the overall arrival structure can be determined; the time window can then be reduced and the full source spectrum included.

In SAFARI-FIPP it is possible to calculate the pulse responses for many receiver ranges and depths through a single solution pass, and a fixed start of the time window is therefore inconvenient. Instead one can choose a 'running' window defined by

$$t_{\min}(r) = r/c_r, \tag{131}$$

where r is the range and c_r is a constant called the reduction velocity. This constant has to be large enough that $t_{\min}(r)$ is smaller than the arrival time of the fastest signal in order to avoid wrap-around. In most applications c_r is conveniently chosen to be equal to the fastest wave speed in the problem.

5. Installation of SAFARI

The SAFARI package consists of the three main programs SAFARI-FIPR, SAFARI-FIP and SAFARI-FIPP and a number of subroutines, most of which are common for the three main programs.

All output from the SAFARI modules is produced in graphics form, either as standard curve plots or three-dimensional contour plots. The plotting is performed by two main programs, FIPPLOT and CONTUR, which have to be called after execution of the calculating programs.

At SACLANTCEN the programs are implemented on an FPS164 Attached Processor linked to a VAX 8600. The programs are therefore highly vectorised, and a number of FPS164 library subroutines are used. Apart from these and a few critical subroutines used for generating the kernel of the Green's function written in APAL64 assembler plus special subroutines for asynchronous I/O, the codes are written entirely in FORTRAN 77. A special FORTRAN 77 library with simulations of these special subroutines is available, however. The codes for the FPS164 and the VAX are therefore basically identical. The fact that standard FORTRAN 77 has been used makes installation possible on any computer satisfying the hardware requirements.

5.1. PRECISION REQUIREMENTS

The solution algorithm is stable for any machine precision, but the argument of the exponential function has to be truncated accordingly, in order to avoid arithmetic overflow. The maximum argument is set in each of the main programs through the variable AM. For VAX single precision a value of 65 is used, whereas 300 is used for 64-bit machines such as the FPS164 and the CRAY.

Although the actual precision has no influence on the stability, it affects the dynamic range of the results, but double precision will only be required in very special cases.

5.2. MEMORY REQUIREMENTS

The codes will run in their default version on any machine with more than 250 k words of memory, where one word corresponds to a real number in the actual precision. It is, however, possible to reduce the array sizes to allow installation on machines with less memory. The array sizes are basically controlled by three parameters defined in most subroutines. If changes are made, they therefore must be made in all source files. The parameters are:

NLA: Maximum number of layers in environmental model, including the upper and lower halfspaces. The default is NLA = 24.

NP: Maximum number of wavenumber samples. In SAFARI-FIPP NP is also the maximum allowed number of frequency samples. Due to the use of an RFFT for the frequency/time transform, the corresponding maximum number of time samples is 2NP. The default is NP = 4096.

NRD: Maximum number of source and receiver depths. The default is NRD = 1001.

It is obvious that the array sizes may also be increased by any amount allowed by the available hardware.

5.3. SOURCE FILES

The main programs are placed in separate source files, but the subroutines have been grouped together in a few relatively large files according to their use. In the following the source files and their contents are described.

SJEFIPR30.FOR The reflection coefficient program SAFARI-FIPR version 3.0, which uses the SAFARI solution technique to determine the reflection coefficients of any horizontally stratified fluid/solid halfspace. The implemented output options are

- Modulus and phase as function of grazing angle for a selected number of frequencies.
- Modulus and phase as function of frequency for a selected number of grazing angles.
- Modulus contoured *vs* frequency and grazing angle.
- There is a choice between calculation of the P-P reflection coefficient and the P-SV reflection coefficient. The last, of course, only have meaning for a solid upper halfspace.

SJEFIP30.FOR The transmission loss program SAFARI-FIP version 3.0, which for a single frequency solves the wave equation for a horizontally stratified environment. The output is controlled by a number of options. Some of the features are

- Solid, liquid or vacuum isovelocity layers and half spaces. Variable velocity allowed in fluid layers.
- Interface roughness (all interface types).
- Cylindrical or plane geometry.
- Multiple sources (vertical line arrays).
- Multiple receivers.
- Calculation of normal stress (pressure in fluids).
- Calculation of vertical particle velocities.
- Calculation of horizontal particle velocities.
- Depth averaging of calculated field properties.
- Range/depth contouring of field properties.
- Complex integration contour for use in lossless cases.

SJEFIPP30.FOR The pulse program SAFARI-FIPP version 3.0, which solves the wave equation for a horizontally stratified environment at a selected number of frequencies. Some of the features are

- Solid, liquid or vacuum isovelocity layers and half spaces. Variable velocity allowed in fluid layers.

  [illegible]terface roughness.
- Cylindrical or plane geometry.
- Multiple sources (vertical line arrays).
- Multiple receivers.
- Several choices of source pulse shapes.
- Synthetic hydrophone signals.
- Synthet[illegible] [illegible]ismograms. These can be plotted separately for each receiver or [illegible]acke[illegible] [illegible] stacking can be performed in either range or depth.
- Dispersion curves for normal modes.
- Dispersion curves for seismic interface waves.
- Complex [illegible] [illegible]ration contour.

FIPPLOT.FOR The main program FIPPLOT, which performs all plotting of results except for contour plots. FIPPLOT is based on the DISSPLA plotting system. The plot data are transfered through two files. One file contain titles, labels, axis limits etc. This file is a formatted file and the default values can be changed by the user. The other file is a formatted file which contains the data for plotting.

CONTUR.FOR The main program and associated subroutines, which perform the contour plotting optionally using a DISSPLA compatible plotting package or the raster package UNIFAS. The two-file interface to the calculating programs is also used here.

FIPPSJE30.FOR High-level subroutines used by all programs.

FIPTSJE30.FOR High-level subroutines used by SAFARI-FIP.

FIPRSJE30.FOR Subroutines used only by SAFARI-FIPR.

FIPSSJE30.FOR Lower-level subroutines used by all programs, i.e. basically all subroutines involved in determining the depth-dependent Green's functions.

FIPUSJE30.FOR Subroutines used by all programs for generation of printout and plot files.

APMATHSIM.FOR Subroutines simulating the APMATH64 library of the FPS164 Attached Processor. Also contains FORTRAN equivalents to those subroutines, which in the FPS164-version are written in APAL64 assembler.

5.4. COMPILING THE SAFARI CODES

The compilation is straightforward, since no special options are needed. Thus for VAX/VMS,

```
$ FOR/LIST SJEFIP30
$ FOR/LIST SJEFIPP30
$ FOR/LIST SJEFIPR30
$ FOR/LIST FIPPLOT
$ FOR/LIST CONTUR
$ FOR/LIST FIPPSJE30
$ FOR/LIST FIPSSJE30
$ FOR/LIST FIPRSJE30
```

```
$ FOR/LIST FIPTSJE30
$ FOR/LIST FIPUSJE30
$ FOR/LIST APMATHSIM
```

For convenience the subroutines are placed in two libraries:

```
$ LIBR/CREATE APMATH64 APMATHSIM
$ LIBR/CREATE SAFLIB FIPPSJE30,FIPSSJE30,FIPTSJE30,-
    FIPUSJE30,FIPRSJE30
```

The compilation of SAFARI for the FPS164 is described in Appendix A.

5.5. LINKING THE SAFARI CODES

The linking of the five executable modules is performed as follows under VAX/VMS:

```
$ LINK/EXE=VAXFIP30 SJEFIP30,SAFLIB/LIB,APMATH64/LIB
$ LINK/EXE=VAXFIPP30 SJEFIPP30,SAFLIB/LIB,APMATH64/LIB
$ LINK/EXE=VAXFIPR30 SJEFIPR30,SAFLIB/LIB,APMATH64/LIB
$ LINK FIPPLOT,DISSPLA/LIB
$ LINK CONTUR,DISSPLA/LIB,UNIRAS/LIB
```

where DISSPLA.OLB is a library containing the DISSPLA subroutines; UNIRAS.OLB is the UNIRAS library if available. If UNIRAS is not available, the call to the subroutine MAINRAS in the main program included in CONTUR.FOR must be removed. DISSPLA can of course be exchanged with any other plotting system available.

The linking of SAFARI for the FPS164 is described in Appendix A.

5.6. RUNNING THE SAFARI CODES

The programs are now ready to run. On the VAX it is most convenient to make one command file with parameter input for each program:

FIPR.COM

```
$ ASSIGN/USER 'P1'.DAT FOR001    !INPUT DATA FILE
$ ASSIGN/USER 'P1'.PLP FOR019    !PLOT PARAMETERS (FIPPLOT)
$ ASSIGN/USER 'P1'.PLT FOR020    !PLOT DATA FILE (FIPPLOT)
$ ASSIGN/USER 'P1'.CDR FOR028    !CONTOUR PLOT PARAMETERS
```

```
$ ASSIGN/USER 'P1'.BDR FOR029    !CONTOUR DATA FILE
$ RUN VAXFIPR30                  !EXECUTE SAFARI-FIPR
$ ASSIGN/USER 'P1'.PLP FOR019    !ASSIGN PLOT FILES TO
$ ASSIGN/USER 'P1'.PLT FOR020    !LOGICAL NAMES USED BY FIPPLOT
$ RUN FIPPLOT                    !EXECUTE FIPPLOT
$ ASSIGN/USER 'P1'.CDR FOR055    !ASSIGN CONTOUR FILES TO
$ ASSIGN/USER 'P1'.BDR FOR017    !LOGICAL NAMES USED BY CONTUR
$ RUN CONTUR                     !EXECUTE CONTUR
```

FIP.COM

```
$ ASSIGN/USER 'P1'.DAT FOR001    !INPUT DATA FILE
$ ASSIGN/USER 'P1'.PLP FOR019    !PLOT PARAMETERS (FIPPLOT)
$ ASSIGN/USER 'P1'.PLT FOR020    !PLOT DATA FILE (FIPPLOT)
$ ASSIGN/USER 'P1'.CDR FOR028    !CONTOUR PLOT PARAMETERS
$ ASSIGN/USER 'P1'.BDR FOR029    !CONTOUR DATA FILE
$ RUN VAXFIP30                   !EXECUTE SAFARI-FIP
$ ASSIGN/USER 'P1'.PLP FOR019    !ASSIGN PLOT FILES TO
$ ASSIGN/USER 'P1'.PLT FOR020    !LOGICAL NAMES USED BY FIPPLOT
$ RUN FIPPLOT                    !EXECUTE FIPPLOT
$ ASSIGN/USER 'P1'.CDR FOR055    !ASSIGN CONTOUR FILES TO
$ ASSIGN/USER 'P1'.BDR FOR017    !LOGICAL NAMES USED BY CONTUR
$ RUN CONTUR                     !EXECUTE CONTUR
```

FIPP.COM

```
$ ASSIGN/USER 'P1'.DAT FOR001    !INPUT DATA FILE
$ ASSIGN/USER 'P1'.PLP FOR019    !PLOT PARAMETERS (FIPPLOT)
$ ASSIGN/USER 'P1'.PLT FOR020    !PLOT DATA FILE (FIPPLOT)
$ ASSIGN/USER 'P1'.CDR FOR028    !CONTOUR PLOT PARAMETERS
$ ASSIGN/USER 'P1'.BDR FOR029    !CONTOUR DATA FILE
$ RUN VAXFIPP30                  !EXECUTE SAFARI-FIPP
$ ASSIGN/USER 'P1'.PLP FOR019    !ASSIGN PLOT FILES TO
$ ASSIGN/USER 'P1'.PLT FOR020    !LOGICAL NAMES USED BY FIPPLOT
$ RUN FIPPLOT                    !EXECUTE FIPPLOT
```

The command files shown here of course have to be extended with the definition of the proper directories. However, this is installation dependent and therefore not included here. The preparation of command files for running SAFARI on the FPS164 is described in Appendix A. Details on running FIPPLOT and CONTUR are given in Appendixes B and C respectively .

Assume that a file INPUT.DAT has been prepared for SAFARI-FIP. The user then only needs to give the command

```
$ @FIP INPUT
```

and the program will run. All files related to the actual run will have the same names except for the extensions. Similarly in batch:

```
$ SUBMIT FIP/PARAM=INPUT
```

The preparation of input files is described separately for the different SAFARI modules in the following sections.

6. Running SAFARI-FIPR

The SAFARI-FIPR module calculates the plane-wave reflection coefficients for an arbitrarily stratified fluid/solid halfspace. The layer above the interface of interest should be replaced by an infinite halfspace with the properties existing just above the interface. The code will then automatically place a compressional line source in the upper halfspace and, for each selected grazing angle and frequency, use the global matrix technique to calculate the complex amplitude of the resulting upgoing plane wave in the upper halfspace. The complex reflection coefficient then follows directly by division with the complex amplitude at the interface of the incoming wave produced by the source. The complex reflection coefficient R_C is most conveniently displayed as modulus $|R_C|$ and phase $\tan^{-1}(\mathrm{Im}[R_C]/\mathrm{Re}[R_C])$. In underwater acoustics it is common, however, to represent the modulus by the corresponding *reflection loss* defined by

$$R_{\mathrm{dB}} = -20 \log |R_C|$$

and this is the parameter displayed in the graphic output produced by SAFARI-FIPR.

The results are presented in graphic form as curve plots showing the dependence of the reflection loss and phase shift as function of either grazing angle or frequency. Further, there is an optional choice of reflection loss contours *vs* grazing angle and frequency.

All inputs to SAFARI-FIPR are read from the file currently assigned to the logical file FOR001. Before running the program the user has to assign the file containing the input data to this logical name. It is most convenient to include this assignment in a general command file also assigning file names to the logical names of the output files, as described in Subsect. 5.6.

In the following the preparation of the input files will be discussed in detail followed by an outline of the necessary numerical considerations.

6.1. INPUT FILES FOR SAFARI-FIPR

The input data are structured in 9 blocks. The first 5 blocks, shown in Table 2, specify the title, options, environmental parameters, together with the desired grasing angle and frequency sampling. The last 4 blocks, outlined in Table 3, contain axis specifications for the graphical output. Some of these blocks should always be included and others only if certain options have been specified. The single blocks and parameters are described in detail in the following.

Table 2
Parameters of SAFARI-FIPR input files: Calculation and environmental parameters

Block		Parameter	Units	Limits
I	TITLE:	title of run	–	≤ 80 char.
II	opt1 opt2 ...:	output options	–	≤ 40 char.
III	NL:	number of layers, incl. halfspaces	–	NL ≥ 2
	D:	depth of interface	m	–
	CC:	compressional speed	m/s	CC ≥ 0
	CS:	shear speed	m/s	–
	AC:	compressional attenuation	dB/λ	AC ≥ 0
	AS:	shear attenuation	dB/λ	AS ≥ 0
	RO:	density	g/cm^3	RO ≥ 0
	RG:	rms value of interface roughness	m	–
	CL:	correlation length of roughness	m	CL > 0
IV	FMIN:	minimum frequency	Hz	FMIN > 0
	FMAX:	maximum frequency	Hz	FMAX > 0
	NRFR:	number of frequencies	–	NRFR ≥ 1
	NFOU:	plot output increment	–	NFOU ≥ 0
V	AMIN:	minimum grasing angle	deg	AMIN ≥ 0
	AMAX:	maximum grasing angle	deg	AMAX ≥ 0
	NRAN:	number of grasing angles	–	NRAN ≥ 1
	NAOU:	plot output increment	–	NAOU ≥ 0

Table 3
Parameters of SAFARI-FIPR input files: Plot parameters

Block		Parameter	Units	Limits
VI[1]	ALEF:	left border of angle axis	deg	–
	ARIG:	right border of angle axis	deg	–
	ALEN:	length of angle axis	cm	ALEN > 0
	AINC:	distance between tick marks	deg	AINC > 0
	RALO:	lower border of R-loss axis	dB	–
	RAUP:	upper border of R-loss axis	dB	–
	RFLN:	length of loss and phase axes	cm	RFLN > 0
	RFIN:	R-loss axis tick mark interval	dB	RFIN > 0
VII[2]	FLEF:	left border of frequency axis	Hz	–
	FRIG:	right border of frequency axis	Hz	–
	FLEN:	length of frequency axis	cm	FLEN > 0
	FINC:	distance between tick marks	Hz	FINC > 0
	RFLO:	lower border of R-loss axis	dB	–
	RFUP:	upper border of R-loss axis	dB	–
	RFLN:	length of loss and phase axes	cm	RFLN > 0
	RFIN:	R-loss axis tick mark interval	dB	RFIN > 0
VIII[3]	ALEF:	left border of angle axis	deg	–
	ARIG:	right border of angle axis	deg	–
	ALEN:	length of angle axis	cm	ALEN > 0
	AINC:	distance between tick marks	deg	AINC > 0
	FRLO:	lower border of frequency axis	Hz	FRLO > 0
	FRUP:	upper border of frequency axis	Hz	FRUP > 0
	OCLN:	length of one octave	cm	OCLN > 0
	NTKM:	number of tick marks per octave	–	NTKM > 0
	ZMIN:	minimum contour level	dB	–
	ZMAX:	maximum contour level	dB	–
	ZINC:	contour level increment	dB	ZINC > 0
IX[4]	VLEF:	wave speed at left border	m/s	–
	VRIG:	wave speed at right border	m/s	–
	VLEN:	length of wave speed axis	cm	VLEN > 0
	VINC:	wave speed tick mark distance	m/s	VINC > 0
	DVUP:	depth at upper border	m	–
	DVLO:	depth at lower border	m	–
	DVLN:	length of depth axis	cm	DVLN > 0
	DVIN:	depth axis tick mark interval	m	DVIN > 0

[1] Only for NFOU > 0. [2] Only for NAOU > 0. [3] Only for option C. [4] Only for option Z.

BLOCK I – TITLE

Lines:	1
Required:	Always
Syntax:	TITLE
Format:	A80
Description:	TITLE: Title of run. Maximum 80 characters.

BLOCK II – OPTIONS

Lines:	1
Required:	Always
Syntax:	`opt1 opt2 opt3 ...`
Format:	Free. Maximum 40 alphanumeric characters.
Description:	Series of alphanumeric characters specifying the desired options. The following are implemented at present:

`C`: Loss contours plotted *vs* frequency and grazing angle.

`M`: This is the default option, which therefore never needs to be specified. It calculates the P-P reflection loss as function of angle and frequency.

`P`: Phase angle of reflection coefficient plotted in addition to the default reflection loss.

`S`: This option replaces the default P-P wave reflection coefficient by the P-SV wave reflection coefficient.

`Z`: Plot of velocity profiles.

BLOCK III – ENVIRONMENTAL DATA

Lines: ≥ 3
Required: Always
Syntax:

```
NL
D(1) CC(1) CS(1) AC(1) AS(1) RO(1) RG(1) CL(1)
D(2) CC(2) CS(2) AC(2) AS(2) RO(2) RG(2) CL(2)
:
D(NL)CC(NL)CS(NL)AC(NL)AS(NL)RO(NL)RG(NL)CL(NL)
```

Description:

`NL`: Number of layers, including the upper and lower halfspaces. These should always be included, even in cases where they are vacuum. In this regard it should be noted that the reflection coefficient is always calculated for the uppermost interface, with the incoming wave being a downward-going plane P-wave in the upper halfspace. This halfspace is therefore not allowed to be vacuum.

`D()`: Depth z in m of upper boundary of layer or halfspace. The reference depth can be choosen arbitrarily, and `D()` is allowed to be negative. For layer no. 1, i.e. the upper halfspace, this parameter is dummy.

`CC()`: Velocity c_c of compressional waves in m/s. If specified to 0.0, the layer or halfspace is vacuum.

`CS()`: Velocity c_s of shear waves in m/s. In order to be physically meaningful, it is required that $c_s \leq \sqrt{0.75}c_c$. If specified to 0.0, the layer or halfspace is fluid. If $c_s < 0$, then $|c_s|$ represents the compressional velocity at the bottom of the actual layer, which is treated as fluid with $1/c(z)^2$ varying linearly with depth.

`AC()`: Attenuation γ_c of compressional waves in dB/Λ. If the layer is fluid, and `AC()` is specified as 0.0, then an empirical water attenuation is used.

BLOCK III – (Continued)

Description:

AS(): Attenuation γ_s of shear waves in dB/Λ. For the attenuations to be physically meaningful, it is required that

$$\frac{\gamma_s}{\gamma_c} \leq \frac{3}{4}\left(\frac{c_c}{c_s}\right)^2$$

RO(): Density ρ in g/cm^3.

RG(): RMS roughness of interface in m. `RG(1)` is dummy. If `RG` > 0 the Kirchhoff approximation is used for the scattering loss, i.e. `CL` $\rightarrow \infty$. This is computationally faster than doing the full scattering theory, but it is only applicable for small roughnesses and large correlation lengths. To invoke the full non-Kirchhoff scattering RG must be specified equal to the negative rms roughness, i.e. `RG` < 0.

CL(): Correlation length of roughness in m. This parameter is only required if non-Kirchhoff scattering has been selected, i.e. `RG` < 0.

BLOCK IV – FREQUENCY DATA

Lines: 1
Required: Always
Syntax: `FMIN FMAX NRFR NFOU`
Format: Free
Description:

`FMIN`: Minimum frequency in Hz.
`FMAX`: Maximum frequency in Hz.
`NRFR`: Number of frequencies ($\geq$ 1). If the contour option `C` was specified the samples will be placed equidistantly on a logarithmic frequency axis; otherwise the sampling will be equidistant on a linear frequency axis.
`NFOU`: If `NFOU` > 0 a plot of reflection loss (and phase shift if option `P` was chosen) as function of grazing angle is generated for each `NFOU` frequency. If `NFOU` = 0 no plots as function of grazing angle will be produced.

BLOCK V – GRAZING ANGLE DATA

Lines: 1
Required: Always
Syntax: `AMIN AMAX NRAN NAOU`
Format: Free
Description:

`AMIN`: Minimum grazing angle in degrees.
`AMAX`: Maximum grazing angle in degrees.
`NRAN`: Number of angles.
`NAOU`: If `NAOU` > 0 a plot of reflection loss (and phase shift if option P was chosen) as function of frequency is produced for each `NAOU` angle. If `NAOU` = 0 no plots of reflection lose as function of frequency are generated.

BLOCK VI – PLOT DATA / REFLECTION LOSS AND PHASE VS GRAZING ANGLE

Lines: 2

Required: If NFOU > 0

Syntax:

```
ALEF ARIG ALEN AINC
RALO RAUP RALN RAIN
```

Format: Free

Description:

- **ALEF:** Grazing angle in degrees corresponding to left border of plots.
- **ARIG:** Right border of grazing angle axis.
- **ALEN:** Length of angle axis in cm.
- **AINC:** Distance in degrees between tick marks on grazing angle axis.
- **RALO:** Reflection loss in dB corresponding to lower border of plot. For phase shift plots the phase angle axis will automatically cover the interval −180° to 180°. This interval can, however, be changed as described in Appendix B.
- **RAUP:** Upper border in dB.
- **RALN:** Length of reflection loss and phase shift axes in cm.
- **RAIN:** Distance in dB between tick marks for loss axis.

BLOCK VII – PLOT DATA / REFLECTION LOSS AND PHASE VS FREQUENCY

Lines: 2

Required: If NAOU > 0

Syntax:

```
FLEF FRIG FLEN FINC
RFLO RFUP RFLN RFIN
```

Format: Free

Description:

- **FLEF:** Frequency in Hz corresponding to left border of plots.
- **FRIG:** Right border frequency axis.
- **FLEN:** Length of frequency axis in cm.
- **FINC:** Distance in Hz between tick marks on frequency axis.
- **RFLO:** Reflection loss in dB corresponding to lower border of plot. For phase shift plots the phase angle axis will automatically cover the interval −180° to 180°. This interval can, however, be changed as described in Appendix B.
- **RFUP:** Upper border of reflection loss axis in dB.
- **RFLN:** Length of reflection loss and phase shift axes in cm.
- **RFIN:** Distance in dB between tick marks on loss axis.

BLOCK VIII – PLOT DATA / ANGLE-FREQUENCY CONTOURS

Lines: 3

Required: If option C was specified.

Syntax:

```
ALEF ARIG ALEN AINC
FRLO FRUP OCLN NTKM
ZMIN ZMAX ZINC
```

Format: Free

Description:

- **ALEF:** Grazing angle in degrees corresponding to left border of contour plots.
- **ARIG:** Right border of grazing angle axis on contour plot.
- **ALEN:** Length of grazing angle axis in cm.
- **AINC:** Distance in degrees between tick marks on angle axis.
- **FRLO:** Frequency in Hz corresponding to lower border of plot. Since the frequency axis will be logarithmic, **FRLO** > 0.
- **FRUP:** Frequency corresponding to upper border of plot.
- **OCLN:** Size parameter specifying number of cm per octave on frequency axis.
- **NTKM:** Number of tick marks per octave.
- **ZMIN:** Lower limit in dB of reflection loss interval for which contour lines are to be plotted.
- **ZMAX:** Upper limit in dB of reflection loss interval for which contour lines are to be plotted.
- **ZINC:** Distance in dB between contour lines.

BLOCK IX – PLOT DATA / VELOCITY PROFILE

Lines: 2

Required: If option Z was specified in Block II.

Syntax:

```
VLEF VRIG VLEN VINC
DVUP DVLO DVLN DVIN
```

Format: Free

Description:

VLEF:	Left border value of velocity in m/s.
VRIG:	Right border value of velocity in m/s.
VLEN:	Length of velocity axis in cm.
VINC:	Distance between tick marks in m/s.
DVUP:	Depth at upper border of plot in m.
DVLO:	Depth at lower border of plot in m.
DVLN:	Length of depth axis in cm.
DVIN:	Distance in m between tick marks on depth axis.

6.2. NUMERICAL CONSIDERATIONS

Since the determination of plane-wave reflection coefficients does not involve any numerical evaluation of integral transforms, the only numerical problem is related to the discretization of the environmental model. When modeling real data where only a few environmental data are known, it is obvious that the model has to be re-run several times in order to fit a discrete stratified model. On the other hand the accuracy requirements are very limited, and there are no purely numeric considerations involved. This is, however, the case when the SAFARI-FIPR reflection coefficients have to be compared to those obtained by other numerical models, which is very common in relation to the verification of new algorithms. Some reflection coefficient codes, e.g. those based on finite differences, assume a linearly varying sound velocity profile between the sampling points, whereas SAFARI assumes either isovelocity layers or a sound speed varying non-linearly between the sampling points, Eq. (5). It is therefore necessary that the number of profile sampling points is so large that the differences between the interpolation techniques has insignificant effect on the calculated sound field. It is not possible to give any specific rules in this regard since the effect depends on the frequencies and grazing angles of interest. If isovelocity layers are used to represent the profile, a layer thickness of $\frac{1}{4}\Lambda$ will usually be sufficient. For the inhomogeneous fluid layers, however, the thickness can be chosen much larger. In any case the profile discretization should be controlled by checking the convergence.

6.3. SAFARI-FIPR EXAMPLES

In this section a few characteristic examples will be given of the use of SAFARI-FIPR for determining plane-wave reflection coefficients. The examples here have been chosen from underwater acoustics, but problems from seismology and ultrasonics are treated in an identical manner. Several other examples can be found in [20–27].

The environment considered in the present, and in all following examples for the transmission loss and pulse models, is characterized by a water depth of 100 m and a bottom consisting of a silt layer of 20 m thickness overlying a homogeneous sub-bottom of coarse sand. The material properties of the bottom are given in Table 4.

Table 4
Material parameters for ocean bottom

Layer	Thickness	Wave speed		Attenuation		Density
	H (m)	c_c (m/s)	c_s (m/s)	γ_c (dB/Λ)	γ_s (dB/Λ)	ρ (g/cm^3)
Silt	20.0	1600	400	0.2	0.5	1.8
Sand	∞	1800	600	0.1	0.2	2.0

■ *6.3.1.* SAFARI-FIPR *case 1: Reflection coefficients vs grazing angle*

This test case concerns the determination of the plane-wave reflection coefficient of the ocean bottom as function of grazing angle at a single frequency of 50 Hz. The data file is given in Table 5.

When running SAFARI-FIPR with the above data file, 3 plots are produced (Fig. 6). Figure 6a shows the calculated reflection loss with the velocity profile plot inserted. Note that the loss is very small for grazing angles less than the critical angle for the sub-bottom, $\theta_{c2} = \cos^{-1}(1500/1800) = 33.6°$. At a frequency of 50 Hz no significant transition happens at the sediment critical angle, $\theta_{c1} = \cos^{-1}(1500/1600) = 20.4°$. The main effect of the low shear speeds is the non-vanishing reflection loss at grazing angles smaller than critical. Figure 6b shows the associated phase shift as function of grazing angle. Again the transition at the sub-bottom critical angle is apparent. Here it should be noted that no phase unwrapping is performed; therefore the discontinuous behaviour at 33.6° in fact represents a 360° phase change.

■ *6.3.2.* SAFARI-FIPR *case 2: Loss contours vs frequency and angle*

In this example we calculate the reflection loss as a function of grazing angle over 4 frequency octaves from 20 to 320 Hz and generate a contour plot. The environment is the same as case 1, and the data file is given in Table 6.

The contour plot generated by SAFARI-FIPR for this case is shown in Fig. 7a. Figure 7b shows the plot obtained when the contour program CONTUR is re-run with the UNIRAS option, as described in Appendix C. The dark areas indicate high loss, the light ones low loss. Note that the contour levels have been changed to a spacing of 2 dB in Fig. 7b.

Note that at the low frequencies the reflection properties are dominated by the critical angle $\theta_{c2} = 33.6°$ of the sub-bottom, whereas for the higher frequencies a series of 'resonance ridges' of high loss appear, asymptotically approaching the sediment critical angle, $\theta_{c1} = 20.4°$. This behaviour is typical for layered media.

Table 5
SAFARI-FIPR case 1 data file

Data file	Description	Notes
SAFARI-FIPR case 1	title	
P Z	options: P – phase plot, Z – velocity profile	1,2
3	number of layers	
0 1500 0 0 0 1 0	layer 1 (upper halfspace, water)	3
0 1600 400 0.2 0.5 1.8 0	layer 2 (sediment)	4
20 1800 600 0.1 0.2 2.0 0	layer 3 (sub-bottom)	4
50 50 1 1	frequency 50 Hz, NFOU = 1	5
0 90 181 0	angle interval 0 to 90°, 181 samples	5,6
0 90 20 30	angle axis for plots	6
0 15 12 5	loss axis for plots	6
0 2000 10 1000	velocity axis for profile plot	
-20 40 10 20	depth axis for profile plot	

[1] In order to obtain plots of the phase shift in addition to the default plot of the reflection loss, option P has been specified.

[2] Option Z is specified to get a plot of the velocity profile. This option requires that the axis specifications are given at the end of the data file. In the present case the profile is plotted from a depth 20 m above the bottom to 40 m below.

[3] Note that the 100 m thick water column has been replaced by an infinite halfspace with the properties of the water. For convenience the ocean bottom has been selected as origin for the depth axis. This is, however, arbitrary, and 100 m could be added to all depths without influencing the results.

[4] Since both interfaces are plane the rms roughness is specified as 0 in all cases, and the correlation lengths have been omitted.

[5] By specifying NFOU = 1, plots of the reflection data as a function of grazing angle will be produced for each frequency, in this case of course only one. NAOU = 0 indicates that no plots of reflection loss as a function of frequency are requested.

[6] The reflection coefficient will be calculated in 181 equidistantly-spaced points in the angular interval 0 to 90°, and the plots will show the reflection loss and phase shift over the whole interval. The loss axis is specified to cover the interval 0 to 15 dB.

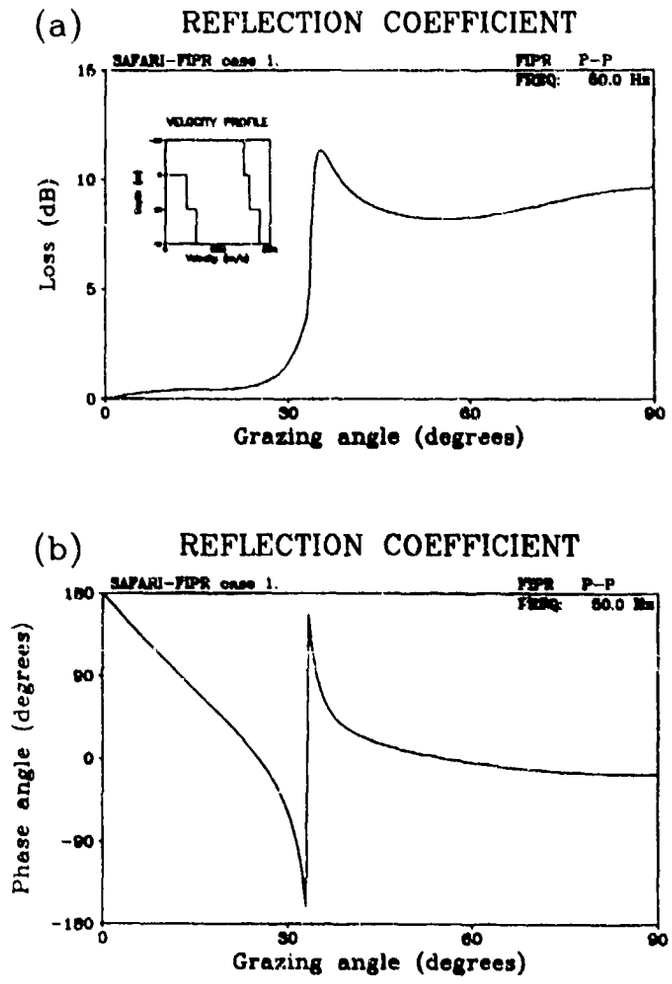

Fig. 6. Results for SAFARI-FIPR case 1: (a) reflection loss as function of grazing angle, with velocity profile inserted; (b) phase shift as function of grazing angle

Table 6
SAFARI-FIPR case 2 data file

Data file	Description	Notes
SAFARI-FIPR case 2	title	
C	option **C** – contour plot of reflection loss	1
3	number of layers	
0 1500 0 0 0 1 0	layer 1 (upper halfspace, water)	
0 1600 400 0.2 0.5 1.8 0	layer 2 (sediment)	
20 1800 600 0.1 0.2 2.0 0	layer 3 (sub-bottom)	
20 320 41 0	frequency interval 20 to 320 Hz, 41 samples	2
0 90 181 0	angle interval 0 to 90°, 181 samples	2
0 90 20 30	angle axis for contour plot	3
20 320 3 1	frequency axis for contour plot	3
1 10 1	contour levels	4

[1] Option **C** is specified to create a contour plot of the reflection loss *vs* angle and frequency.

[2] When option **C** is selected, the 41 selected frequency samples are placed equidistantly on a logarithmic frequency axis. The sampling in angle is the same as above, but note that both **NFOU** and **NAOU** have been set to 0 in order to disable the creation of the normal curve plots produced in case 1.

[3] The parameters for the angle axis are given exactly as for the curve plots in case 1. However, for the logarithmic frequency axis the total length of the axis is not specified. Instead the length of one octave is given in cm, here 3 cm. The tick marks are controlled by the last parameter in the line, in this case one tick mark per octave is plotted.

[4] The last line in the data file specifies that contour lines are to be plotted for each 1 dB in the interval 1 to 10 dB.

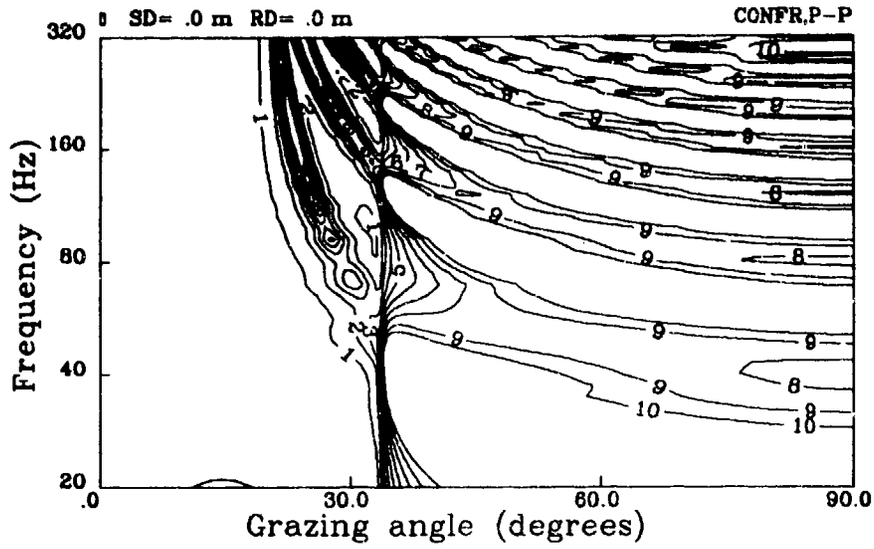

a

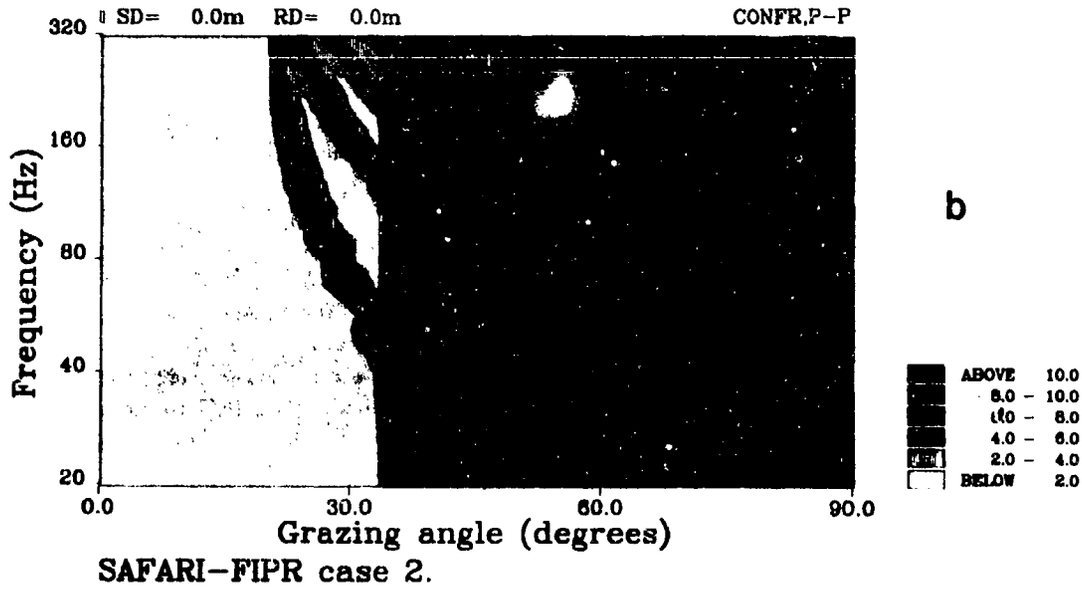

b

Fig. 7. **Results for SAFARI-FIPR case 2: (a) contour plot of reflection loss as function of grazing angle and frequency produced by the DISSPLA package; (b) contour plot produced by UNIRAS.**

■ 6.3.3. SAFARI-FIPR *case 3: Reflection loss at rough ice layer*

The last example of using SAFARI-FIPR concerns the determination of the reflection loss appearing at a randomly rough ice layer. This problem from arctic acoustics is included for two purposes. First of all it illustrates how to include the effect of interface roughness in the calculations. Secondly it is an example of a problem where the environment has to be turned upside down as SAFARI-FIPR always places the source in the upper halfspace.

It is assumed that an ice layer of average thickness 3.9 m covers a water column with a constant sound speed of 1500 m/s. The free surface of the ice layer is stochastically rough with an rms elevation of 0.6 m. The underside of the ice has an rms roughness

Table 7
SAFARI-FIPR case 3a data file

Data file	Description	Notes
`SAFARI-FIPR case 3a`	title	
`N`	option N – normal reflection loss	1
`3`	number of layers	
`0 1500 0 0 0 1 0`	layer 1 (upper halfspace, water)	2
`0 3000 1600 1.0 2.5 0.9 1.9`	layer 2 (ice layer)	3
`3.9 0 0 0 0 0 0.6`	layer 3 (vacuum)	4
`1 50 50 0`	frequency interval 1 to 50 Hz, 50 samples	5
`10 10 1 1`	angle interval 10°, 1 sample.	5
`0 50 20 10`	frequency axis for plot	6
`0 0.2 12 0.1`	loss axis for plot	6

[1] Option N means that the default reflection loss is to be calculated. This option need not to be specified, but the option field should always be represented by one line, which in this case could be empty.

[2] The environment has been turned upside down. Therefore the upper halfspace is water. Note that the depth and roughness parameters are dummy for the upper halfspace, the depth of the first interface and its roughness data should be given together with the material properties of the first real layer, i.e. layer 2.

[3] The roughness of the water/ice interface is specified to be 1.9 m. Since this is a positive number, the correlation length is assumed to be infinite and has therefore been omitted. The scattering theory based on the Kirchhoff approximation will be applied in this case.

[4] The roughness of the free ice surface is specified to be 0.6 m, again the correlation length is infinite.

[5] The frequency interval is chosen to be 1 to 50 Hz, and since the contour option C was not selected, the 50 samples will be placed equidistantly on a linear frequency axis. The calculation is to be performed at only one grazing angle, NANG = 1 and NAOU = 1.

[6] In contrast to the case for the contour plot, the frequency axis is here linear, and the parameters are given in the usual way.

of 1.9 m. Initially the correlation length is assumed to be infinite. The ice has a compressional velocity of $c_c = 3000$ m/s, a shear velocity of $c_s = 1600$ m/s and a density of 0.9 g/cm^3. The compressional and shear attenuations are 1.0 dB/Λ and 2.5 dB/Λ, respectively. The data file given in Table 7 is set up to calculate the reflection loss as function of frequency at a fixed grazing angle of 10°.

The resulting plot of the reflection loss as function of frequency is shown in Fig. 8a. Note the expected increase in the loss with increasing frequency. Now assume that the correlation length for the roughness of the water/ice interface is 40 m, and not infinite as above. Then the data file would look as shown in Table 8. As can be observed, the data file is identical to the one above except for the line stating the environmental data for the ice layer.

Table 8
SAFARI-FIPR case 3b data file

Data file	Description	Notes
SAFARI-FIPR case 3b	title	
N	option N – normal reflection loss	
3	number of layers	
0 1500 0 0 0 1 0	layer 1 (upper halfspace, water)	
0 3000 1600 1.0 2.5 0.9 -1.9 40	layer 2 (ice layer)	1
3.9 0 0 0 0 0 0.6	layer 3 (vacuum)	
1 50 50 0	frequency interval 1 to 50 Hz, 50 samples	
10 10 1 1	angle interval 10°, 1 sample	
0 50 20 10	frequency axis for plot	
0 0.2 12 0.1	loss axis for plot	

[1] By specifying the negative rms value of the roughness, the non-Kirchhoff scattering theory will be applied, and in this case the correlation length (40 m) has to be given as a last number in the same line.

The resulting reflection-loss curve is shown in Fig. 8b. There is a significant effect of the finite correlation length in the actual frequency interval, but at higher frequencies the non-Kirchhoff result will approach the Kirchhoff result. More examples treating interface roughness can be found in [24,25].

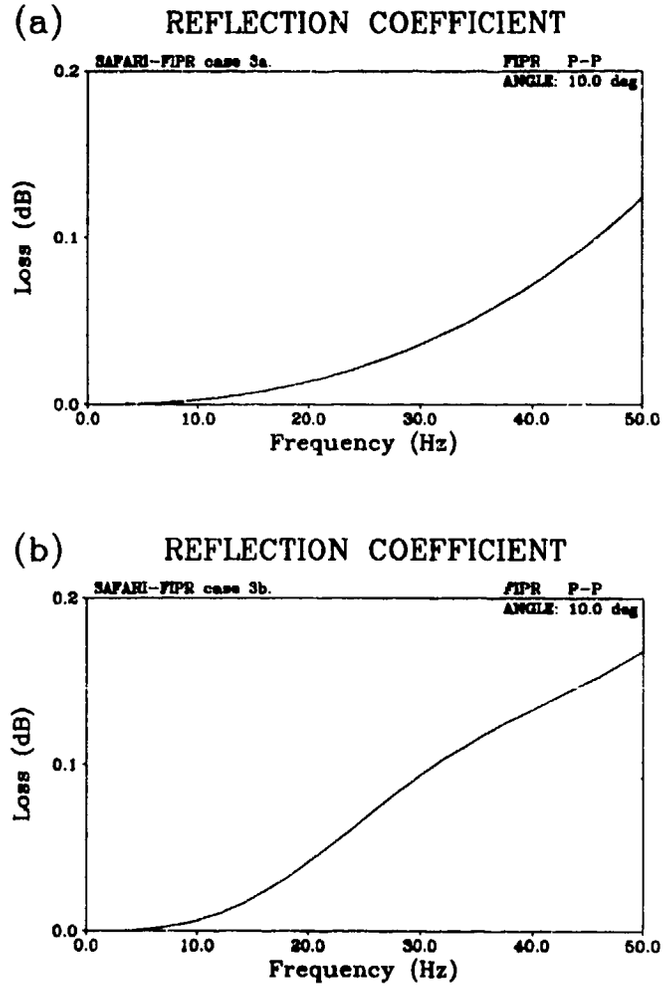

Fig. 8. **Results for SAFARI-FIPR case 3: (a) reflection loss at rough ice layer as function of frequency at grazing angle 10°, correlation length $L = \infty$; (b) reflection loss at rough ice layer as function of frequency at grazing angle 10°, correlation length $L = 40$ m.**

7. Running SAFARI-FIP

The SAFARI-FIP module performs single-frequency calculation of the total wavefield at any number of depths and ranges for either a single compressional source or a vertical phased source array. In both cases the sources may be either point sources or line sources, yielding axisymmetric and plane fields, respectively.

In the case of a single source in a fluid medium, the source strength S_ω is normalized to yield a pressure of 1 Pa at 1 m distance from the source. For both a compressional source and a point force in a solid medium the source strength is normalized to yield a normal stress σ_{zz} of 1 Pa, 1 m *below* the source. The graphical results are always given in dB and for the pressure or normal stress they therefore directly correspond to the standard definition of the transmission loss. For the phased arrays, the source strength of each individual source is divided by the total number of sources in order to get a maximum level in the generated beams which is independent of the number of sources. It is common in both underwater acoustics and seismology to measure particle velocities by means of geophones, and these parameters are therefore included as optional outputs. Since the particle velocities are vector parameters depending not only on the receiver position but also on the direction, there is no logical 'transmission loss' definition as in the case of the scalar pressure. In the graphical output these parameters are therefore given directly in dB relative to 1 m/s for a source strength of 1 Pa at 1 m distance. Thus the dB values for pressure and particle velocity will in general be offset with respect to each other. For a plane wave in a fluid with density ρ and sound speed c_c, the offset is determined by the relation between pressure p and particle velocity v, $|p| = \rho c_c |v|$, i.e. approximately 123 dB for water.

For all parameters the output is available both as standard curve plots *vs* depth or range and as contour plots showing the field variation in both depth and range.

All inputs to SAFARI-FIP are read from the file currently assigned to the logical file FOR001. Before running the program the user has to assign the file containing the input data to this logical name. The most convenient approach is to include this assignment in a general command file which also assigns file names to the logical names of the output files as described in Subsect. 5.6.

A successful use of SAFARI-FIP is highly dependent on how the parameters are specified, in particular those related to the truncation and discretization of the horizontal wavenumber interval. We will therefore in the following first describe the preparation of the input files in detail and then outline some important numerical considerations.

Table 9
Parameters of SAFARI-FIP input files: Calculation and environmental parameters

Block		Parameter	Units	Limits
I	TITLE :	title of run	–	≤ 80 char.
II	opt1 opt2 ...:	output options	–	≤ 40 char.
III	FREQ:	source frequency	Hz	> 0
	COFF:	integration contour offset	dB/Λ	COFF ≥ 0
IV	NL:	number of layers, incl. halfspaces	–	NL ≥ 2
	D:	depth of interface	m	–
	CC:	compressional speed	m/s	CC ≥ 0
	CS:	shear speed	m/s	–
	AC:	compressional attenuation	dB/Λ	AC ≥ 0
	AS:	shear attenuation	dB/Λ	AS ≥ 0
	RO:	density	g/cm^3	RO ≥ 0
	RG:	rms value of interface roughness	m	–
	CL:	correlation length of roughness	m	CL > 0
V	SD:	source depth (mean for array)	m	–
	NS:	number of sources in array	–	NS > 0
	DS:	vertical source spacing	m	DS > 0
	AN:	grazing angle of beam	deg	–
	IA:	array type	–	1 ≤ IA ≤ 5
	FD:	focal depth of beam	m	FD ≠ SD
VI	RD1:	depth of first receiver	m	–
	RD2:	depth of last receiver	m	RD2 > RD1
	NR:	number of receivers	–	NR > 0
	IR:	plot output increment	–	IR ≥ 0
VII	CMIN:	minimum phase velocity	m/s	CMIN > 0
	CMAX:	maximum phase velocity	m/s	–
VIII	NW:	number of wavenumber samples	–	$NW = 2^M$
	IC1:	first sampling point	–	IC1 ≥ 1
	IC2:	last sampling point	–	IC2 ≤ NW

7.1. INPUT FILES FOR SAFARI-FIP

The input data are structured in 13 blocks. The first eight, shown in Table 9, specify the title, options, frequency, environmental parameters, source and receiver

geometry, and finally the wavenumber sampling parameters. The last 5 blocks, outlined in Table 10, contain axis specifications for the graphical output. Some of these blocks should always be included and others only if certain options have been specified. The single blocks and parameters are described in detail in the following.

Table 10
Parameters of SAFARI-FIP input files: Plot parameters

Block		Parameter	Units	Limits
IX	RMIN:	minimum range on plots	km	–
	RMAX:	maximum range on plots	km	–
	RLEN:	length of x-axis for all plots	cm	RLEN > 0
	RINC:	distance between tick marks	km	RINC > 0
X[1]	TMIN:	minimum transmission loss	dB	–
	TMAX:	maximum transmission loss	dB	–
	TLEN:	length of vertical TL axes	cm	TLEN > 0
	TINC:	distance between tick marks	dB	TINC > 0
XI[2]	DCUP:	minimum depth for plots	m	–
	DCLO:	maximum depth for plots	m	–
	DCLN:	length of depth axis	cm	DCLN > 0
	DCIN:	distance between tick marks	m	DCIN > 0
XII[3]	ZMIN:	minimum contour level	dB	–
	ZMAX:	maximum contour level	dB	–
	ZINC:	contour level increment	dB	ZINC > 0
XIII[4]	VLEF:	wave speed at left border	m/s	–
	VRIG:	wave speed at right border	m/s	–
	VLEN:	length of wave speed axis	cm	VLEN > 0
	VINC:	wave speed tick mark distance	m/s	VINC > 0
	DVUP:	depth at upper border	m	–
	DVLO:	depth at lower border	m	–
	DVLN:	length of depth axis	cm	DVLN > 0
	DVIN:	depth-axis tick mark interval	m	DVIN > 0

[1] Only for options A, D, I and T. [2] Only for options C and D. [3] Only for option C.
[4] Only for option Z.

BLOCK I – TITLE

Lines:	1
Required:	Always
Syntax:	TITLE
Format:	A80
Description:	TITLE: Title of run. Maxim · 80 characters.

BLOCK II – OPTIONS

Lines: 1
Required: Always
Syntax: opt1 opt2 opt3 ...
Format: Free. Maximum 40 alphanumeric characters.
Description: Series of alphanumeric characters specifying the desired options. The following are implemented at present:

- A: Depth-averaged transmission loss plotted for each of the selected field parameters (N, V, H). The averaging is performed over the specified number of receivers (Block VI).
- C: Range/depth contour plot for transmission loss. A separate contour plot will be produced for every selected parameter (N, V, H).
- D: Plots of transmission loss *vs* depth produced for the ranges determined by the range axis parameters RMIN, RMAX and RINC (Block IX).
- H: Calculation of horizontal particle velocity.
- I: Hankel transform integrands are plotted for each of the selected field parameters (N, V, H).
- J: Complex integration contour. The contour is shifted into the upper halfplane by an offset controlled by the input parameter COFF (Block III).
- L: Linear vertical source array.
- N: Calculation of normal stress σ_{zz} (equal to negative pressure in fluids).
- P: Plane geometry. The sources will be line sources instead of point sources as used in the default cylindrical geometry.
- T: Transmission loss plotted as function of range for each of the selected field parameters (N, V, H).
- V: Calculation of vertical particle velocity.
- X: If sources are present in a solid medium, these will be considered vertical point forces (line forces in plane geometry) rather than omnidirectional sources.
- Z: Plot of velocity profile.

BLOCK III – FREQUENCY

Lines: 1
Required: Always
Syntax: FREQ, COFF
Format: Free
Description:

FREQ: Frequency f in Hz, at which calculation has to be performed.

COFF: Integration contour offset. Specified in dB/Λ, where Λ is the wavelength at the source depth SD. Since only the horizontal part of the integration contour is considered, this parameter should not be chosen so large that the amplitudes at the ends of the integration interval become significant. In lossless cases too small values will give sampling problems at the normal modes and other singularities. For intermediate values, the result is independent of the choice of COFF, but a good value to choose is one that gives 60 dB at the longest range considered in the FFT, i.e.

$$\mathrm{COFF} = 60 c_c(z_s)/f r_{\max}$$

where the maximum FFT range is

$$r_{\max} = \mathrm{NW}/f(c_{\min}^{-1} - c_{\max}^{-1}).$$

This value is the default which is applied if COFF is specified as 0.0.

BLOCK IV – ENVIRONMENTAL DATA

Lines: ≥ 3
Required: Always
Syntax:

```
NL
D(1) CC(1) CS(1) AC(1) AS(1) RO(1) RG(1) CL(1)
D(2) CC(2) CS(2) AC(2) AS(2) RO(2) RG(2) CL(2)
:
D(NL)CC(NL)CS(NL)AC(NL)AS(NL)RO(NL)RG(NL)CL(NL)
```

Description:

`NL`: Number of layers, including the upper and lower halfspaces. These should always be included, even in cases where they are vacuum.

`D()`: Depth z in m of upper boundary of layer or halfspace. The reference depth can be choosen arbitrarily, and `D()` is allowed to be negative. For layer no. 1, i.e. the upper halfspace, this parameter is dummy.

`CC()`: Velocity c_c of compressional waves in m/s. If specified as 0.0, the layer or halfspace is a vacuum.

`CS()`: Velocity c_s of shear waves in m/s. In order to be physically meaningful, it is required that $c_s \leq \sqrt{0.75}c_c$. If specified as 0.0, the layer or halfspace is fluid. If $c_s < 0$, it represents the compressional velocity at the bottom of the actual layer, which is treated as a fluid with $1/c(z)^2$ varying linearly with depth.

`AC()`: Attenuation γ_c of compressional waves in dB/λ. If the layer is fluid, and `AC()` is specified as 0.0, then an empirical water attenuation is used.

`AS()`: Attenuation γ_s of shear waves in dB/λ. For the attenuations to be physically meaningful, it is required that

$$\frac{\gamma_s}{\gamma_c} \leq \frac{3}{4}\left(\frac{c_c}{c_s}\right)^2$$

BLOCK IV – (Continued)

Description:

RO(): Density ρ in g/cm^3.

RG(): RMS roughness of interface in m. RG(1) is dummy. If RG > 0 the Kirchhoff approximation is used for the scattering loss, i.e. CL $\rightarrow \infty$. This is computationally faster than doing the full scattering theory, but it is only applicable for small roughnesses and large correlation lengths. To invoke the full non-Kirchhoff scattering RG must be specified equal to the negative rms roughness, i.e. RG < 0.

CL(): Correlation length of roughness in m. This parameter is only required if non-Kirchhoff scattering has been selected, i.e. RG < 0.

BLOCK V – SOURCE DATA

Lines: 1
Required: Always
Syntax: Option L: SD NS DS AN IA FD
else: SD
Format: Free
Description:

SD: Source depth z, in m. If option L has been specified, SD defines the mid-point of the vertical source array.
NS: Number of sources in the array.
DS: Source spacing in m.
AN: Specifies the nominal grazing angle of the generated beam in degrees. AN > 0 corresponds to downward propagation.
IA: Array type
[1] Rectangular weighted array
[2] Hanning weighted array
[3] Hanning weighted focused array
[4] Gaussian weighted array
[5] Gaussian weighted focused array
FD: Focal depth in m for an array of type 3 or 5.

BLOCK VI – RECEIVER DATA

Lines: 1
Required: Always
Syntax: RD1 RD2 NR IR
Format: Free
Description:

RD1: Receiver depth in m. If the calculations are to be performed for more than one receiver, i.e. NR > 1, then RD1 specifies the uppermost receiver.

RD2: If NR > 1 this parameter determines the depth of the lowermost receiver. If NR = 1, then this parameter is dummy.

NR: Number of receivers in depth.

IR: If options T or I have been specified, plots will be generated for each IR receiver depth. This parameter is useful if option C or A have been choosen, and integrands or transmission loss curves are wanted only for a limited number of depths.

BLOCK VII – PHASE VELOCITIES

Lines: 1
Required: Always
Syntax: `CMIN CMAX`
Format: Free
Description:

`CMIN`: Minimum phase velocity c_{min} in m/s. Determines the upper limit of the truncated horizontal wavenumber space:

$$k_{max} = 2\pi f / c_{min}.$$

`CMAX`: Maximum phase velocity c_{max} in m/s. Determines the lower limit of the truncated horizontal wavenumber space:

$$k_{min} = 2\pi f / c_{max}.$$

In plane geometry (option P) `CMAX` may be specified as negative. In this case, the negative wavenumber spectrum will be included with $k_{min} = -k_{max}$, yielding correct solution also at zero range. Contour offset (option J) is not allowed in this case.

BLOCK VIII – WAVENUMBER SAMPLING

Lines: 1
Required: Always
Syntax: `NW IC1 IC2`
Format: Free
Description:

`NW`: Number of sampling points in wavenumber space. Should be an integer power of 2, i.e. `NW` $= 2^M$. The sampling points are placed equidistantly in the truncated wavenumber space determined by `CMIN` and `CMAX`

`IC1`: Number of the first sampling point, where the calculation is to be performed. If `IC1` $>$ 1, then the Hankel transform is zeroed for sampling points 1,2...`IC1` $-$ 1, and the discontinuity is smoothed.

`IC2`: Number of the last sampling point where the calculation is to be performed. If `IC2` $<$ `NW`, then the Hankel transform is zeroed for sampling points `IC2` + 1, . . . `NW`, and the discontinuity is smoothed by Hermite polynomial extrapolation.

BLOCK IX – PLOT DATA / RANGE AXES

Lines: 1
Required: Always
Syntax: RMIN RMAX RLEN RINC
Format: Free
Description:

RMIN: Minimum range r_{min} in km. Determines the starting value for the x-axis of transmission loss and contour plots. RMIN is also the first range for which transmission loss *vs* depth will be plotted if option D is selected.

RMAX: Maximum range r_{max} in km. This parameter only defines the end of the x-axis of transmission loss and contour plots. The range interval of calculation is defined by r_{min} and the truncation and discretization of the wavenumber space.

RLEN: Length of x-axis in cm of all plots, i.e. also the length of the transmission loss axis if option D is selected.

RINC: Range interval between tick marks on the x-axes of transmission loss and contour plots. Also determines the range interval between plots of transmission loss *vs* depth for option D. For integrand plots all scaling and labelling is automatic.

BLOCK X – PLOT DATA / TRANSMISSION LOSS AXES

Lines: 1 for each field parameter (N, V, H).
Required: If options A, D, I or T were specified.
Syntax: TMIN TMAX TLEN TINC
Format: Free
Description:

TMIN: Minimum transmission loss in dB. For plots of transmission loss *vs* range (options A and T), TMIN determines the upper border. In the case of transmission loss *vs* depth (option D), it determines the right border of the plot.

TMAX: Maximum transmission loss in dB. Determines the lower border (for options A and T) or left border (for option D) of transmission loss plots. It should be noted, that the reference for the particle velocities is 1 m/s, when the reference pressure is 1 Pa (1 N/m^2) at 1 m distance from the source. If option L has been specified, i.e. more than one source is present, then the reference pressure of each source is divided by the number of sources. This ensures that the order of magnitude of the field parameters are independent of the number of sources in the array.

TLEN: Length of y-axes in cm for transmission loss and integrand plots. For option D, the transmission loss is represented by the x-axis and the length is therefore determined by RLEN .

TINC: Number of dB between tick marks on transmission loss axes. Scaling and labeling of integrand plots is automatic.

BLOCK XI – PLOT DATA / DEPTH AXES

Lines: 1
Required: If options C or D were specified.
Syntax: DCUP DCLO DCLN DCIN
Format: Free
Description:

DCUP: Minimum depth in m for both contour plots and plots of transmission loss *vs* depth.
DCLO: Maximum depth in m for both contour plots and plots of transmission loss *vs* depth.
DCLN: Length in cm of depth axes.
DCIN: Difference in m between tick marks on depth axes.

BLOCK XII – PLOT DATA / CONTOUR LEVELS

Lines: 1 for each selected parameter (N, V, H).
Required: If option C was specified.
Syntax: ZMIN ZMAX ZINC
Format: Free
Description:

ZMIN: Lower limit in dB of transmission loss interval for which contour lines are to be plotted.
ZMAX: Upper limit in dB of transmission loss interval for which contour lines are to be plotted.
ZINC: Difference in dB between contours.

BLOCK XIII – PLOT DATA / VELOCITY PROFILE

Lines: 2

Required: If option Z was specified in Block II.

Syntax:

```
VLEF VRIG VLEN VINC
DVUP DVLO DVLN DVIN
```

Format: Free

Description:

VLEF:	Left border value of velocity in m/s.
VRIG:	Right border value of velocity in m/s.
VLEN:	Length of velocity axis in cm.
VINC:	Distance between tick marks in m/s.
DVUP:	Depth at upper border of plot in m.
DVLO:	Depth at lower border of plot in m.
DVLN:	Length of depth axis in cm.
DVIN:	Distance in m between tick marks on depth axis.

7.2. NUMERICAL CONSIDERATIONS

When SAFARI-FIP is to be applied to a propagation problem, the first difficulty that arises is related to the discretization of the environmental model. When modelling real data collected in an area where only a few environmental data are known, it is generally necessary to re-run the code several times in order to fit a discrete stratified model; on the other hand the accuracy requirements will usually be limited, and there will be no purely numerical considerations involved. However, the choice of environmental model is important in cases where the SAFARI results have to be compared to those obtained by other numerical models, which is very common in relation to the verification of new algorithms. Many codes, like the normal mode and parabolic equation models, assume a linearly varying sound velocity profile between the sampling points, whereas SAFARI assumes either isovelocity layers or a sound speed varying non-linearly between the sampling points, Eq. (5). It is therefore necessary for the number of profile sampling points to be so large that the difference between the interpolation techniques has no significant effect on the calculated sound field. It is not possible to give any specific rules in this regard since the effect depends on many factors such as frequency, water depth and the receiver range of interest. But if isovelocity layers are used to represent the profile, a layer thickness of $\frac{1}{4}\Lambda$ will usually be sufficient. For the inhomogeneous layers, however, the thickness can be chosen to be much larger. In any event the profile discretization should be controlled by checking the convergence.

The actual choice of parameters controlling the wavenumber integration is far more critical. There are essentially 5 parameters: `CMIN`, `CMAX`, `NW`, `IC1` and `IC2`, but they cannot be chosen independently from other parameters, in particular the range interval of interest (Block IX), because of the wrap-around problem. Further, both source and receiver depths influence the choice of integration parameters, e.g. in the waveguide problem the presence of the normal modes will require much higher sampling rate if the source and receiver are inside the waveguide than if one of them is buried in the bottom. There are no general rules which can be used to automate the wavenumber integration. The only way to obtain accurate results is to change the integration parameters until convergence is obtained.

Clearly, when making parameter studies, convergence tests are not required for every small change in the environmental parameters. However, convergence tests must be done for at least one characteristic example before proceeding with a complete propagation study. A user with a reasonable knowledge of the physics of waveguide problems will – after gaining some experience – be able to determine the proper parameters relatively quickly. All problems are, however, not equally easy to predict, and it is therefore advisable – also for the experienced user – to use the following guidelines for estimating the integration parameters for every new application of SAFARI-FIP.

1. Select the horizontal phase velocities `CMIN` and `CMAX` such that all significant wave phenomena are included, i.e. `CMIN` should be chosen to be 10–20%

smaller than the smallest wave speed in the problem and CMAX should be a very large number, e.g. CMAX = 1E8. If evanescent waves are known to be present CMIN may have to be even smaller.

2. Select a few characteristic receiver depths.
3. Select a reasonably small number of sampling points NW, and run the code with option I to obtain plots of the integration kernels.
4. Repeat steps 1 to 3 with decreasing CMIN until all significant wavenumber components are within the integration interval. Then read the wavenumber limits $k_{\min}$ and $k_{\max}$ from the plot or calculate them directly as $k_{\min} = 2\pi f/c_{\max}$ and $k_{\max} = 2\pi f/c_{\min}$.
5. Select the range interval (RMIN, RMAX) of interest, and convert from km to m to obtain $r_{\min}$ and $r_{\max}$. For the FFT integration to 'reach' $r_{\max}$ the necessary number of sampling points must be larger than $N_{\min} = r_{\max}(k_{\max} - k_{\min})/2\pi\}$. Choose the smallest M for which NW $= 2^M > N_{\min}$. Set IC1 = 1 and IC2 = NW.
6. If the integration kernels plotted out in step 3 are very 'peaky' due to low loss in the waveguide, select option J and specify COFF = 0 to invoke the default contour offset. The experienced user can choose a specific value of COFF as described in Block III above.
7. Now select option T and calculate the transmission loss.
8. Double the number of sampling points NW (remember to double IC2 as well) and re-calculate.
9. Repeat step 8 until a stable transmission loss curve is obtained.
10. Now the number of receivers can be increased and the other options C, A and Z can be specified, as desired. Remember to change the plot parameters accordingly, see Table 10.

This is the standard procedure which is only applicable if the number of sampling points NW is reasonably small, at least smaller than the maximum allowed for the actual installation. If this is not the case, there are two different ways to proceed. If the computation time is not important and the actual computer allows it, a larger version can be installed, and the procedure above is repeated or continued. In many cases, however, the computation time will become unacceptable using this approach, and the second possible approach has to be taken. This, however, requires a little more knowledge concerning the physics of the actual problem.

As discussed earlier, each horizontal wavenumber component k corresponds to a specific conical or plane wave propagating at grazing angle θ, where $k = k_m \cos\theta$, k_m being the medium wavenumber of layer m. Therefore the small wavenumbers correspond to steep propagation, and $k = k_m$ corresponds to horizontal propagation. It is well known for the waveguide problem that the waves propagating at grazing

angles larger than the critical angle θ_c at the bottom will suffer a large attenuation for every bottom bounce and will therefore yield an insignificant contribution to the total field at longer ranges. This so-called *continuous* part of the wavenumber spectrum $0 \leq k \leq k_c$ can therefore be ignored for long range propagation. This is in fact the approximation made in most normal mode models where only the *discrete* part $k_c < k < k_m$ of the spectrum is considered. In SAFARI-FIP the wavenumber spectrum can be reduced by specifying a smaller value of CMAX. This will obviously lead to a smaller wavenumber spectrum, and thus to larger ranges covered by the FFT integration. Due to the fact that the wavenumber spectrum is a continuous function of k, an arbitrary truncation point may give rise to numerical artifacts such as wrap-around. The truncation is therefore usually determined in the following way:

1. Carry out steps 1 to 3 above.
2. By inspection of the integration kernels, choose a truncation point in the continuous spectrum where the amplitude is small. Calculate the corresponding phase velocity c_t. If only a single receiver depth is required choose CMAX $= c_t$ and proceed to next step. If more receiver depths are involved a universal truncation point with vanishing amplitude can usually not be found. In these cases and when the kernel has significant amplitude in the whole continuous spectrum, choose CMAX somewhat larger than c_t. Then use IC1 to specify the first sampling point where the calculation should start, and SAFARI will automatically taper the discontinuity. The same procedure is of course applicable if the wavenumber spectrum is truncated at the large wavenumber end, which requires a proper choice of CMIN and IC2.
3. Now perform steps 5 to 8 above.
4. If determination of both short and long range propagation is required, calculate the full-spectrum solution to a reasonable and convenient range as described above. Then compare the solutions to ensure that they overlap. If this is not the case – which will only very rarely happen – change the truncation point to include more of the *continuous* spectrum and re-calculate the long-range field until there is an overlapping region of identical results.

To the inexperienced user the procedure outlined here may seem very cumbersome, but as mentioned above the test of convergence is not needed for every small change in the parameters, and after a few trials it will probably seem a very logical procedure.

7.3. SAFARI-FIP EXAMPLES

Using basically the same environmental model as for the SAFARI-FIPR examples, we will here demonstrate the different features of SAFARI-FIP by a series of examples. These have been chosen such that also the numerical considerations involved in the wavenumber integration are illustrated.

In all cases the water depth will be 100 m and the ocean bottom is assumed to have the properties given in Table 4.

■ *7.3.1.* SAFARI-FIP *case 1: Seismic interface wave propagation*

In the first example we will calculate the transmission loss at 5 Hz for a source depth of 95 m and a receiver depth of 100 m and for ranges out to 5 km. This is done by specifying the data file given in Table 11.

After running SAFARI-FIP with this data file, the plot program FIPPLOT will produce the plots shown in Fig. 9. The kernel in the wavenumber integral representation of the normal stress at depth 100 m is shown in Fig. 9a. As can be observed, there are two distinct peaks. The large peak at a wavenumber of 0.07 m^{-1} is the fundamental interface mode. The second peak at a wavenumber of 0.017 m^{-1} is a virtual mode associated with propagation in the water column. Figure 9b shows the calculated transmission loss, clearly displaying an interference pattern produced by the interface mode and the virtual mode. It should be pointed out that the integration contour has not been offset in this case because no discrete normal modes are present. Had the frequency been chosen a little higher, however, the virtual mode would have moved into the discrete spectrum and given rise to a very sharp peak in the integration kernel. In that case option J could conveniently be selected, but this is dealt with in the following example.

As can be observed from Fig. 9a, the amplitude of the integration kernel is not insignificant at the truncation point defined by the parameter IC2. However, due to the tapering of the discontinuity and the fact that the exponential function is rapidly varying at the large wavenumbers, the influence of the truncation is insignificant. The significance of the truncation can of course be checked by increasing the value of IC2 and comparing the results.

Table 11
SAFARI-FIP case 1 data file

Data file	Description	Notes
SAFARI-FIP case 1	title	
N I T	options	1
5.0	frequency 5 Hz	
4	number of layers	
0 0 0 0 0 0 0	layer 1 (upper halfspace, vacuum)	2
0 1500 0 0 0 1 0	layer 2 (isovelocity water column)	2
100 1600 400 0.2 0.5 1.8 0	layer 3 (silt sediment)	
120 1800 600 0.1 0.2 2.0 0	layer 4 (sand sub-bottom)	
95	source depth 95 m	
100 100 1 1	receiver depth 100 m	
100 1E8	phase velocities CMIN and CMAX	3
2048 1 1000	wavenumber sampling parameters	4
0.0 5.0 20 1.0	range axis parameters	
20 80 12 10	transmission-loss axis parameters	

[1] Option N indicates that the normal stress (= − pressure) should be calculated. The I option will produce a plot of the depth-dependent Green's function, i.e. the kernel in the integral representation for the normal stress at the selected receiver depth. Option T will generate a plot of the transmission loss as function of range.

[2] The sea surface is introduced by including a vacuum upper halfspace, and the sea surface is chosen as the origin for the depth axis.

[3] In order to include the propagation directions close to vertical, CMAX has been set to a very large number such that $k_{min} \approx 0$. Since the source is close to the seabed and the frequency is relatively low, seismic interface waves will be excited. CMIN should therefore be chosen somewhat smaller than the smallest wave speed in the problem, i.e. the sediment shear speed 400 m/s. A value of 250 m/s would probably be sufficiently low. However, due to the link between the wavenumber and range sampling, Eq. (115), this would lead to a relatively course range sampling, $\Delta r \simeq c_{min}/f = 50$ m. To reduce this to 20 m, CMIN is specified as 100 m/s.

[4] The number of wavenumber sampling points, NW, is specified as $2048 = 2^{11}$, but since no wave phenomena are expected with phase velocities smaller than 200 m/s, the depth-dependent Green's function is only calculated for the first 1000 sampling points (IC1 = 1, IC2 = 1000), automatically invoking the discontinuity tapering.

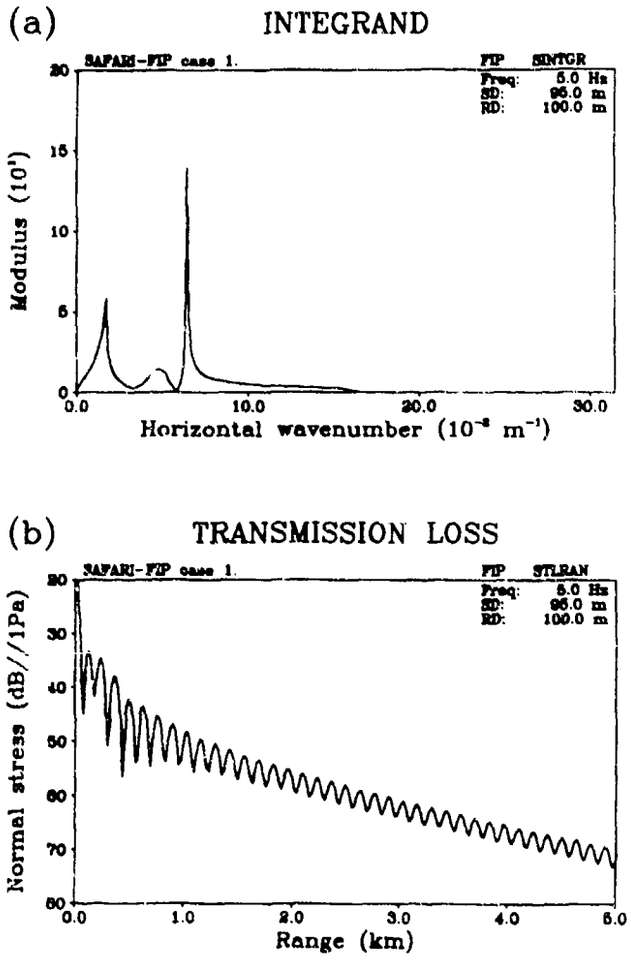

Fig. 9. **Results for SAFARI-FIP case 1: (a) depth-dependent Green's function as function of horizontal wavenumber; (b) calculated transmission loss as function of range.**

7.3.2. SAFARI-FIP *case 2: Normal mode propagation*

As a second example, a propagation problem is chosen where the interface wave is unimportant. Because of the characteristic exponential amplitude decay away from the guiding boundary, the interface wave is insignificant when either the source or the receiver is far away from the sea-bed in terms of wavelength. Typically, the contribution to the total field by the interface wave is insignificant if the source is one wavelength away from the sea-bed and if discrete modes are present in the water column. We will therefore place a 30 Hz source at mid-water depth and again calculate the transmission loss out to 5 km range for a receiver at the ocean bottom. To demonstrate how a velocity profile in the water column is specified, it is assumed that the sound speed has been measured to be 1500 m/s at the surface, 1480 m/s at 30 m depth, and 1490 m/s at the sea-bed. The data file is set up as shown in Table 12.

The results are shown in Fig. 10. Figure 10a shows the integration kernel with the velocity profile plot inserted. Two discrete modes are apparent, and a third mode is just around cut-off at the medium wavenumber for compressional waves in the sub-bottom, $k = 2\pi f/1800 \simeq 0.105$. The resulting transmission loss plotted in Fig. 10b is clearly dominated by the interference pattern produced by the 2 discrete modes for ranges larger than 1 km.

Table 12
SAFARI-FIP case 2 data file

Data file	Description	Notes
SAFARI-FIP case 2	title	
N I T J Z	options	1
30 0	frequency and contour offset	2
5	number of layers	
0 0 0 0 0 0 0	layer 1 (upper halfspace, vacuum)	
0 1500 -1480 0 0 1 0	layer 2 (water layer)	3
30 1480 -1490 0 0 1 0	layer 3 (water layer)	3
100 1600 400 0.2 0.5 1.8 0	layer 4 (silt sediment)	
120 1800 600 0.1 0.2 2.0 0	layer 5 (sand sub-bottom)	
50	source depth 50 m	
100 100 1 1	receiver depth 100 m	
700 1E8	phase velocities CMIN and CMAX	4
1024 1 512	wavenumber sampling parameters	5
0.0 5.0 20 1.0	range axis parameters	
20 80 12 10	transmission-loss axis parameters	
1450 1550 10 25	velocity axis for profile plot	1
0 100 10 20	depth axis for profile plot	1

[1] The first 3 options are the same as specified in case 1, but here option J has been specified to invoke the contour offset since discrete modes are present at this frequency. Further, option Z will generate a plot of the velocity profile in the water column. The associated axis specifications are given at the end of the data file.

[2] The frequency is specified as 30 Hz and the default contour offset will be applied since COFF = 0.

[3] By specifying a negative value for the shear speed, SAFARI will interpret the number as the negative of the compressional speed at the bottom of the layer, i.e. at the next interface. The solution obtained assumes a linear depth variation of $1/c_c^2$ within the layer.

[4] Although it can be demonstrated that the part of the spectrum with phase velocities smaller than ≈ 1400 m/s yields no significant contribution to the total field, a relatively small value of CMIN has been selected. This is again done in order to obtain a reasonable range sampling. In the present case $\Delta r \simeq c_{min}/f = 23.3$ m.

[5] As in the former case, by specifying IC2 = 512 the insignificant second half of the wavenumber spectrum is not calculated.

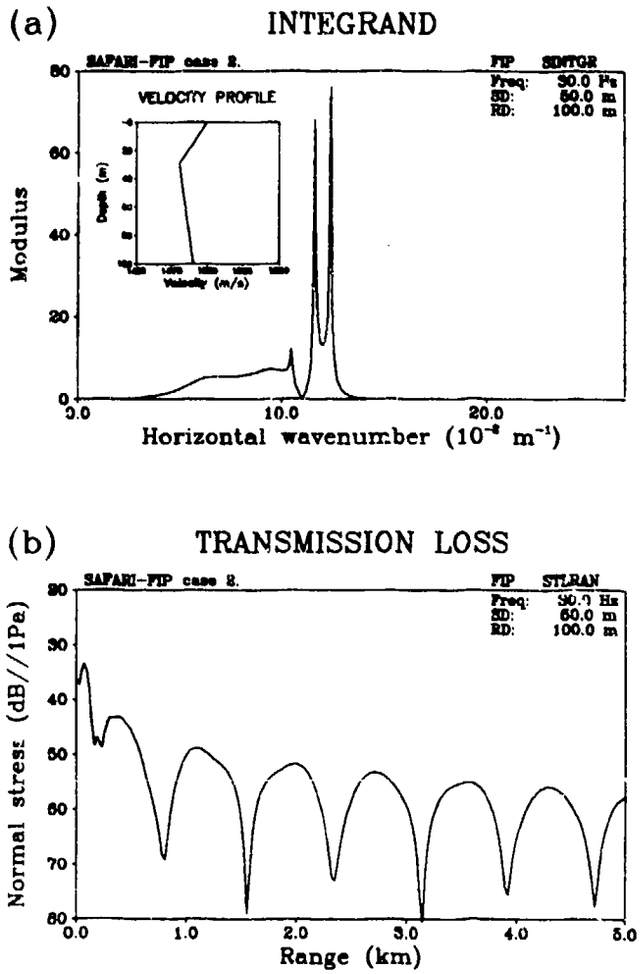

Fig. 10. **Results for SAFARI-FIP case 2: (a) depth-dependent Green's function as function of horizontal wavenumber with velocity-profile plot inserted; (b) calculated transmission loss as function of range.**

■ *7.3.3.* SAFARI-FIP *case 3: Transmission loss vs depth and range*

Next, we take exactly the same problem considered in case 2, but calculate the transmission loss at several receiver depths, both in the water column and in the sediment, and produce a contour plot of the loss as a function of range and depth. Further, we produce a plot of the transmission loss averaged over depth as a function of range. The data file is given in Table 13.

The resulting plot of the depth-averaged transmission loss is shown in Fig. 11a. Note that the averaging removes the interference pattern seen at the individual receiver depths, Fig. 10b. The contour plot produced by the CONTUR program is shown in Fig. 11b. The periodic pattern for ranges longer than a couple of kilometres is typical for a 2-mode propagation problem. The actual contouring grid size is indicated by the small 'box' at the upper left corner of the plot.

Figure 12 shows two out of a total of 5 plots of transmission loss *vs* depth produced by option D.

Table 13
SAFARI-FIP case 3 data file

Data file	Description	Notes
SAFARI-FIP case 3	title	
N C A D J	options	1
30 0	frequency and contour offset	
5	number of layers	
0 0 0 0 0 0 0	layer 1 (upper halfspace, vacuum)	
0 1500 -1480 0 0 1 0	layer 2 (water layer)	
30 1480 -1490 0 0 1 0	layer 3 (water layer)	
100 1600 400 0.2 0.5 1.8 0	layer 4 (silt sediment)	
120 1800 600 0.1 0.2 2.0 0	layer 5 (sand sub-bottom)	
50	source depth 50 m	
0.1 120 41 40	receiver depths 0.1–120 m	2
1350 1E8	phase velocities CMIN and CMAX	3
1024 1 950	wavenumber sampling parameters	4
0.0 5.0 20 1.0	range axis parameters	5
20 80 12 10	transmission-loss axis parameters	
0 120 12 20	depth axis for contour plot	
40 70 6	contour levels in dB	

[1] Option C will create a contour plot of the transmission loss as a function of depth and range, whereas option A will calculate the depth-averaged transmission loss over the specified number of receiver depth. Option D will generate plots of transmission loss *vs* depth at the ranges defined by the range axis parameters, see note 5 below.

[2] 41 receivers will be placed equidistantly in the depth interval 0.1–120 m. Note that the first receiver is not placed on the surface where the field is known to vanish and thus has an undefined dB level. The last parameter in this line is IR = 40. This parameter is dummy in the present case; but if option I or T had been specified, an integrand or transmission loss plot would be created for every 40 receiver depth, i.e. here for the first and last depth only.

[3] Compared to case 2, the wavenumber interval is smaller here, since a very fine range sampling is not crucial for the contour plots as a consequence of the CONTUR program performing a smooth interpolation between the data points. The present choice of CMIN and CMAX translates into a range step of $\Delta r \simeq 45$ m.

[4] The tapering is again activated by specifying IC2 = 950.

[5] The range axis parameters are applied to both the plot of the depth-averaged transmission loss and the contour plot. Further, they determine the ranges for which transmission loss vs depth will be plotted (option D). Thus, these plots will be produced at the ranges corresponding to the tick marks on the range axis.

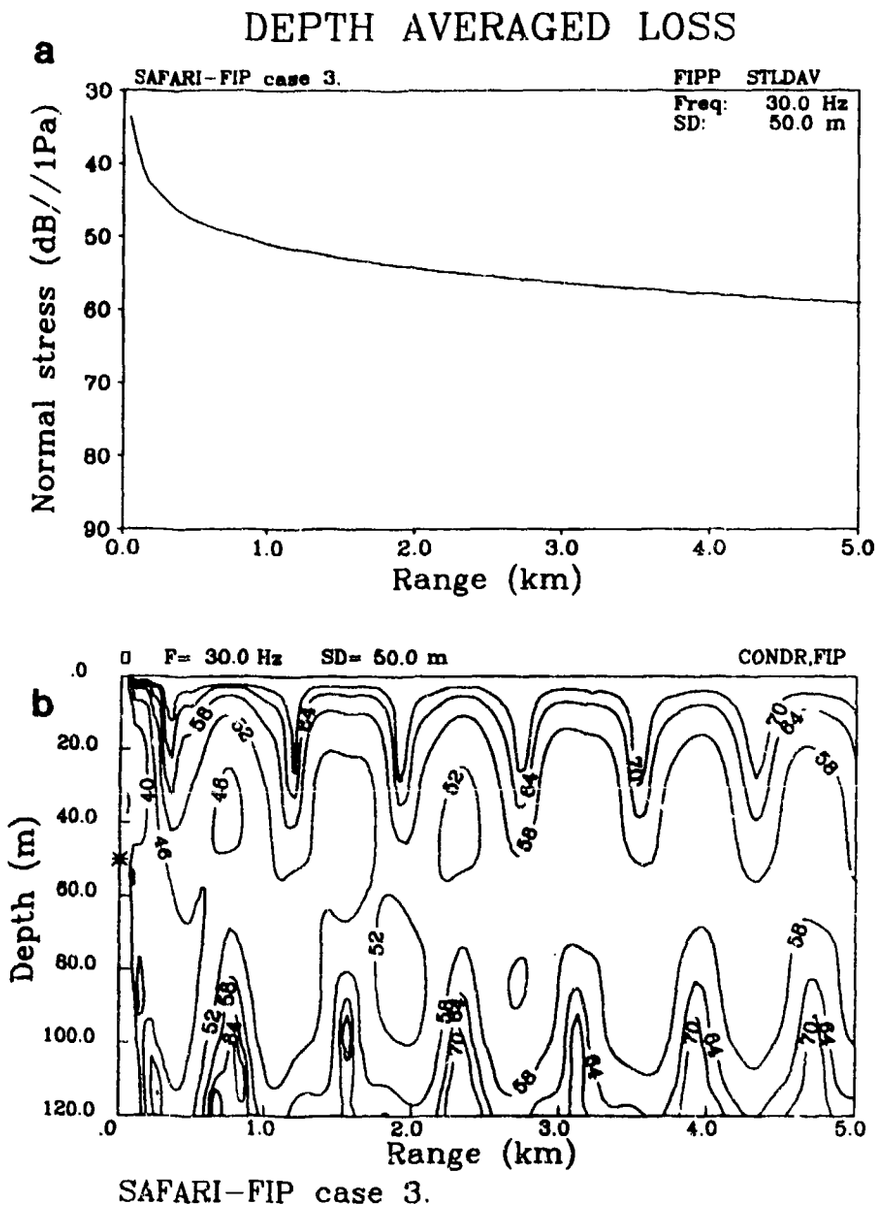

Fig. 11. **Results for SAFARI-FIP case 3: (a) depth-averaged transmission loss as function of range; (b) contour plot of transmission loss as function of range and depth.**

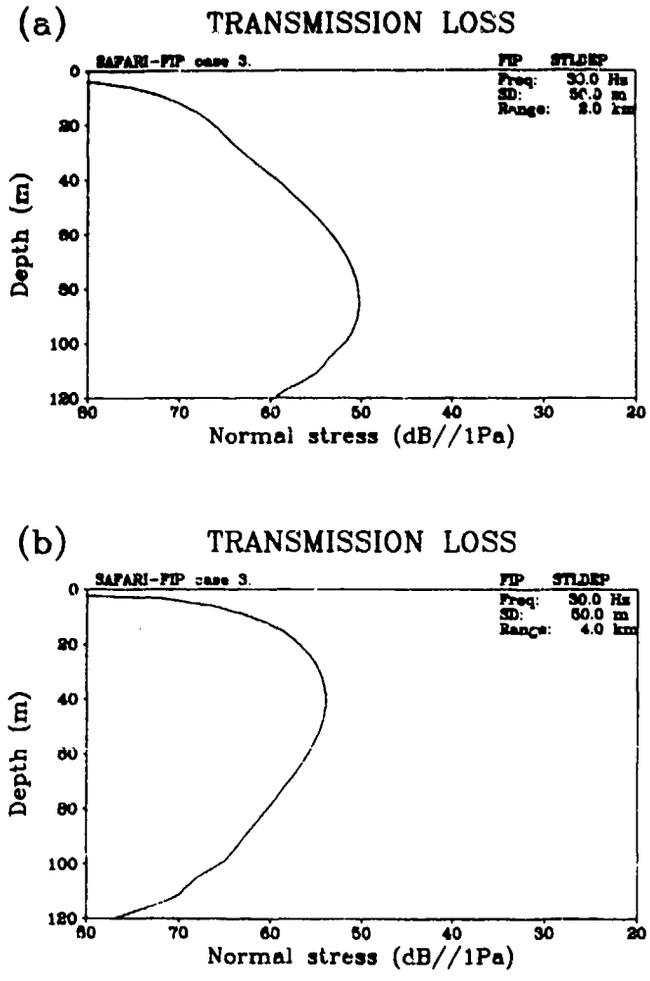

Fig. 12. Results for SAFARI-FIP case 3: (a) transmission loss *vs* depth at 2 km range; (b) transmission loss *vs* depth at 4 km range.

■ 7.3.4. SAFARI-FIP *case 4: Long-range propagation*

In this example it is demonstrated how long-range propagation problems are treated by properly truncating the integration interval. The problem considered is exactly the same as in case 2, but now the transmission loss should be calculated out to a range of 50 km. If the wavenumber interval was left unchanged, several thousand sampling points would be required. It is well known, however, that except for very short ranges – typically less than a few water depths – the field will be entirely dominated by the two propagating normal modes, clearly showing up as sharp peaks in the integrand plot of Fig. 10a. The long-range propagation loss can therefore be calculated by including only the discrete part of the spectrum containing the two modes, significantly reducing the required sampling. This is done by creating the data file given in Table 14.

The resulting plots of the integration kernel and the transmission loss are shown in Fig. 13. As can be observed, the wavenumber interval has been properly truncated.

Table 14
SAFARI-FIP case 4 data file

Data file	Description	Notes
SAFARI-FIP case 4	title	
N I T J	options	
30 0	frequency and contour offset	
5	number of layers	
0 0 0 0 0 0 0	layer 1 (upper halfspace, vacuum)	
0 1500 -1480 0 0 1 0	layer 2 (water layer)	
30 1480 -1490 0 0 1 0	layer 3 (water layer)	
100 1600 400 0.2 0.5 1.8 0	layer 4 (silt sediment)	
120 1800 600 0.1 0.2 2.0 0	layer 5 (sand sub-bottom)	
50	source depth 50 m	
100 100 1 1	receiver depth 100 m	
1300 1750	phase velocities CMIN and CMAX	1
512 46 465	wavenumber sampling parameters	2
0.0 50 20 10	range axis parameters	
40 120 12 20	transmission-loss axis parameters	

[1] A proper value of CMAX is found by observing the full integrand in Fig. 10a. An obvious point to truncate is where the amplitude vanishes at the wavenumber 0.11 m^{-1}, corresponding to a phase velocity of 1712 m/s. The actual value of CMAX has been chosen a little larger, as 1750 m/s. The value of CMIN is less critical, but 1300 m/s has been chosen to yield a reasonable range sampling.

[2] Since CMAX was not chosen equal to the actual value corresponding to the wavenumber where the integrand amplitude was zero, IC1 is given a value which will start calculation at this particular point. Also, since the integrand amplitude is known to be insignificant at the high wavenumber end of the selected interval, IC2 is set to a value smaller than NW.

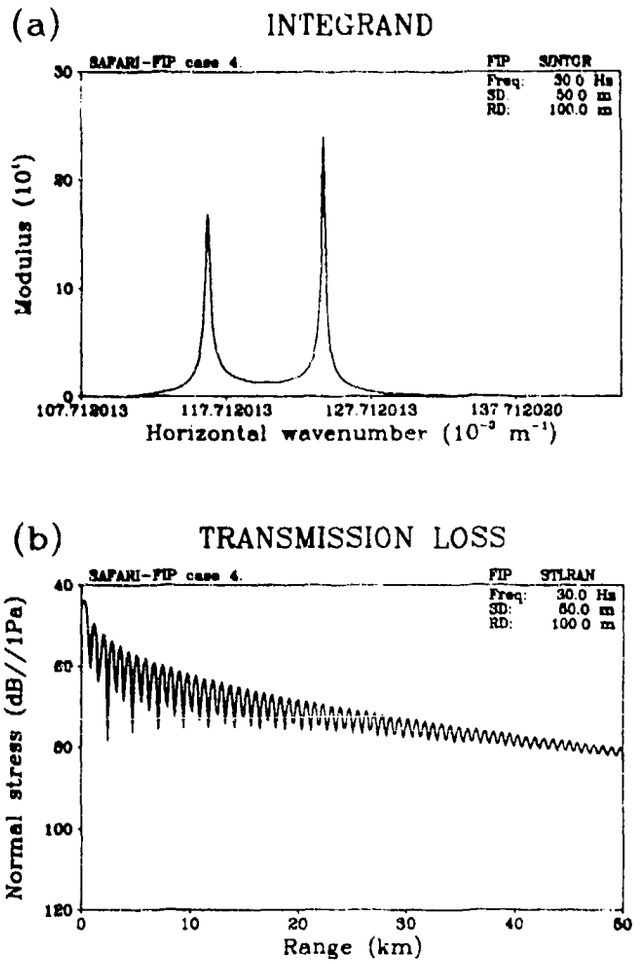

Fig. 13. Results for SAFARI-FIP case 4: (a) truncated integration kernel as function of horizontal wavenumber; (b) calculated transmission loss as function of range.

■ 7.3.5. SAFARI-FIP case 5: Beam propagation

In this last example it is demonstrated how SAFARI-FIP is applied to a beam propagation problem. A linear vertical array, placed at mid-water depth in the environment treated in case 1, is generating a 1000 Hz gaussian beam impinging on the bottom at a nominal grazing angle of 25°. The task is to investigate the reflection and transmission characteristics of this beam by generating a contour plot of the sound-pressure field in depth and range. The data file is set up in Table 15.

The contour plot produced by means of the DISSPLA plot package is shown in Fig. 14a, whereas Fig. 14b shows the corresponding UNIRAS contour plot with dark shading indicating high levels. Since the angle of incidence of the beam is between the critical angles of the silt layer and the sub-bottom, the incident beam is both reflected and transmitted at the water/sediment interface whereas the transmitted beam is totally reflected at the sediment/subbottom interface. The resulting complex beam-splitting reflectivity pattern is easily observed. More beam examples can be found in [21,22,26,27].

Table 15
SAFARI-FIP case 5 data file

Data file	Description	Notes
SAFARI-FIP case 5	title	
P N C L	options	1
1000	frequency 1 kHz	
4	number of layers	2
65 1500 0 0 0 1 0	layer 1 (upper halfspace, water)	2
65 1500 0 0 0 1 0	layer 2 (isovelocity water layer)	2
100 1600 400 0.2 0.5 1.8 0	layer 3 (silt sediment)	
120 1800 600 0.1 0.2 2.0 0	layer 4 (sand sub-bottom)	
50 41 0.75 25.0 4 100	source array parameters	3
50 125 51 52	receiver depths 50 to 125 m	
1500 5000	phase velocities CMIN and CMAX	4
2048 1400 1950	wavenumber sampling parameters	5
0.0 0.3 20 0.05	range axis for contour plot	
50 125 12 25	depth axis for contour plot	
24 54 6	contour levels in dB	

[1] Option P indicates that the sources are line sources rather than point sources. The calculations are therefore performed in plane geometry, and the calculated parameter is the normal stress, option N. Option C generates a contour plot of the field in depth and range. Finally, option L indicates that the field is generated by a vertical linear array.

[2] Since only the first bottom bounce of the beam is of interest, the sea surface is removed by replacing the water column by an infinite halfspace. Note that a dummy interface has been introduced just below the lowermost source in the array. This is a 'trick', reducing the computation time in cases where many sources and receivers are present. This is due to the fact that the homogeneous solution within a layer has to be superimposed with the direct source field – an operation which must be performed for every source/receiver combination within each layer. In the present case the introduction of the dummy interface reduces the number of receivers present in the source layer to the uppermost 10, and the savings in computational effort more than compensates for the additional computation involved in adding an extra interface. It is left as an exercise to the user to demonstrate this.

[3] Since option L was chosen, all 7 source parameters have to be specified. The mid-point of the array is 50 m, i.e. in the middle of the water column. The array has 41 elements with a spacing of 0.75 m, i.e. half a wavelength. The total array length is therefore 30 m. The steering angle is 25° downward with respect to horizontal. The array is of type 4, indicating a Gaussian, non-focusing shading. The focal depth, specified to the depth of the sea-bed, is therefore dummy in this case

[4] Although the wavenumber spectrum of the parallel beam will be relatively narrow, almost the whole spectrum of propagation angles in the water has been included in order to get a reasonable range sampling.

[5] The wavenumber sampling parameters have been chosen such that only the non-vanishing part of the spectrum is included. This can be shown by adding option I to obtain plots of the integration kernel.

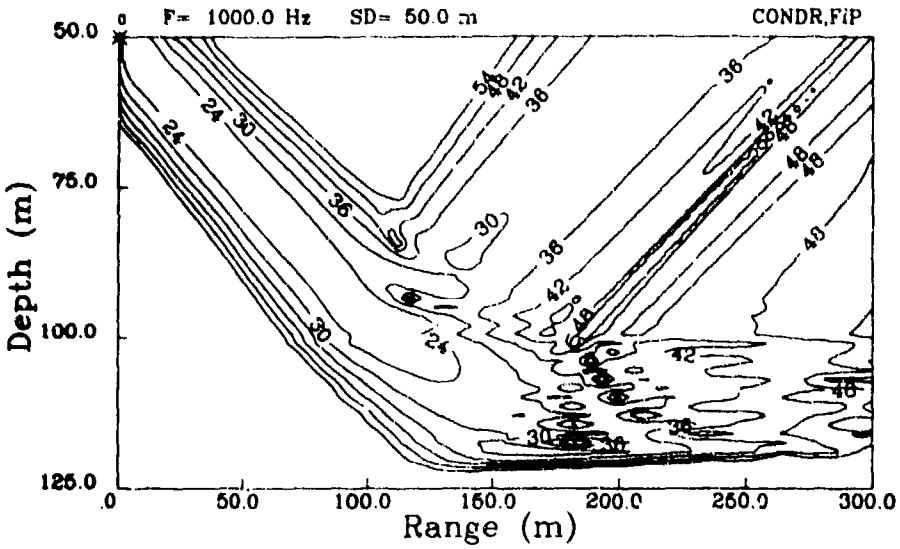

SAFARI- FIP case 5.

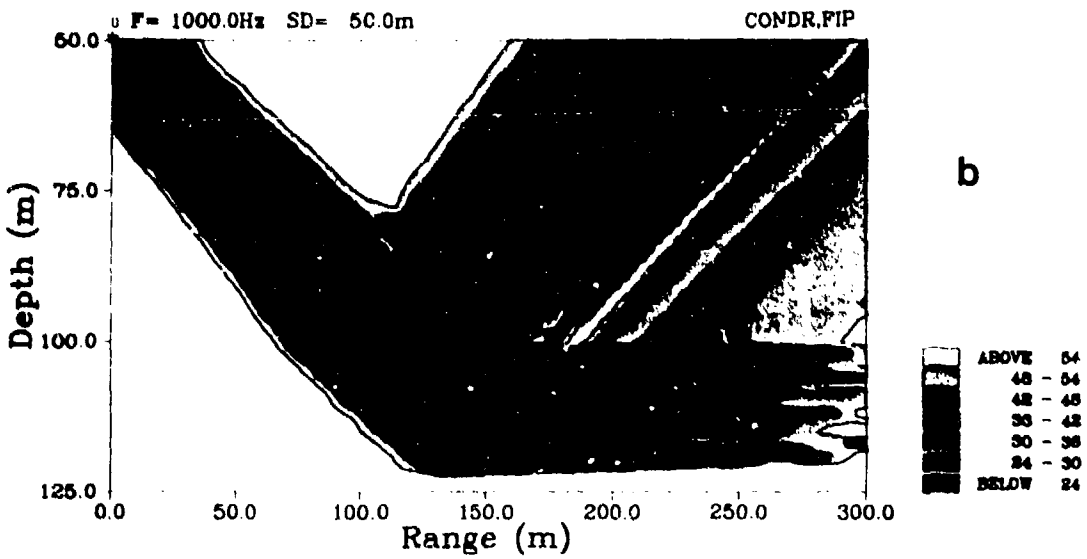

SAFARI–FIP case 5.

Fig. 14. **Results for SAFARI-FIP case 5: (a) contours in depth and range of beam-generated acoustic field produced by the DISSPLA package; (b) contour plot produced by UNIRAS.**

8. Running SAFARI-FIPP

The SAFARI-FIPP module calculates the depth-dependent Green's function for a selected number of frequencies and determines the pulse response at a given receiver position by evaluating first the wavenumber integral, Eq. (13), and then the frequency integral, Eq. (8). As was the case for SAFARI-FIP, both stresses and particle velocities can be determined, and the field may be produced by either point or line sources. By arranging the sources in a vertical phased array, pulsed beam propagation can be analysed.

The time response is of course dependent on the pulse shape at the source. In SAFARI-FIPP the user can either select one of the five internal pulse shapes or create an external file containing any desired pulse shape. In either case the source pulse is defined as the pressure pulse produced at a distance of 1 m from the source (for solids the negative of the normal stress 1 m *below* the source). The time dependence is therefore *not* directly that of the forcing term in the potential wave equation, Eq. (6). This is important to note when comparing the SAFARI-FIPP solutions with those obtained by other codes.

The pulse response output is available as either individual pulse plots for single receivers or as stacked plots, where the stacking can be performed in either range or depth. For the individual plots the time series are produced in true units, i.e. Pa for stresses and m/s for particle velocities, again assuming that the source pulse shape is given in Pa. For the stacked plots the individual traces are scaled according to certain rules specified in the following.

All inputs to SAFARI-FIPP are read from the file currently assigned to the logical file FOR001. Before running the program the user has to assign the file containing the input data to this logical name. The most convenient approach is to include this assignment in a general command file which also assigns file names to the logical names of the output files, as described in Subsect. 5.6.

As was the case for the single-frequency module, successful use of SAFARI-FIPP is highly dependent on the parameters specified, in particular those related to the truncation and discretization for carrying out numerical integrations. It is obvious that the additional frequency integration performed in SAFARI-FIPP makes this module even more difficult to use than SAFARI-FIP. It is therefore important that the user be extremely confident in running SAFARI-FIP before trying to use the pulse model. In the following the preparation of input files is first discussed in detail and then the numerical considerations particular to the pulse model are addressed.

Table 16
Parameters of SAFARI-FIPP input files: Calculation and environmental parameters

Block		Parameter	Units	Limits
I	TITLE :	title of run	–	≤ 80 char.
II	opt1 opt2 ...:	output options	–	≤ 40 char.
III	FREQ:	source centre frequency	Hz	> 0
	COFF:	integration contour offset	dB/Λ	COFF ≥ 0
IV	NL:	number of layers, incl. halfspaces	–	NL ≥ 2
	D:	depth of interface	m	–
	CC:	compressional speed	m/s	CC ≥ 0
	CS:	shear speed	m/s	–
	AC:	compressional attenuation	dB/Λ	AC ≥ 0
	AS:	shear attenuation	dB/Λ	AS ≥ 0
	RO:	density	g/cm^3	RO ≥ 0
	RG:	rms value of interface roughness	m	–
	CL:	correlation length of roughness	m	CL > 0
V	SD:	source depth (mean for array)	m	–
	NS:	number of sources in array	–	NS > 0
	DS:	vertical source spacing	m	DS > 0
	AN:	grazing angle of beam	deg	–
	IA:	array type	–	1 ≤ IA ≤ 5
	FD:	focal depth of beam	m	FD ≠ SD
VI	RD1:	depth of first receiver	m	–
	RD2:	depth of last receiver	m	RD2 > RD1
	NR:	number of receivers	–	NR > 0
VII	CMIN:	minimum phase velocity	m/s	CMIN > 0
	CMAX:	maximum phase velocity	m/s	–
VIII	NW:	number of wavenumber samples	–	NW ≥ 1
	IC1:	first sampling point	–	IC1 ≥ 1
	IC2:	last sampling point	–	IC2 ≤ NW
	IINC:	integrand plot increment	–	IINC ≥ 0
IX	NT:	number of time samples	–	NT= 2^M
	F1:	low frequency limit	Hz	F1 ≥ 0
	F2:	high frequency limit	Hz	F2 >F1
	DT:	time sampling increment	s	DT > 0
	RO:	first receiver range	km	–
	DR:	receiver range increment	km	DR ≠ 0
	NRAN:	number of ranges	–	NRAN ≥ 0

8.1. INPUT FILES FOR SAFARI-FIPP

The input data are structured in 13 blocks. The first nine, described in Table 16, specify the title, options, frequency, environmental parameters, source and receiver geometry and finally the wavenumber and frequency integration parameters. The last four blocks, described in Table 17, contain axis specifications for the graphical output. Some of these blocks should always be included and others only if certain options have been specified. The single blocks and parameters are described in detail in the following.

Table 17
Parameters of SAFARI-FIPP input files: Plot parameters

Block		Parameter	Units	Limits
X[1]	CRED:	reduction velocity	m/s	CRED ≥ 0
	TMIN:	start of time window	s	–
	TMAX:	end of time window	s	–
	TLEN:	length of time aixs	cm	TLEN > 0
	TINC:	distance between tick marks	s	TINC > 0
XI[2]	SPLO:	lower limit of stacked plots	m or km	–
	SPUP:	upper limit of stacked plots	m or km	–
	SPLN:	length of stacking axis	cm	SPLN > 0
	SPIN:	distance between tick marks	m or km	SPIN > 0
XII[3]	NMOD:	number of modes	–	NMOD ≥ 1
	FMIN:	min. freq. dispersion curves	Hz	FMIN ≥ 0
	FMAX:	max. freq. dispersion curves	Hz	FMAX > 0
	FLEN:	lenght of frequency axis	cm	FLEN > 0
	FINC:	frequency tick mark spacing	Hz	FINC > 0
	GVLO:	min. phase/group velocity	m/s	GVLO > 0
	GVUP:	max. phase/group velocity	m/s	GVUP > 0
	GVLN:	lenght of velocity axis	cm	GVLN > 0
	GVIN:	velocity tick mark spacing	m/s	GVIN > 0
XIII[4]	VLEF:	wave speed at left border	m/s	–
	VRIG:	wave speed at right border	m/s	–
	VLEN:	length of wave speed axis	cm	VLEN > 0
	VINC:	wave speed tick mark distance	m/s	VINC > 0
	DV' :	depth at upper border	m	–
	DVLO:	depth at lower border	m	–
	DVLN:	length of depth axis	cm	DVLN > 0
	DVIN:	depth axis tick mark interval	m	DVIN > 0

[1] Only for option R or NRAN > 0. [2] Only for options S and D. [3] Only for option G.
[4] Only for option Z.

BLOCK I – TITLE

Lines:	1
Required:	Always
Syntax:	TITLE
Format:	A80
Description:	TITLE: Title of run. Maximum 80 characters.

BLOCK II – OPTIONS

Lines:	1
Required:	Always
Syntax:	`opt1 opt2 opt3...`
Format:	Free. Maximum 40 alphanumeric characters.
Description:	Series of alphanumeric characters specifying the desired options. The following are implemented at present:

`B`: If this option is specified the slowness interval (or phase velocity interval) will be held constant at all frequencies. As a default procedure, the wavenumber interval will be determined from the specified phase velocities and the maximum frequency and will then be held constant at all lower frequencies. The `B` option should be used when only a certain part of the angular spectrum is considered, e.g. the discrete spectrum containing normal modes. On the other hand, when evanescent waves are considered, e.g. seismic interface waves, the wavenumber interval should be held constant in order to include the whole exponential 'tail' at the low frequencies; thus in these cases the `B` option should be omitted. It is always a good habit to check the integrand at a selected number of frequencies (`XINC` > 0)

`D`: For each selected range the pulses will be plotted in a depth-stacked format. This is the VSP (vertical seismic profiling) type of output used in seismology. No geometrical spreading compensation is performed in the depth-stacked format, but a common scaling factor determined for the upper trace is applied. As for option `S`, the scaling is performed individually for each stacked plot; the amplitudes for different ranges therefore cannot be directly compared. The depth-stacked plots, however, can be rescaled by running FIPPLOT with option `RES`.

`F`: The Filon integration scheme is used for the wavenumber integration instead of the standard scheme based on the trapezoidal rule.

BLOCK II – (Continued)

Description:

G: Dispersion curves are plotted for a selected number of interface modes and normal modes. The modes are not found directly by searching for singularities but indirectly by localising maxima in the depth-dependent Green's function. The user should therefore be sure that the mode of interest is present at the selected depth at all frequencies. Otherwise a 'false' mode may be found, leading to discontinous dispersion curves.

H: Horizontal particle velocity is calculated.

J: Complex wavenumber integration contour is applied. The contour is shifted into the upper halfplane by an offset controlled by the input parameter COFF (Block III).

L: Sources are arranged in a vertical line array.

N: Normal stress σ_{zz} ($= -p$ in fluids) is calculated.

P: Plane geometry. The sources will be line sources instead of point sources as used in the default cylindrical geometry.

R: Plot of source pulse at 1 m distance from a single source will be produced together with a plot of the associated frequency spectrum. The chosen source pulse is filtered to exclude frequencies outside the interval considered in the calculation (Block IX).

S: For each selected receiver depth the pulses are plotted in a range-stacked format. The vertical axis of the plots represents the range, and each receiver trace is placed with the zero-line at the corresponding range value. In order to remove the effect of spherical spreading, the amplitudes are first multiplied by the range of the actual receiver, and then a common scaling factor is applied to all traces. This factor is determined such that the trace for the first receiver range does not overlap the next trace. This scaling is performed individually for each receiver depth; thus the amplitudes for different receivers cannot be directly compared. The scaling may be changed by running the plot program FIPPLOT with the RES option as described in Appendix B.

BLOCK II – (Continued)

Description:

V: Vertical particle velocity is calculated.

X: If sources are present in a solid medium, these will be considered vertical point forces (line forces in plane geometry) rather than omnidirectional sources.

Z: Plot of velocity profile is generated.

n: Digit determining the desired source pulse, defined as the pressure or normal stress produced at 1 m distance from the source. There are five internal pulse shapes, shown together with their normalised frequency spectra in Figs. 15 to 19. The user can, however, create any desired pulse shape in an external file and read it in by specifying $n = 0$. The internal pulse shapes in pressure (negative of normal stress) are functions of time t and the centre angular frequency $\omega_c = 2\pi f_c$ as follows:

[1] This is the default source pulse, defined by the function

$$f(t) = 0.75 - \cos\omega_c t + 0.25\cos 2\omega_c t, \qquad 0 \le t \le T = 1/f_c.$$

[2] This source pulse has the shape

$$f(t) = \sum_{i=1}^{3} A_i i^2 \cos(2\pi i t/T), \qquad 0 \le t \le T = 1.55/f_c.$$

where $A_1 = 0.48829$, $A_2 = -0.14128$ and $A_3 = 0.01168$, ensuring vanishing first and second derivatives at $t = 0$ and $t = T$.

BLOCK II – (Continued)

Description:

[3] A single sine period

$$f(t) = \sin \omega_c t, \qquad 0 \le t \le T = 1/f_c.$$

[4] This option creates a source pulse with a time dependence consisting of 4 sine periods, weighted with a Hanning window,

$$f(t) = \tfrac{1}{2} \sin \omega_c t \left(1 - \cos \tfrac{1}{4}\omega_c t\right), \qquad 0 \le t \le T = 4/f_c.$$

[5] The last internal source pulse is the one often used in seismology [14],

$$f(t) = \sin \omega_c t - \tfrac{1}{2} \sin 2\omega_c t, \qquad 0 \le t \le T = 1/f_c.$$

If option [0] is specified the source pulse is read from the file currently assigned to the logical unit 66. This file should be formatted and contain the amplitude sampled with the same interval as specified by the parameter DT (Block IX), and with one sample per record. The duration of the source pulse is determined automatically by detection of the end-of-file.

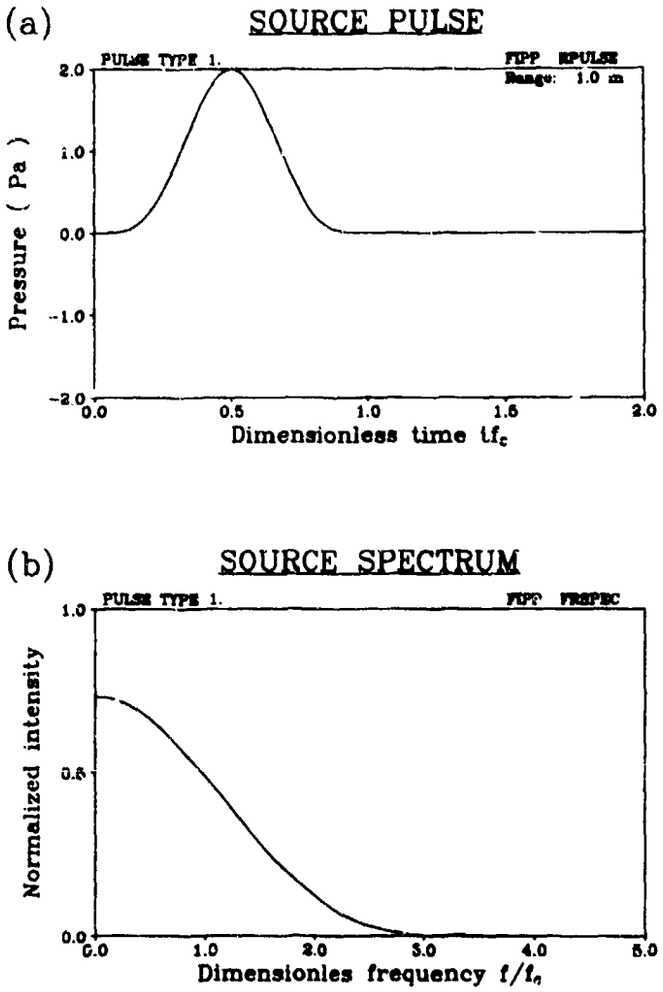

Fig. 15. **SAFARI-FIPP source pulse no. 1 and its frequency spectrum.**

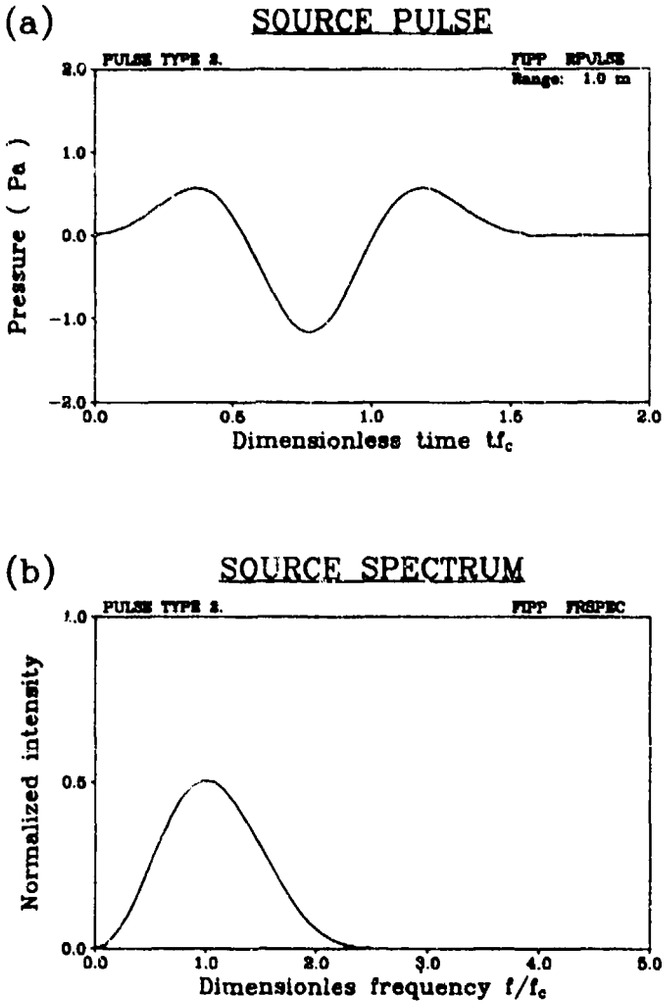

Fig. 1b. SAFARI-FIPP source pulse no. 2 and its frequency spectrum.

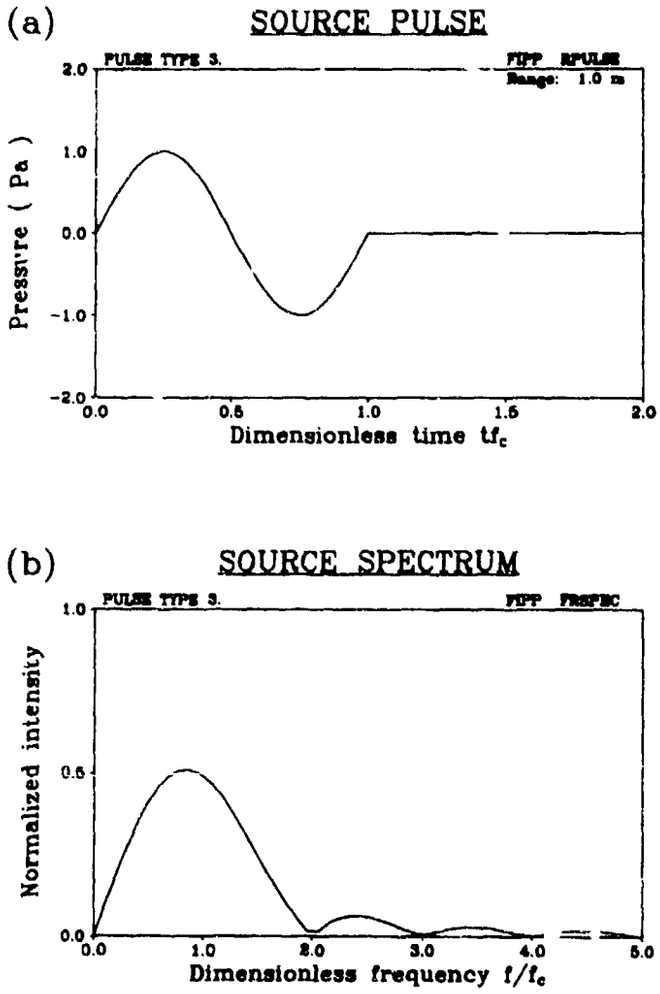

Fig. 17. **SAFARI-FIPP source pulse no. 3 and its frequency spectrum.**

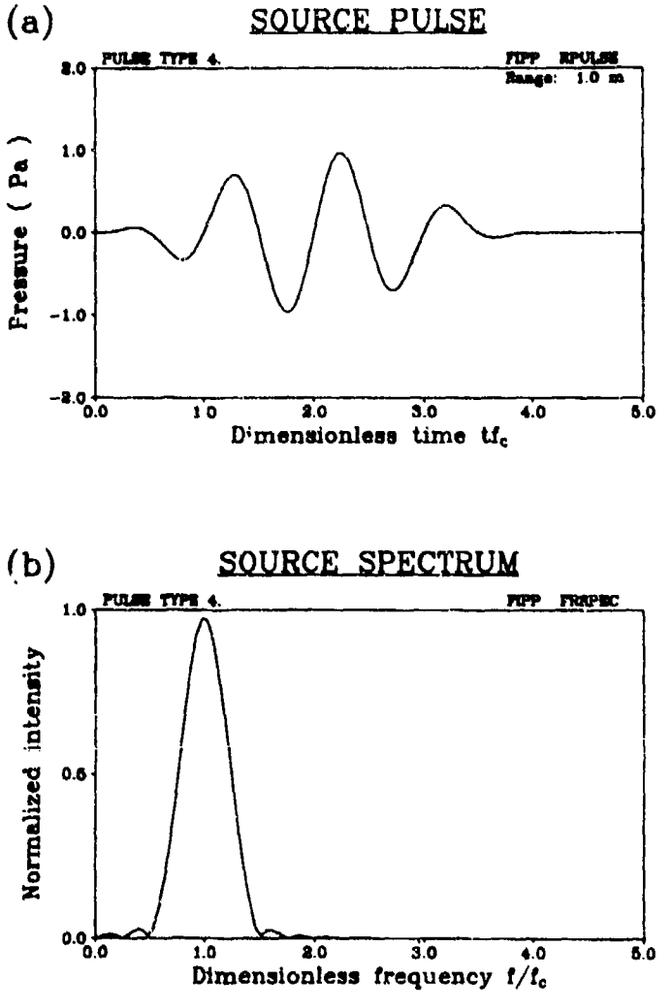

Fig. 18. SAFARI-FIPP source pulse no. 4 and its frequency spectrum.

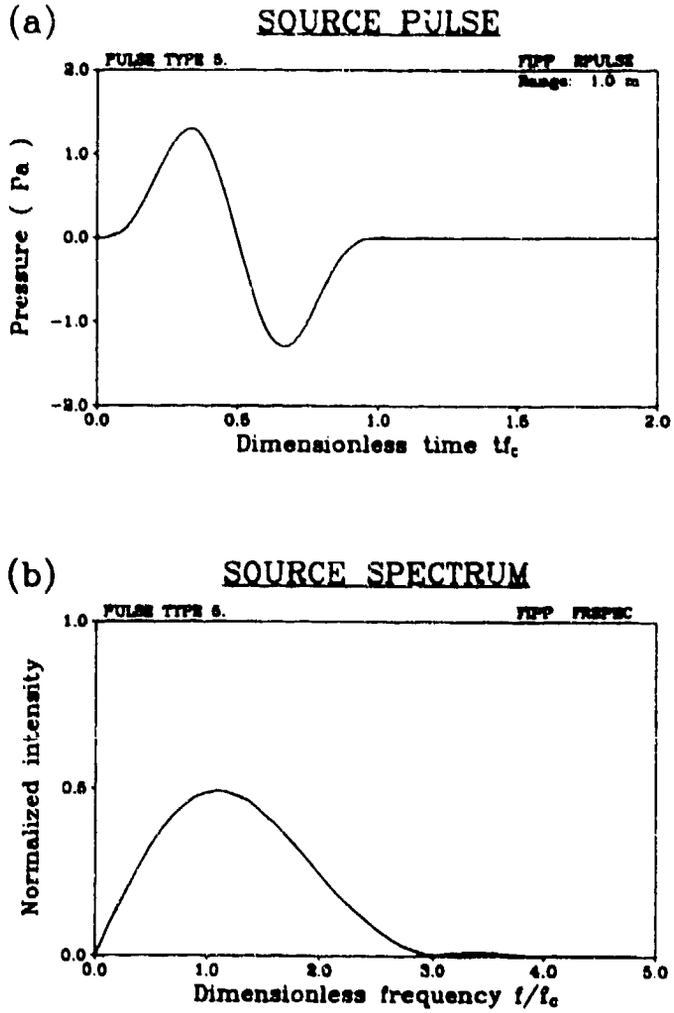

Fig. 18. SAFARI-FIPP source pulse no. 5 and its frequency spectrum.

BLOCK III – FREQUENCY

Lines: 1
Required: Always
Syntax: FREQ, COFF
Format: Free
Description:

FREQ: Centre frequency f_c of source spectrum in Hz.

COFF: Wavenumber integration contour offset. To be specified in dB/Λ, where Λ is the wavelength at the source depth SD. Since only the horizontal part of the integration contour is considered, this parameter should not be chosen so large that the amplitudes at the ends of the integration interval become significant. In lossless cases too small values will give sampling problems at the normal modes and other singularities. For intermediate values, the result is independent of the choice of COFF, but it is recommended to use a value which at the centre frequency f_c is the same as that used by SAFARI-FIP for the same number of sampling points, i.e.

$$\mathtt{COFF} = 60 c_c(z_s)(c_{\min}^{-1} - c_{\max}^{-1})/\mathtt{NW}.$$

This value is the default which is applied if option J is specified and COFF = 0.

BLOCK IV – ENVIRONMENTAL DATA

Lines: ≥ 3
Required: Always
Syntax:

```
NL
D(1) CC(1) CS(1) AC(1) AS(1) RO(1) RG(1) CL(1)
D(2) CC(2) CS(2) AC(2) AS(2) RO(2) RG(2) CL(2)
:
D(NL)CC(NL)CS(NL)AC(NL)AS(NL)RO(NL)RG(NL)CL(NL)
```

Description:

NL: Number of layers, including the upper and lower halfspaces. These should always be included, even in cases where they are vacuum.

D(): Depth z in m of upper boundary of layer or halfspace. The reference depth can be choosen arbitrarily, and D() is allowed to be negative. For layer no. 1, i.e. the upper halfspace, this parameter is dummy.

CC(): Velocity c_c of compressional waves in m/s. If specified as 0.0, the layer or halfspace is a vacuum.

CS(): Velocity c_s of shear waves in m/s. In order to be physically meaningful, it is required that $c_s \leq \sqrt{0.75}c_c$. If specified as 0.0, the layer or halfspace is fluid. If $c_s < 0$, it represents the compressional velocity at the bottom of the actual layer, which is treated as fluid with $1/c(z)^2$ varying linearly with depth.

AC(): Attenuation γ_c of compressional waves in dB/λ. If the layer is fluid, and AC() is specified as 0.0, then an empirical water attenuation is used.

AS(): Attenuation γ_s of shear waves in dB/λ. For the attenuations to be physically meaningful, it is required that

$$\frac{\gamma_s}{\gamma_c} \leq \frac{3}{4}\left(\frac{c_c}{c_s}\right)^2$$

BLOCK IV – (Continued)

Description:

RO(): Density ρ in g/cm^3.

RG(): RMS roughness of interface in m. RG(1) is dummy. If RG > 0 the Kirchhoff approximation is used for the scattering loss, i.e. CL $\rightarrow \infty$. This is computationally faster than doing the full scattering theory, but it is only applicable for small roughnesses and large correlation lengths. To invoke the full non-Kirchhoff scattering RG must be specified equal to the negative rms roughness, i.e. RG < 0.

CL(): Correlation length of roughness in m. This parameter is only required if non-Kirchhoff scattering has been selected, i.e. RG < 0.

BLOCK V – SOURCE DATA

Lines: 1
Required: Always
Syntax: Option L: SD NS DS AN IA FD
else: SD

Format: Free
Description:

SD: Source depth z_s in m. If option L has been specified, SD defines the mid-point of the vertical source array.
NS: Number of sources in the array.
DS: Source spacing in m.
AN: Specifies the nominal grazing angle of the generated beam in degrees. AN > 0 corresponds to downward propagation.
IA: Array type
[1] Rectangular weighted array
[2] Hanning weighted array
[3] Hanning weighted focused array
[4] Gaussian weighted array
[5] Gaussian weighted focused array
FD: Focal depth in m for an array of type 3 or 5.

BLOCK VI – RECEIVER DATA

Lines: 1
Required: Always
Syntax: RD1 RD2 NR
Format: Free
Description:

RD1: Receiver depth in m. If the calculations are to be performed for more than one receiver, i.e. NR > 1, then RD1 specifies the uppermost receiver.

RD2: If NR > 1 this parameter determines the depth of the lowermost receiver. If NR = 1, then the parameter RD2 is dummy.

NR: Number of receiver depths considered.

BLOCK VII – PHASE VELOCITIES

Lines: 1
Required: Always
Syntax: `CMIN CMAX`
Format: Free
Description:

`CMIN`: Minimum phase velocity c_{min} in m/s. Determines the upper limit of the truncated horizontal wavenumber space:

$$k_{max} = 2\pi f / c_{min}$$

where f is the actual frequency if option B was selected; otherwise f is the maximum frequency F2. In this last case k_{max} will therefore be independent of frequency.

`CMAX`: Maximum phase velocity c_{max} in m/s. Determines the lower limit of the truncated horizontal wavenumber space:

$$k_{min} = 2\pi f / c_{max}$$

where f is the actual frequency if option B was selected; otherwise f is the maximum frequency F2. In this last case k_{min} will therefore be independent of frequency. In plane geometry (option P) CMAX may be specified as negative, and the negative wavenumber spectrum will then be included with $k_{min} = -k_{max}$, yielding a correct solution also at zero range. Contour offset (option J) is not allowed in this case.

BLOCK VIII – WAVENUMBER SAMPLING

Lines: 1
Required: Always
Syntax: NW IC1 IC2 IINC
Format: Free
Description:

NW: Number of sampling points in wavenumber space. Since the Fast Field technique is not used for the wavenumber integration, NW may be any positive integer. By specifying NW = 1 the propagation of a single plane or conical wave component may be analysed. Apart from this trivial case, the sampling points are placed equidistantly in the truncated wavenumber space determined by CMIN and CMAX. If the default trapezoidal rule integration is applied, it is recommended to choose NW so large that the wavenumber sampling Δk_c at the centre frequency satisfies the inequality

$$\Delta k_c r_{max} < \tfrac{1}{4}\pi$$

where r_{max} is the maximum range considered in the calculations. For the Filon scheme a smaller number of sampling points may be chosen, but this depends on how smooth the integration kernel is. In any case the sampling should be checked by convergence tests.

IC1: Number of the first sampling point, at which the calculation is to be performed. If IC1 > 1, then the Hankel transform is zeroed for sampling points 1,2 ... IC1-1, and the discontinuity is smoothed.

IC2: Number of the last sampling point where the calculation is to be performed. If IC2 < NW, then the Hankel transform is zeroed for sampling points IC2 +1, ... NW, and the discontinuity is smoothed by Hermite polynomial extrapolation.

IINC: If this parameter is an integer > 0 then integrand plots will be produced for each IINC frequency considered in the calculation.

BLOCK IX – TIME, FREQUENCY AND RANGE PARAMETERS

Lines: 1
Required: Always
Syntax: `NT F1 F2 DT RO DR NRAN`
Format: Free
Description:

`NT`: Number of sampling points in time domain. Should be an integer power of 2. To avoid aliasing it is extremely important, that the time window (`NT*DT`) is chosen large enough to contain the entire time signal at all the selected ranges.

`F1`: Lower limit of frequency band considered. Should be given in Hz.

`F2`: Upper limit of frequency band considered. Should be given in Hz. If `F2` is specified as having a value greater than the Nyquist frequency 0.5/`DT`, it will be replaced by the Nyquist frequency in the calculations. It should be noted that a simple rectangular weighting is applied to the frequency window defined by `F1` and `F2`. To avoid 'ringing' in the pulse responses due to the abrupt truncation, it is therefore required that `F1` and `F2` be chosen where the source frequency spectrum has a minimum, see Figs. 15 to 19.

`DT`: Interval between samples in time domain. Should be given in seconds. See notes above.

`RO`: Range in km for first receiver.

`DR`: Spacing in km between receivers (horizontal direction).

`NRAN`: Number of ranges. Pulse plots will be produced for each of the selected field parameters at each receiver range.

BLOCK X – TIME WINDOW PARAMETERS

Lines: 2

Required: For option R and if NRAN > 0

Syntax:

```
CRED
TMIN TMAX TLEN TINC
```

Format: Free

Description: This block determines the time window applied in all calculations and plots of pulse responses. For integrand plots all scaling and labeling is automatic.

CRED: Reduction velocity c_r in m/s. The pulse calculations and the pulse plotting are performed in the reduced time $t_r = t - r/c_r$. To avoid aliasing the reference velocity should be chosen larger than the largest group velocity in the problem. If CRED is specified as 0.0, the reduced time will be set equal to the real time, $t_r = t$.

TMIN: Minimum time in seconds. Determines the starting point for the reduced time axis in pulse plots.

TMAX: Maximum time in seconds. Determines the end point of the reduced time axis in pulse plots.

TLEN: Length of time axis in cm.

TINC: Time interval between tick marks on the time axis in seconds.

BLOCK XI – STACKED PLOT PARAMETERS

Lines: 1
Required: For options D and S
Syntax: SPLO SPUP SPLN SPIN
Format: Free
Description:

SPLO: Lower limit of y-axis in stacked pulse plots. If the range-stacked format has been chosen (option S) then SPLO should be in km. For the depth-stacked format (option D) it should be given in m. SPLO should be chosen such that enough space is available for keeping the negative amplitudes of the lowermost trace within the plot frame.

SPUP: Upper limit of y-axis in stacked pulse plots. Same units as SPLO Again space should be available for the trace closest to SPUP

SPLN: Length in cm of y-axis of stacked pulse plots.

SPIN: Interval between tick marks on y-axis of stacked pulse plots. Same units as SPLO and SPUP

BLOCK XII – PLOT DATA / DISPERSION CURVES

Lines: 3

Required: If option G has been specified.

Syntax:

```
NMOD
FMIN FMAX FLEN FINC
GVLO GVUP GVLN GVIN
```

Format: Free

Description:

- `NMOD`: Number of modes for which phase and group velocity curves are to be plotted. In this context the term 'modes' covers not only the normal modes, but all significant peaks in the Hankel transform integrand, thus also including seismic interface modes. The modes are counted in the usual way, i.e. from low phase velocities towards high phase velocities.
- `FMIN`: Minimum frequency in Hz. Determines the starting point of the x-axis.
- `FMAX`: Maximum frequency in Hz. Determines the end point of the x-axis.
- `FLEN`: Length of frequency axis in cm.
- `FINC`: Tick mark interval for frequency axis.
- `GVLO`: Minimum velocity in m/s. Determines the starting point of the y-axis for dispersion curve plots.
- `GVUP`: Maximum velocity in m/s. Determines the end point of the y-axis.
- `GVLN`: Length in cm of velocity axis for dispersion plots.
- `GVIN`: Velocity tick mark interval in m/s.

BLOCK XIII – PLOT DATA / VELOCITY PROFILE

Lines: 2

Required: If option Z was specified in Block II.

Syntax:

```
VLEF VRIG VLEN VINC
DVUP DVLO DVLN DVIN
```

Format: Free

Description:

VLEF:	Left border value of velocity in m/s.
VRIG:	Right border value of velocity in m/s.
VLEN:	Length of velocity axis in cm.
VINC:	Distance between tick marks in m/s.
DVUP:	Depth at upper border of plot in m.
DVLO:	Depth at lower border of plot in m.
DVLN:	Length of depth axis in cm.
DVIN:	Distance in m between tick marks on depth axis.

8.2. NUMERICAL CONSIDERATIONS

It must be assumed that the user is confident with the numerical problems involved in running the reflection coefficient and transmission loss models SAFARI-FIPR and SAFARI-FIP before trying to use the much more complicated pulse code. We will therefore at this point concentrate on the numerical considerations particular to the pulse code. For guidelines concerning the selection of environmental models, the user is referred to the previous sections.

The first thing the user has to select is a proper source pulse, which can either be one of the internal pulses or one created by the user and placed in a file that can be read by SAFARI-FIPP. After selecting the centre frequency f_c, the frequency bandwidth, defined by the parameters F1 and F2, is chosen such that the amplitude of the source spectrum is small at the truncation points. This is easily done by inspection of the frequency spectrum of the source pulse.

Next, the time sampling DT is selected. If chosen too large, the pulse plots will become very 'peaky', but in most cases 10 sampling points per period at the centre frequency f_c will be sufficient, i.e. DT $= 0.1/f_c$. The total time window T is of course dependent on the total number of time samples NT, but it is usually convenient to postpone the determination of this parameter until later.

Instead we select at this point the parameters controlling the wavenumber sampling. The numerical considerations in this regard are identical to those described for SAFARI-FIP, but the wide frequency band is a complicating factor. First an appropriate slowness interval, defined by CMIN and CMAX, should be selected, which is most conveniently done in the following way:

1. Select three characteristic frequencies, typically the centre frequency and one at each end of the frequency interval.
2. Determine the necessary wavenumber interval for each frequency as described for SAFARI-FIP.
3. Now determine whether the wavenumber interval should be held constant at all frequencies (default) or should vary such that the slowness interval is constant (option B) and select values of CMIN and CMAX accordingly.

If only a certain spectral part (limited and frequency-independent beamwidth) is being considered, then option B must be selected, but in this case the procedure above is used to determine proper truncation points, and, as was the case for SAFARI-FIP, the truncation may have to be tapered by selecting proper values of IC1 and IC2.

The number of wavenumber sampling points is a parameter which is even more critical in the present case than for transmission loss calculations where an error of a fraction of a dB is usually acceptable. This is due to the fact that not only the amplitude but also the phase of each frequency component has to be accurate in order

to yield a correct pulse response. Although a convergence test could be performed by using SAFARI-FIP at a few selected frequencies, it will usually be necessary to perform the convergence test on the full pulse problem. For the inexperienced user, however, it is advisable to perform a convergence test for SAFARI-FIP at least at the centre frequency to obtain reasonable initial estimates of the number of wavenumber samples. It should be stressed that although the Filon integration scheme (option F) is not default it is highly recommended due to the increased accuracy and reduced sampling requirements.

An initial convergence test for the wavenumber sampling is most conveniently done together with the one necessary for determining the length of the time window, $T =$ NT * DT. This is done in the following way:

1. Select a narrow frequency window around the centre frequency, typically F1 = $0.8f_c$ and F2 = $1.2f_c$.
2. Choose CRED and NT such that the time window of length T is believed to contain all arrivals. As the frequency sampling interval is inversely proportional to the length of the time window, $\Delta f = 1/T$, NT should be chosen as small as possible in order to limit the calculation time. CRED is most conveniently taken to be the highest wave speed in the problem.
3. Select pulse type 4 which has the narrowest spectrum.
4. Run SAFARI-FIPP to obtain pulse responses at all ranges.
5. If the pulse response at longer ranges become 'noisy', it indicates that the wavenumber sampling is insufficient. Increase the sampling and re-run until the 'noise' disappears. Remember that the very narrow frequency band will yield considerable 'ringing' of the pulse, which should not be confused with the undersampling noise. The amount of 'ringing' of the source pulse can be checked by selecting option R, which produces a plot of the source pulse filtered by the rectangular window determined by F1 and F2.
6. When the result is stable, increase the time window by changing either NT or DT. The true arrivals will be invariant to the change in time window, whereas the arrivals which are wrapped around will change position. Repeat until the wrap-around disappears.
7. The pulse type is now changed to the desired one and the frequency window is extended accordingly, usually containing the entire main lobe of the spectrum. The full response is then calculated. If high-frequency noise again appears at the long ranges, the wavenumber sampling must be increased. On the other hand it will only rarely be necessary to change the time window again.
8. As usual: *When the result is stable, it is the final result.*

It is clear that this convergence test procedure can become extremely time consuming since the computation time is proportional to both the number of frequencies

and the number of wavenumber samples. It is therefore important that the user selects reasonably low initial values, which again requires that he is already confident with the wavenumber sampling concepts of the single frequency SAFARI-FIP module. Further, it is extremely important that the user has a substantial knowledge of time/frequency analysis by means of FFTs in order to be able to properly select the time/frequency parameters and to pinpoint and remove the different numerical artifacts such as wrap-around and ringing.

8.3. SAFARI-FIPP EXAMPLES

The use of SAFARI-FIPP for calculating the full time response will here be illustrated by a few examples, all treating propagation in the sample environment used for the SAFARI-FIPR and SAFARI-FIP test cases, i.e. a shallow water environment with 100 m water depth and the layered bottom given in Table 4.

■ *8.3.1.* SAFARI-FIPP *case 1: Dispersion curves*

In this and the next example we use SAFARI-FIPP to model the propagation of seismic interface waves along the ocean sea-bed. One of the numerical problems particular to the pulse model is the determination of the necessary time window in order to avoid wrap-around. As described above, the starting time is easily determined from the maximum wave speed in the problem. The length of the time window, however, requires a little more skill to determine, in particular in cases where very slow interface waves are present. However, SAFARI-FIPP has the option of calculating group velocities of the interface wave, which is a very valuable tool in this regard. In this first example we will therefore calculate the dispersion curves in the frequency interval 1–12 Hz for the slowest fundamental interface mode associated with the environment treated in SAFARI-FIP case 1. To do this, the data file given in Table 18 is set up.

The resulting dispersion curves are shown in Fig. 20. The minimum group velocity is observed to be 280 m/s. If the pulse response has to be calculated out to a range of 2.5 km and no reduced time is applied, the length of the time window required in order to avoid wrap-around is $T = 10$ s.

Table 18
SAFARI-FIPP case 1 data file

Data file	Description	Notes
SAFARI-FIPP case 1	title	
V G	options	1
3	centre frequency 3 Hz	2
4	number of layers	
0 0 0 0 0 0 0	layer 1 (vacuum halfspace)	
0 1500 0 0 0 1 0	layer 2 (water column)	
100 1600 400 0.2 0.5 1.8 0	layer 3 (silt sediment)	
120 1800 600 0.1 0.2 2.0 0	layer 4 (sand sub-bottom)	
95	source depth 95 m	
100 100 1	receiver depth 100 m	
300 1E8	phase velocity interval	3
250 1 250 0	wavenumber sampling parameters	4
512 1.0 12.0 .01 0.5 0.5 0	frequency sampling parameters	5
1	number of modes	6
0 12 20 2	frequency axis parameters	
200 600 12 100	velocity axis parameters	

[1] It is indicated by option G that the dispersion characteristics of one or more modes should be determined. Option V indicates that the depth-dependent Green's function for the vertical particle velocity is used for finding the peak corresponding to the interface mode.

[2] The centre frequency is specified as 3 Hz, but this parameter has no influence on the dispersion calculation.

[3] The wavenumber interval is chosen so large that the fundamental interface mode is known to be included at the maximum frequency of 12 Hz. Note that option B was not specified. The wavenumber spectrum is therefore constant and equal to the one determined by the maximum frequency.

[4] The wavenumber sampling is not extremely critical for the G option because a bisection technique is used to iterate onto the correct position of the modal peak.

[5] The frequency interval has been chosen as 1 to 12 Hz, and to obtain a frequency sampling interval of $\Delta f = 0.2$ Hz, the time sampling parameters have been adjusted to yield a total time window of length $T = 1/\Delta f \simeq 5$ s. Since NRAN = 0, no pulse plots are generated, but we have in any case chosen $\Delta t = 0.01$ s, which is the sampling required to nicely represent graphically a wave of frequency 12 Hz. The appropriate number of time samples therefore follows as $NT = 2^9 = 512$.

[6] In order to determine the width of the time window for the following pulse calculations, only the group velocity of the fundamental interface mode is required.

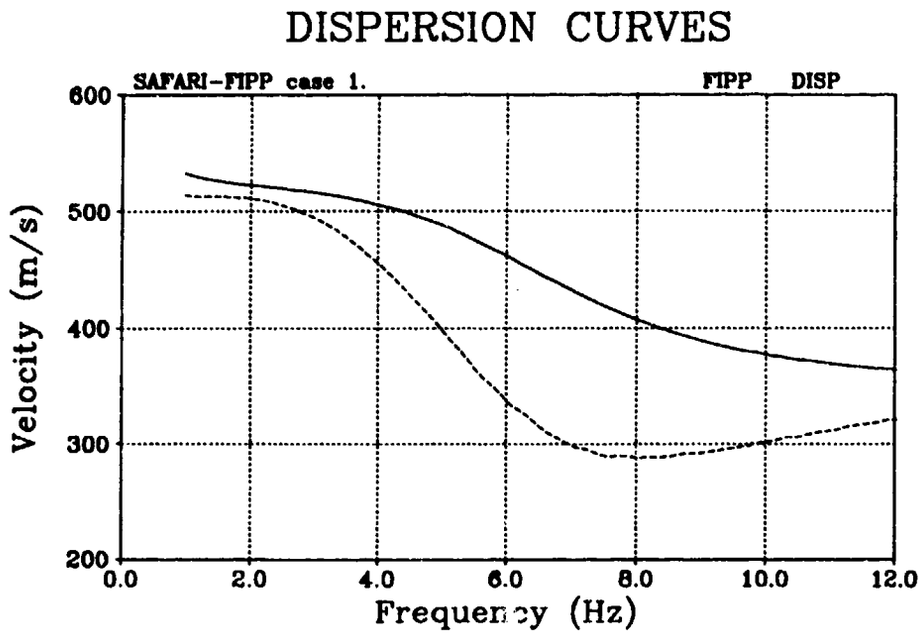

Fig. 20. SAFARI-FIPP case 1: dispersion curves for the fundamental interface mode in a stratified sea-bed. The solid curve indicates the phase velocity and the dashed curve the group velocity.

■ *8.3.2.* SAFARI-FIPP *case 2: Seismic interface wave propagation*

In this example we calculate the time response of 5 vertical geophones on the ocean bottom, spaced 500 m apart out to a range of 2.5 km, using a source of type 2 with a centre frequency of 5 Hz. The environment is exactly as in the previous example. This is done by specifying the data file given in Table 19.

The resulting stacked plots of the time behaviour of the vertical and horizontal particle velocities are shown in Fig. 21a and b, respectively. Note that the amplitudes have been multiplied by range before being plotted. The highly dispersive nature of the slow seismic interface wave is characteristic for this type of propagation situation. Although not particularly evident in the present case, it is also characteristic that the horizontal component shows a second interface mode more pronounced than the vertical component. For a more detailed description of the behaviour of seismic interface waves, reference is made to [16–18]. In Fig. 21b for the horizontal component, the first arrival is the lowest waterborne normal mode, which is only weakly present on the vertical component. This arrival also contains a head wave arising from the sub-bottom, but this wave is not easily isolated from the waterborne mode.

Table 19
SAFARI-FIPP case 2 data file

Data file	Description	Notes
SAFARI-FIPP case 2	title	
V H S 2 F J	options	1
5 0	centre frequency 5 Hz	2
4	number of layers	
0 0 0 0 0 0 0	layer 1 (vacuum halfspace)	
0 1500 0 0 0 1 0	layer 2 (water column)	
100 1600 400 0.2 0.5 1.8 0	layer 3 (silt sediment)	
120 1800 600 0.1 0.2 2.0 0	layer 4 (sand sub-bottom)	
95	source depth 95 m	
100 100 1	receiver depth 100 m	
300 1E8	phase velocity interval	3
1024 1 950 0	wavenumber sampling parameters	4
2048 0.0 12.5 .006 0.5 0.5 5	frequency sampling parameters	5
0	reduction velocity	6
0 10 20 2	time axis for stacked plots	7
0 3 15 0.5	range axis for stacked plots	8

[1] Options V and H are specified in order to calculate both vertical and horizontal particle velocities. Since option S has been selected, the time responses will be displayed in a range-stacked format. A source pulse of type 2 has been selected. Option F invokes the Filon integration scheme which requires less sampling points than the default trapezoidal-rule integration scheme. Finally, the J option is specified to move the wavenumber integration contour out into the complex plane. This is not necessary for the interface wave, which is itself highly attenuated, but, as was demonstrated in SAFARI-FIP case 1, normal modes will become important for frequencies above the centre frequency of 5 Hz. Therefore a significantly larger number of sampling points than the actual 1024 would be required at the higher frequencies in the band. Note that option B was not specified because the exponential decay of the wavenumber integration kernel will be very slow at the low frequencies in cases where interface waves are important.

[2] The centre frequency is specified as 5 Hz. By inspection of Fig. 16b it is clear that the source pulse will contain significant energy up to a frequency of 12.5 Hz, which is therefore selected as the upper limit for the calculations. The default contour offset is applied by specifying COFF = 0.

[3] As in case 1, a wide wavenumber spectrum is used in order to encompass all real angles of propagation and all evanescent waves that are present.

[4] The number of wavenumber samples selected is 1024, which translates into $\Delta k\, r_{max} \simeq 0.64 < \frac{1}{4}\pi$, i.e. sufficient also for the standard trapezoidal rule integration and therefore more than enough for the selected Filon scheme. The last parameter IINC is set to 0 in order not to create any wavenumber integrand plots. By selecting IC2 as 950 the tapering is invoked, to take care of possible discontinuities at the high wavenumber truncation point.

[5] The frequency interval selected is 0 to 12.5 Hz, which is an appropriate choice for pulse type 2, see Fig. 21. The total time window is chosen a little larger than 10 s by specifying DT = 0.006 and NT = 2048. The ranges where pulses are to be calculated are determined by the last 3 parameters. In the present case there are 5 receiver ranges spaced 500 m apart in the interval 500 to 2500 m. Note that ranges are always given in km.

[6] Due to the short ranges involved, no time reduction is applied; therefore CRED = 0.

[7] The time axis on all generated plots is specified to contain a window of width 10 s, starting at 0 s. The length of the time axis selected is 20 cm.

[8] Since the receivers are placed at ranges between 0.5 and 2.5 km, the range axis for the stacked plots has been chosen to range from 0 to 3.0 km in order not to truncate the first and last trace.

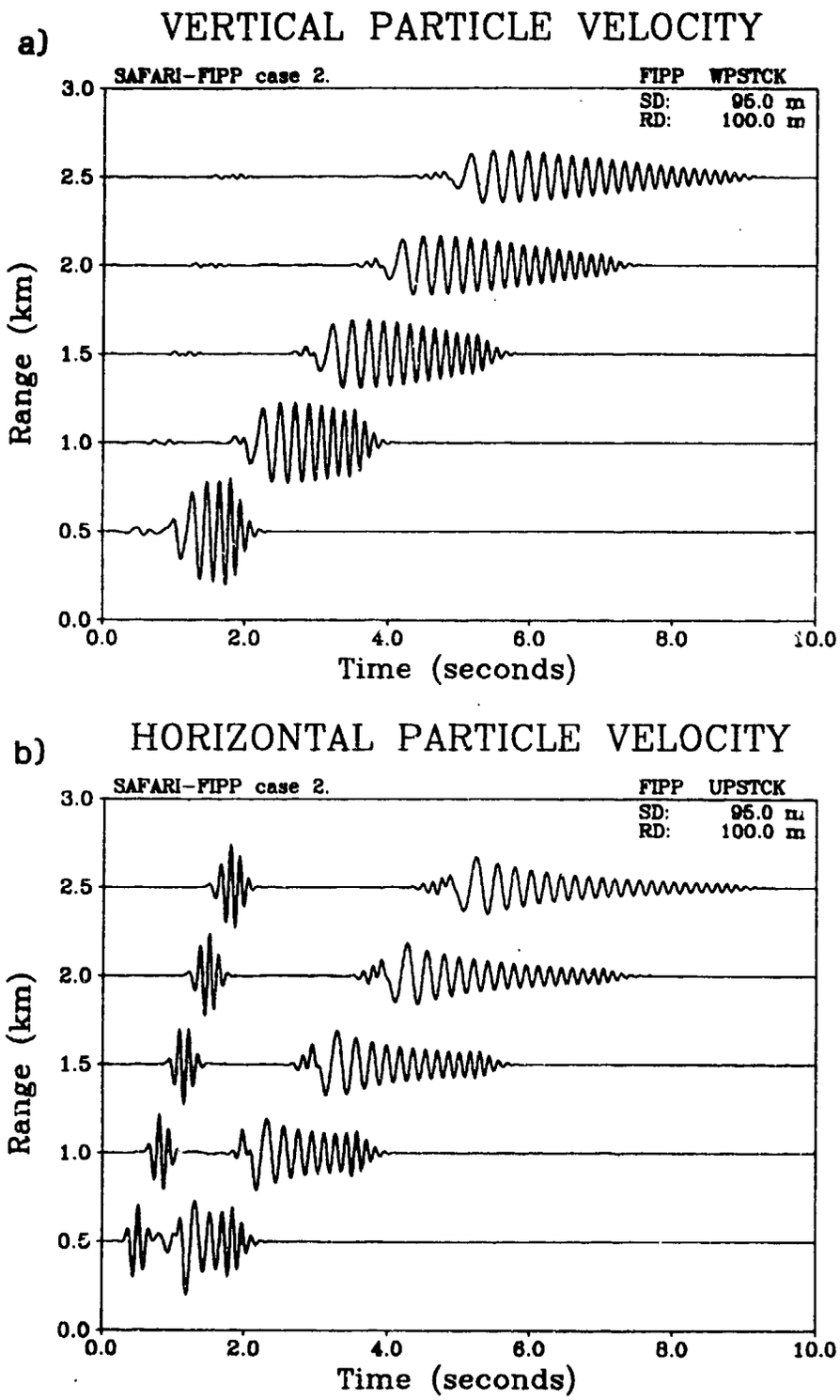

Fig. 21. **Results for SAFARI-FIPP case 2: (a) stacked plot of vertical particle velocity traces; (b) corresponding horizontal particle velocity traces.**

8.3.3. SAFARI-FIPP case 3: Normal mode propagation

In this last example the stacking in depth instead of range will be demonstrated by calculating the field produced at a vertical array of hydrophones for a source at 50 m depth and with range offsets of 5 and 10 km. The environment is the same as treated in examples SAFARI-FIP 2 and 3, and the source is assumed to be of type 4 with a centre frequency of 30 Hz. Only the discrete part of the wavenumber spectrum wil be included in order to demonstrate how the truncation of the integration interval is introduced in the pulse calculations. The data file is given in Table 20.

The resulting stacked plots are shown in Fig. 22. Note the two arrivals corresponding to the two normal modes. As expected, the first arrival is the first mode with its largest amplitude at approximately 60 m depth. The second mode arrives 0.2 to 0.3 s later, and it has a low anplitude at 60 m depth. By comparing the results for the two different ranges, the characteristic dispersion of the modes is evident.

Table 20
SAFARI-FIPP case 3 data file

Data file	Description	Notes
SAFARI-FIPP case 3	title	
N D 4 J F B	options	1
30 0	centre frequency 30 Hz	
5	number of layers	
0 0 0 0 0 0 0	layer 1 (vacuum halfspace)	
0 1500 -1480 0 0 1 0	layer 2 (water layer)	
30 1480 -1490 0 0 1 0	layer 3 (water layer)	
100 1600 400 0.2 0.5 1.8 0	layer 4 (silt sediment)	
120 1800 600 0.1 0.2 2.0 0	layer 5 (sand sub-bottom)	
50	source depth 50 m	
90 10 9	receiver depths 10 to 90 m	2
1450 1700	phase velocities CMIN and CMAX	3
550 50 500 0	wavenumber sampling parameters	3
1024 15 75 0.0012 5 5 2	frequency sampling parameters	4
1500	reduction velocity	5
0 1 20 0.2	time axis for stacked plots	6
100 0 15 20	depth axis for stacked plots	7

[1] Option N indicates that the normal stress, equal to the negative value of the acoustic pressure, should be calculated. The depth stacking is invoked by specifying option D, and the wavenumber contour offset, option J, is again applied. Option F selects the Filon integration scheme, and finally option B indicates that the phase velocity interval (or slowness interval) should be held constant at all frequencies in contrast to the former example, where the wavenumber interval was held constant. The B option is essential when the calculations involve only a limited beamwidth.

[2] There are 9 receivers in the vertical array, with the lowermost receiver at 90 m depth and the uppermost at 10 m depth. The deepest receiver has been specified first, since the amplitude scaling is controlled by the first receiver depth, and the amplitude is expected to be larger at the bottom than at the pressure-release surface.

[3] As in example SAFARI-FIP case 3, the wavenumber interval has been selected to include only propagating normal modes, and the tapering is applied by properly specifying IC1 and IC2. No integrand plots have been requested (IINC = 0), although this feature is often applied to check the wavenumber truncation.

[4] As can be observed from Fig. 18b, the selected frequency interval 15 to 75 Hz will include the whole main lobe of the source frequency spectrum. The time sampling parameters have been chosen to yield a total time window of 1.2 s, which turns out to be sufficient for the ranges selected. As above, a dispersion calculation for the normal modes (2 at the centre frequency) could have been performed in advance.

[5] Since the fast-bottom head wave has been excluded from the wavenumber integration interval, no arrivals faster than the water velocity (1500 m/s) are expected. Therefore this velocity has been chosen as reduction velocity.

[6] The time axis covers the first 1 s of the selected time window.

[7] The depth axis for the stacked plots covers the whole water column, leaving enough space for both the first and the last trace.

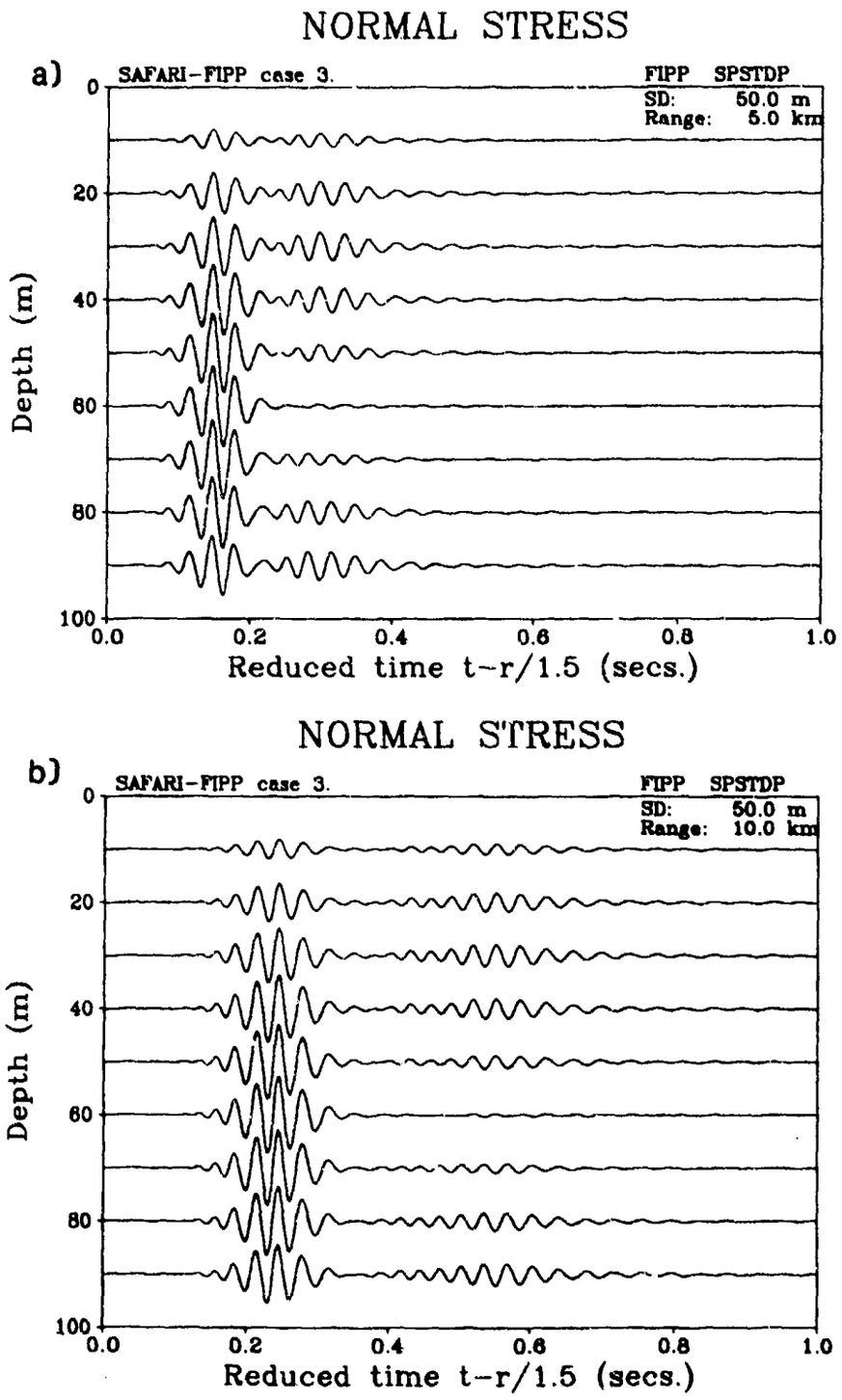

Fig. 22. Results for SAFARI-FIPP case 3: depth-stacked plots of hydrophone traces at two different ranges: (a) 5 km; (b) 10 km.

References

[1] STEPHEN, R.A. A comparison of finite difference and reflectivity seismograms for marine models. *Geophysical Journal of the Royal Astronomical Society*, **72**, 1983: 39–58.

[2] ZIENKIEWITZ, O.C. The Finite Element Method, 3rd edn, Maidenhead, McGraw-Hill, 1977.

[3] TAPPERT, F.D. The parabolic approximation method. *In*: KELLER, J.B. and PAPADAKIS, J.S., *eds*. Wave Propagation and Underwater Acoustics. Berlin, Springer, 1977: pp. 224–287.

[4] JENSEN, F.B. and FERLA, M.C. SNAP: The SACLANTCEN normal-mode acoustic propagation model, SACLANTCEN SM-121, La Spezia, Italy, NATO SACLANT Undersea Research Centre, 1979.

[5] EVANS, R.B. A coupled mode solution for acoustic propagation in a waveguide with stepwise depth variations of a penetrable bottom. *Journal of the Acoustical Society of America*, **74**, 1983: 188–195.

[6] PEKERIS, C.L. Theory of propagation of explosive sound in shallow water. *Memoirs, Geological Society of America*, **27**, 1948.

[7] JARDETZKY, W.S. Period equation for an N-layered halfspace and some related questions, Tech. Rep. Seism. No. 29. Palisades, Columbia University, Lamont Geological Observatory, 1953.

[8] EWING, W.M., JARDETZKY, W.S. and PRESS, F. Elastic Waves in Layered Media. New York, McGraw-Hill, 1957.

[9] THOMSON, W.T. Transmission of elastic waves through a stratified solid, *Journal of Applied Physics*, **21**, 1950: 89–93.

[10] HASKELL, N.A. The dispersion of surface waves in multilayered media. *Bulletin of the Seismological Society of America*, **43**, 1953: 17–34.

[11] KENNETT, B.L.N. Seismic Wave Propagation in Stratified Media. Cambridge, Cambridge University Press, 1983.

[12] KENNETT, B.L.N. Reflections, rays and reverberations, *Bulletin of the Seismological Society of America*, **65**, 1974: 1685–1696.

[13] KUTSCHALE, H.W. Rapid computation by wave theory of propagation loss in the Arctic ocean. Rep. CU-8-73. New York, Columbia University, 1973.

[14] FUCHS, K. and MUELLER, G. Computation of synthetic seismograms with the reflectivity method and comparison with observations. *Geophysical Journal of the Royal Astronomical Society*, **23**, 1971: 417–433.

[15] DINAPOLI, F.R. and DEAVENPORT, R.L. Theoretical and numerical Green's function solution in a plane layered medium. *Journal of the Acoustical Society of America*, **67**, 1980: 92–105.

[16] SCHMIDT, H. Excitation and propagation of interface waves in a stratified sea-bed. *In*: PACE, N.G., *ed.* Acoustics and the Sea-Bed, Bath, UK, Bath University Press, 1983.

[17] JENSEN, F.B. and SCHMIDT, H. Shear properties of ocean sediments determined from numerical modelling of Scholte wave data. *In*: AKAL, T. and BERKSON, J.M., *eds.* Ocean Seismo-Acoustics, New York, Plenum Press, 1986.

[18] SCHMIDT, H. Numerical modelling of seismic interface waves, SACLANTCEN SM-169, La Spezia, Italy, NATO SACLANT Undersea Research Centre, 1984.

[19] SCHMIDT, H. Modelling of pulse propagation in layered media using a new fast field program. *In*: FELSEN, L.B., *ed.* Hybrid Formulation of Wave Propagation and Scattering. Dordrecht, the Netherlands, Nijhoff, 1984.

[20] SCHMIDT, H. and JENSEN, F.B. Efficient numerical solution technique for wave propagation in horizontally stratified environments. *Computers and Mathematics with Applications*, **11**, 1985: 699–715.

[21] SCHMIDT, H. and JENSEN, F.B. A full wave solution for propagation in multilayered viscoelastic media with application to Gaussian beam reflection at fluid-solid interfaces. *Journal of the Acoustical Society of America*, **77**, 1985: 813–825.

[22] SCHMIDT, H. and JENSEN, F.B. Evaluation of experimental techniques for determining the plane wave reflection coefficient at the sea floor. *In*: AKAL, T. and BERKSON, J.M., *eds.* Ocean Seismo-Acoustics. New York, Plenum Press, 1986.

[23] SCHMIDT, H. and TANGO, G. Efficient global matrix approach to the computation of synthetic seismograms. *Geophysical Journal of the Royal Astronomical Society*, **84**, 1986: 331–359

[24] SCHMIDT, H. and KUPERMAN, W.A. A 'finite wave element' approach to the solution of the wave equation in horizontally stratified environments with rough interfaces. *In*: Proceedings of the 11th IMACS World Congress on System Simulation and Scientific Computation, Oslo, Norway, Aug. 5–9, 1985.

[25] KUPERMAN, W.A. and SCHMIDT, H. Rough surface elastic wave scattering in a horizontally stratified ocean. *Journal of the Acoustical Society of America*, **79**, 1986: 1767–1777.

[26] JENSEN, F.B. and SCHMIDT, H. Subcritical penetration of narrow Gaussian beams into sediments. *Journal of the Acoustical Society of America*, **82**, 1987: 574–579.

[27] JENSEN, F.B. and SCHMIDT, H. Nonspecular reflection of bounded acoustic beams from layered viscoelastic halfspaces. *In*: MCCARTHY, M.F. and O'LEARY, P.M., *eds.* Elastic Wave Propagation. Elsevier/North Holland, 1988.

[28] SCHMIDT, H. and GLATTETRE, J. A fast field model for three-dimensional wave propagation in stratified environments based on the global matrix method. *Journal of the Acoustical Society of America*, **78**, 1985: 2105–2114.

[29] ABRAMOWITZ, M. and STEGUN, I.A. Handbook of Mathematical Functions. New York, Dover, 1965.

[30] MORSE, P.M. and INGARD, K.U. Theoretical Acoustics. New York, McGraw-Hill, 1968.

[31] HARKRIDER, D.G. Surface waves in multilayered elastic media, part I: Rayleigh and Love waves from buried sources in a multilayered elastic halfspace. *Bulletin of the Seismological Society of America*, **54**, 1964: 627–679.

[32] KOLSKY, H. Stress Waves in Solids. New York, Dover, 1963.

[33] CHIN, R.C.Y., HEDSTROM, G.W. and THIGPEN, L. Matrix methods in synthetic seismograms. *Geophysical Journal of the Royal Astronomical Society*, **77**, 1984: 483–502.

[34] TSANG, L., BROWN, R., KONG, J.A. and SIMMONS, G. Numerical evaluation of elctromagnetic fields due to dipole antennas. Journal of Geophysical Research, **79**, 1974: 2077–2080.

[35] ANDERSON, W.L. Computation of Green's tensor integrals for three-dimensional electromagnetic problems using fast Hankel transforms, *Geophysics*, **49**, 1984: 1754–1759.

[36] MALLICK, S. and FRAZER, L.N. Practical aspects of reflectivity modeling. *Geophysics*, **52**, 1987: 1355–1364.

[37] FRAZER, L.N. and GETTRUST, J.F. On the generalisation of Filon's method and the computation of oscillatory integrals of seismology. *Geophysical Journal of the Royal Astronomical Society*, **76**, 1984: 461–481.

Appendix A

Installing and running SAFARI on the FPS164

SAFARI is installed at SACLANTCEN on both the VAX 8600 cluster and the FPS164 Attached Processor. The installation on the VAX proceeds exactly as described in Sect. 5. For the FPS164 the simulation of the FPS library functions should of course not be used. Further, the most critical subroutines have been written in APAL64 assembler and a special set of subroutines is available for doing asynchronous I/O to all scratch files. This last feature requires the FPS164 to be equipped with a D64 disk subsystem and to run under the Single Job Executive (SJE) operating system.

The FPS164 version is compiled and linked by means of the following command file:

COMFPS.COM

```
$ SET DEF US5:[SCHMI.ANIS]
$ !
$ !  SUBROUTINES
$ !
$ APFTN64/XOFF=ALL/OPT=2 FIPASJE30
$ APFTN64/XOFF=ALL/OPT=2 FIPSSJE30
$ APFTN64/XOFF=ALL/OPT=2 FIPPSJE30
$ APFTN64/XOFF=ALL/OPT=2 FIPUSJE30
$ APFTN64/XOFF=ALL/OPT=2 FIPTSJE30
$ APFTN64/XOFF=ALL/OPT=2 FIPRSJE30
$ !
$ !  ASSEMBLER SUBROUTINES
$ !
$ APAL64 APCBGE5
$ APAL64 CVMOVI
$ APAL64 CVIMOV
$ !
$ !  SUBROUTINES FOR ASYNCHRONOUS I/O
$ !
$ APFTN64/XOFF=ALL/OPT=2 ASIO4
$ !
$ !  CREATE LIBRARY
$ !
$ APLIBR64/OUT=SAFLIB/IN=(FIPPSJE30,FIPSSJE30,FIPUSJE30,-
    FIPTSJE30,FIPRSJE30,FIPASJE30,APCBGE5,CVMOVI,CVIMOV,ASIO4)
$ !
$ !  MAIN PROGRAMS
$ !
```

```
$ APFTN64/XOFF=ALL SJEFIPP30
$ APLINK64 SJEFIPP30,SAFLIB.AOL
$ APFTN64/XOFF=ALL SJEFIP30
$ APLINK64 SJEFIP30,SAFLIB.AOL
$ APFTN64/XOFF=ALL SJEFIPR30
$ APLINK64 SJEFIPR30,SAFLIB.AOL
$ !
$ !  CREATE AND SUBMIT COMMAND FILE FOR COPYING
$ !  IMAGES INTO FPS164/SJE FILES, HERE UNDER
$ !  ACCOUNT :SCHMI
$ !
$ OPEN/WRITE COM COP.COM
$ WRITE COM "$ SET DEF US5:[SCHMI.ANIS]"
$ WRITE COM "$ SJE"
$ WRITE COM "ATT/W"
$ WRITE COM "ACC :SCHMI"
$ WRITE COM "COPYIN/BI SJEFIP30.IMG,SJEFIP30"
$ WRITE COM "COPYIN/BI SJEFIPP30.IMG,SJEFIPP30"
$ WRITE COM "COPYIN/BI SJEFIPR30.IMG,SJEFIPR30"
$ WRITE COM "DET"
$ WRITE COM "QUIT"
$ CLOSE COM
$ FPSQUE COP
```

Also, a special command file is required for running SAFARI on the FPS164, e.g. for the transmission loss program SAFARI-FIP:

FIP.COM

```
$ SET DEF US5:[SCHMI.ANIS]
$ OPEN/WRITE COM SAFARIFIP.COM
$ WRITE COM "$ SJE"
$ WRITE COM "ATTACH/W 1"
$ WRITE COM "COPYIN ''P1'.DAT,FTN001"
$ WRITE COM ":SCHMI:SJEFIP30"
$ WRITE COM "COPYOUT FTN019,''P1'.PLP"
$ WRITE COM "COPYOUT FTN020,''P1'.PLT"
$ WRITE COM "COPYOUT FTN028,''P1'.CDR"
$ WRITE COM "COPYOUT FTN029,''P1'.BDR"
$ WRITE COM "DETACH"
$ WRITE COM "QUIT"
$ CLOSE COM
$ @SAFARIFIP
$ ASSIGN/USER 'P1'.PLP FOR019
$ ASSIGN/USER 'P1'.PLT FOR020
```

```
$ ASSIGN/USER SYS$COMMAND: SYS$INPUT
$ RUN US6:[SCHMI.VAXFIP]FIPPLOT
$ ASS/USER 'P1'.CDR FOR055
$ ASS/USER 'P1'.BDR FOR017
$ ASS/USER SYS$COMMAND: SYS$INPUT
$ RUN US6:[SCHMI.FIPCON]CONTUR.EXE
```

The two other modules are run by means of similar command files.

Appendix B

Running FIPPLOT

When SAFARI is run by using the command files given in Sect. 5 and Appendix A, the plot program FIPPLOT is automatically executed to obtain the graphical output. The plot data are transferred through two files. The file with extension PLP contains plot parameters such as axis lengths, titles, labels etc, whereas the other file, with extension PLT, contains the actual data values to be plotted. Both files are formatted ASCII files, and it is therefore possible to change the layout of the plots by editing the PLP file and then execute FIPPLOT independently. Further, FIPPLOT has such a general setup that it is easily interfaced to any other numerical code requiring graphical output. We will therefore describe here the structure of the PLP file in detail.

As a characteristic example, the PLP file generating the plot shown in Fig. 11a is as follows:

```
␣1024                          modulo
␣FIPP␣␣STLDAV,CPX,IYA
␣DEPTH AVERAGED LOSS
␣SAFARI-FIP case 3.
␣2                             number of labels
␣Freq:  30.0 Hz$
␣SD: 50.0 m$
␣20.000000                     XLEN
␣12.000000                     YLEN
␣0                             grid type
␣0.000000                      XLEFT
␣5.00000                       XRIGHT
␣1.00000                       XINC
␣1.00000                       XDIV
␣Range (km)$
␣LIN
␣80.0000                       YDOWN
␣20.0000                       YUP
␣10.0000                       YINC
␣1.00000                       YDIV
␣Normal stress (dB//1Pa)$
␣LIN
␣1                             NC
␣112                           N
␣0.044957                      XMIN
␣0.449567-001                  DX
```

```
␣0.000000                    YMIN
␣0.000000                    DY
␣FIP␣␣␣PLTEND
```

Notice especially the initial space (denoted by ␣) which is necessary for FIPPLOT to correctly read the file. The PLP file will always start with a block size modulo, with which the corresponding data file was written. This parameter is a leftover from the versions using binary data files, but for the present version of FIPPLOT this parameter is dummy. The file ends with the PLTEND flag signalling the end-of-file.

Between these two records the blocks of actual plot parameters are specified, in the present case for a single plot only. Any number of blocks could, however, be included, each generating one plot.

The plot parameter block starts with a record specifying a 12-character plot identification (FIPP␣␣STLDAV) followed by a series of 3-character options separated by commas. The files generated by the SAFARI modules will in general not have any options specified, but these are important tools for generating final plots. The following options are currently available:

- **DUP**: The duplex character generator will be used in stead of the default simplex.
- **CPX**: The complex character generator is selected. This is the option chosen for all plots in this report.
- **ITA**: The italic character generator is used.
- **IXA**: Integer format will be used for plotting the x-axis tick mark numbers instead of the default decimal format.
- **IYA**: Integer format will be used for plotting the y-axis tick mark numbers instead of the default decimal format.
- **DSD**: If the plot contains more than one curve (NC > 1), then the first curve will be plotted with a solid line, the second with a dashed line and the third with a dotted line. If more than three curves are plotted, this sequence will be repeated. To generate the dispersion plot in Fig. 20 the DSD option was applied.
- **MRK**: A marker will be plotted for each 10th data point on the curves. In the case of more curves, different markers will be used for each.
- **COL**: This option will plot individual curves in different colours, using the repeatable sequence: red–green–blue–cyan–magenta–yellow.
- **SCA**: The default character size has been selected to yield a reasonable 'balance' of the plot when the length of the x-axis is 20 cm. This option will scale the character size accordingly for larger or smaller sizes. This is particularly important when preparing illustrations for reports and journal papers, where

a uniform character size is desirable, independent of the size of the original plots.

RES: When this option is selected, FIPPLOT will request a scaling factor (1.0 = no scaling) which will be applied to all curves in the plot, but *not* to the axis values. This option is particularly useful for the range and depth-stacked time series produced by SAFARI-FIPP.

TCT: This option is used in connection with the stacked time series plots in order to truncate the amplitude of each trace at a value corresponding to half the distance between traces. Used in particular to avoid overlap of curves when rescaling with a large factor (option RES).

NOP: With this option both the parameters from the PLP file and the data from the PLT file are read but no plot is produced. It is therefore used for time-saving when only selected plots are required.

The next record specifies the main title of the plot, followed by a record containing the title specified in the SAFARI data file for the actual run. This title will be plotted just above the plot frame.

Then follows a sub-block containing the labels to be plotted in the upper right corner of the plot frame. The number of labels (≥ 0) is given first, followed by the label texts, each of which should be on separate lines and terminated by a **$**.

The parameters **XLEN** and **YLEN** specify the length in cm of the x- and y-axis, respectively. The parameter labelled 'grid type' indicates whether a grid should be plotted. A value of 1 will produce a dotted grid as in Fig. 20.

The next 6 records contain the parameters for the x-axis of the plot. **XLEFT** and **XRIGHT** are the data values at the left and right borders of the plot frame, respectively, whereas **XINC** is the distance in the same units between the tick marks. **XDIV** is a multiplication factor which will be applied to both the axis parameters and the data values. After **XDIV** the x-axis label is specified, terminated by a **$**, and finally **LIN** indicates that the x-axis should be linear. Another possibility is a logarithmic axis, which has not yet been implemented, however. The parameters for the y-axis are given in the same way in the next 6 records.

The parameter **NC** specifies the number of curves to be plotted. For each curve a sub-block of 5 records has to be specified. The first parameter **N** indicates the number of points in the curve. If **N** is negative, no curve will be plotted; instead a marker will be plotted at the position of each data point. The parameter **XMIN** is the x-coordinate (range) of the first data point, whereas **DX** is the equidistant spacing. If **DX** had been specified as 0, then the **N** x-coordinates of the data points would be read from the PLT file. In that case **XMIN** would be interpreted as an x-offset to be applied to the curve. The same rules apply to **YMIN** and **DY**. In the actual case the y-values (transmission losses) will therefore be read from the PLT file, and no y-offset

will be applied. The offsets are only used for the stacked time series plots, where it is important to be able to rescale (see option RES above) the amplitudes without changing the trace offset. If both DX and DY are specified as 0, then FIPPLOT will first read all N x-values and then all y-values. As an example of this, reference is made to the PLP file for generating the sound-speed profile plot inserted in Fig. 10a.

When the PLP file has been edited, FIPPLOT is executed with the following command file:

```
$ ASS/USER 'P1'.PLP FOR019
$ ASS/USER 'P1'.PLT FOR020
$ ASS/USER SYS$COMMAND: SYS$INPUT
$ RUN FIPPLOT
```

All plots presented in this report have been edited, and they therefore do not appear exactly as those produced automatically.

Appendix C
Running CONTUR

As was the case for FIPPLOT, the command files given in Sect. 5 and Appendix A will automatically execute the contour plotting program CONTUR. The plot parameters are transferred from SAFARI into the file with extension CDR, whereas the actual contour data are placed in the file with extension BDR. The data file is allowed to be in both ASCII or binary format, but as SAFARI is run both on the VAX and the FPS164 at SACLANTCEN, it has been most convenient to use the ASCII format.

The CDR file can be edited to change the layout of the contour plot. As a typical example, the CDR file used to create the contour plot of Fig. 14b is shown below:

```
CONDR,FIP,FMT,CPX,UNI,TEK
SAFARI-FIP case 5.
SAFFIP5.BDR;1
Range (m)
0.0000                    RMIN
299.8535                  RMAX
0.0000                    XLEFT
300.0000                  XRIGHT
15.0000                   XSCALE
50.0000                   XINC
Depth (m)
50.0000                   YUP
125.0000                  YDOWN
6.2500                    YSCALE
25.0000                   YINC
141.0000                  data points along x-axis
51.0000                   data points along y-axis
1.0000                    DIVX
1.0000                    DIVY
0.0000                    FLAGRC
50.0000                   RDUP
125.0000                  RDLO
50.0000                   source depth (m)
141.0000                  grid points along x-axis
51.0000                   grid points along y-axis
1000.0000                 frequency (Hz)
0.0000                    dummy
5.0000                    CAY
5.0000                    NRNG
21.0000                   ZMIN
```

54.0000	ZMAX
3.0000	ZINC
2.0000	x-origin of plot in inches
0.0000	dummy
2.0000	y-origin of plot in inches
0.0000	NSM
0.1000	HGTPT
0.1400	HGTC
-3.0000	LABPT
1.0000	NDIV
5.0000	NARC
-1.0000	LABC
-1.0000	LWGT

The first record specifies one 5-character option (CONDR) followed by a series of 3-letter options. The CONDR option indicates that the actual contour plot is of the depth-range type and CONTUR will interpret the parameters accordingly. *This option should therefore never be changed.* The first 3-letter option (FIP) is purely for identification and has no further effect. The FMT option indicates that the BDR data file is ASCII formatted (BIN for binary format). These first 3 options should always be present in the specified order, but the options following are optional and can be given in any order. The implemented options are as follows:

DUP: The duplex character generator will be used for DISSPLA plots (MINDIS at SACLANTCEN) instead of the default simplex.

CPX: The complex character generator is selected.

ITA: The italic character generator will be used.

UNI: The UNIRAS plot package will be used to generate a colour or grey-tone contour plot. DISSPLA (MINDIS at SACLANTCEN) is the default plot package.

VTT: The raster plot will be produced on a VT240 terminal. This only has effect if option UNI is specified.

G41: The raster plot will be produced on a Tektronix 4105 terminal. This only has effect if option UNI is specified.

TEK: The raster plot will be produced on a Tektronix 4691 ink jet plotter. This only has effect if option UNI is specified.

PRX: The raster plot will be produced on a Printronix printer. This only has effect if option UNI is specified.

COL: If the option UNI has been selected, a colour raster plot using an in-built colour scale will be generated. By default a grey-tone scale is applied.

VUG: If option **UNI** is selected, a viewgraph will be produced on a Tektronix 4691 or 4692 ink jet plotter.

ROT: The UNIRAS plot will be rotated 90°. Mainly used for generating viewgraphs of plots with the x-axis being larger than the y-axis.

After the option record there is a record containing the title of the plot and a record containing the name of the file containing the data, i.e. the BDR file. Except for 2 records containing the x-axis and y-axis labels, the rest of the records contain numerical parameters, all supplied with a descriptive label. In general only a few of these parameters should be changed. The most important ones are described below.

The lengths of the x- and y-axes are controlled by the parameters **XSCALE** and **YSCALE**, respectively. CONTUR requires these parameters to be specified in coordinate units per cm. **ZMIN** and **ZMAX** specify the limits of the contouring interval, whereas **ZINC** is the contour increment. If UNIRAS is selected, areas with small data values will be coloured with magenta (black in the grey-tone mode). The colour scale then moves through different red tones into blue (white in the grey-tone mode). If, however, **ZMIN** > **ZMAX**, then the colour scale will be inverted by CONTUR. If the default DISSPLA package is selected, only contour lines with identifying numbers are plotted. In the present case, removal of the **UNI** option leads to the contour plot shown in Fig. 14a.

The last important parameter is **NSM**, which controls the amount of smoothing applied to the calculated contours. This parameter can be set to any value between 0 and 10, with 0 corresponding to no smoothing. It is obvious that this parameter should be used with extreme care.

After editing the CDR file, CONTUR may be executed by means of the following command file:

```
$ ASS/USER 'P1'.CDR FOR055
$ ASS/USER 'P1'.BDR FOR017
$ ASS/USER SYS$COMMAND: SYS$INPUT
$ RUN US5:[SCHMI.FIPCON]CONTUR
```

Initial Distribution for SR-113

Ministries of Defence	
JSPHQ Belgium	2
DND Canada	10
CHOD Denmark	8
MOD France	8
MOD Germany	15
MOD Greece	11
MOD Italy	10
MOD Netherlands	12
CHOD Norway	10
MOD Portugal	2
MOD Spain	2
MOD Turkey	5
MOD UK	20
SECDEF US	60
NATO Authorities	
Defence Planning Committee	3
NAMILCOM	2
SACLANT	3
SACLANTREPEUR	1
CINCWESTLANT/ COMOCEANLANT	1
COMSTRIKFLTANT	1
CINCIBERLANT	1
CINCEASTLANT	1
COMSUBACLANT	1
COMMAIREASTLANT	1
SACEUR	2
CINCNORTH	1
CINCSOUTH	1
COMNAVSOUTH	1
COMSTRIKFORSOUTH	1
COMEDCENT	1
COMMARAIRMED	1
CINCHAN	3
SCNR for SACLANTCEN	
SCNR Belgium	1
SCNR Canada	1
SCNR Denmark	1
SCNR Germany	1
SCNR Greece	1
SCNR Italy	1
SCNR Netherlands	1
SCNR Norway	1
SCNR Portugal	1
SCNR Turkey	1
SCNR UK	1
SCNR US	2
French Delegate	1
SECGEN Rep. SCNR	1
NAMILCOM Rep. SCNR	1
National Liaison Officers	
NLO Canada	1
NLO Denmark	1
NLO Germany	1
NLO Italy	1
NLO UK	1
NLO US	1
NLR to SACLANT	
NLR Belgium	1
NLR Canada	1
NLR Denmark	1
NLR Germany	1
NLR Greece	1
NLR Italy	1
NLR Netherlands	1
NLR Norway	1
NLR Portugal	1
NLR Turkey	1
NLR UK	1
Total external distribution	234
SACLANTCEN Library	10
Stock	36
Total number of copies	280